



CATALYTIC PYROLYSIS OF VARIOUS BIOMASS TO AROMATIC
HYDROCARBONS OVER Ni-BASED CATALYSTS

BY

LE KIM HOANG PHAM

A DISSERTATION SUBMITTED IN PARTIAL FULFILLMENT OF THE
REQUIREMENTS FOR THE DEGREE OF DOCTOR
OF PHILOSOPHY (CHEMISTRY)
FACULTY OF SCIENCE AND TECHNOLOGY
THAMMASAT UNIVERSITY
ACADEMIC YEAR 2021
COPYRIGHT OF THAMMASAT UNIVERSITY

THAMMASAT UNIVERSITY
FACULTY OF SCIENCE AND TECHNOLOGY

DISSERTATION

BY

LE KIM HOANG PHAM

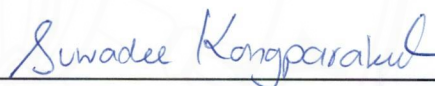
ENTITLED

CATALYTIC PYROLYSIS OF VARIOUS BIOMASS TO AROMATIC HYDROCARBONS OVER
Ni-BASED CATALYSTS

was approved as partial fulfillment of the requirements for
the degree of Doctor of Philosophy (Chemistry)

on July 7, 2022

Chairman



(Associate Professor Suwadee Kongparakul, Ph. D.)

Member and Advisor



(Associate Professor Chantip Samart, D. Eng.)

Member and Co-Advisor



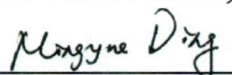
(Dai-Viet N. Vo, Ph. D.)

Member



(Associate Professor Prasert Reuboycharoen, D. Eng.)

Member



(Professor Mingyue Ding, Ph. D.)

Dean



(Associate Professor Nuttont Hongwarittorn, Ph. D.)

Dissertation Title	CATALYTIC PYROLYSIS OF VARIOUS BIOMASS TO AROMATIC HYDROCARBONS OVER Ni-BASED CATALYSTS
Author	Le Kim Hoang Pham
Degree	Doctor of Philosophy (Chemistry)
Department/Faculty/University	Chemistry Faculty of Science and Technology Thammasat University
Dissertation Advisor	Associate Professor Chanatip Samart, D.Eng.
Dissertation Co-Advisor	Dai-Viet N. Vo, Ph.D.
Academic Year	2021

ABSTRACT

The non-noble Ni-based catalyst has been attentive due to its low-cost and high activity in hydro-transfer reactions. However, the selective conversion is still lower compared to noble metal-based catalysts. In this study, we would like to design the modified Ni catalyst by co-doping P and Ce to form Nickel phosphide and bimetallic catalysts, which are supported in N-doping activated carbon. Aiming to study to convert agroforestry residues into valuable chemicals, which are further applied in Jet fuel, we investigated the effect of various biomass types as well as design Ni -based catalysts on upgrading fast pyrolysis oil. In detail, the research includes three parts: Part 1: Studying pyrolysis of 20 biomass samples in Thailand using data analysis to predict the pathway of phenolic formation, which was affected by biomass type and pyrolysis temperature. We found that a significant interaction relationship between lignin, hemicellulose, and pyrolysis temperature on the fraction of phenolic and aromatic hydrocarbon with rich-lignin biomass content and high temperature (550 – 600 °C) in fast catalytic pyrolysis can be an excessive solution to convert the waste material to high alkylphenol content. The statistic was performed to predict the yield of phenolic compounds from each fraction of lignocellulose with temperature.

Part 2 and 3 are the development of nickel phosphide and bi-metallic of Ni-Ce support on N-doping activated charcoal for deoxygenation of pyrolyzed vapor from biomass pyrolysis in case of full H₂ and limited H₂ co-feeding gas, respectively. In the detail, the Ni₂P/N-doping catalyst significantly influenced by the co-ordination of N-doping activated carbon to the formation of pure Ni₂P phase with small particle size. The high selective alkylphenol product (>70%) was observed under mild temperature (300 – 400 °C), under atmospheric pressure in fixed-bed reactors. The Ni₂P/CN50 catalyst can be applied in three cycles without treatment still performed high deoxygenation and prior better than without N-doping.

Last part, the bi-metallic Ni-Ce catalysts with different Ni and Ce loading were tested with different co-feeding gas including H₂, N₂, CO₂, and water. The estimated result is an *in-situ* generation of H₂ by reforming and then immediately hydrodeoxygenation. The results show that the Ni-Ce bimetallic supported on N-doping activated carbon catalyst can be limited to the H₂ atmosphere in hydrodeoxygenation up to 50%. However, to form full free-oxy by hydrodeoxygenation of lignin fragment under mild conditions (400 °C and 1 atm) without H₂ gas co-feeding is still challenged.

Keywords: N-doping carbon; hydrodeoxygenation; Nickel based catalysts; Palm kernel shell

ACKNOWLEDGEMENTS

The doctoral degree is a long journey in my study, in which there are a lot of challenges and barriers. This thesis is the result of not only my efforts but also the support and assistance of many individuals.

First, I would like to express my deepest appreciation to my advisor, Associate Professor Dr.Chanatip Samart, for his continuous encouragement of my doctoral studies and research, as well as his kindness, energy, enthusiasm, and comprehensive knowledge. His mentoring stretched beyond assisting me in completing my studies to enriching my spiritual life.

I especially want to thank my co-Advisor Dr.Dai-Viet N. Vo for his endless support to help me overcome the challenges when the part research was done in Viet Nam. Without your help, the thesis could not be done.

I am also grateful to Associate Professor Dr.Suwadee Kongparakul for serving as chairman, her encouragement, insightful comments, and kindly advise, and Associate Professor Dr.Prasert Reubroycharoen, Professor Mingyue Ding as a lovely committee, for his generous support with effective discussion, suggestions, and questions. I must thank Associate Professor Dr.Nguyen Van Cuong (IUH University) and Dr.Narong Chanlek (Thailand Synchrotron Light Research Institute) for their kind instrument assistance in characterization, as well as all members in laboratory from Thammasat University, Chulalongkorn University, NTT University, and IUH University. Furthermore, I would like to thank the Department of Chemistry, Faculty of Science and Technology, Thammasat University, and Nguyen Tat Thanh University for funding all instruments and allowing me to work on different and intriguing laboratory projects. I also would like to thank the ASEAN scholarship and the NRCT-NSFC Thailand China joint project for giving full financial support for my research at Thammasat University in Thailand.

Finally, I owe a debt of gratitude to my family for their unwavering support during my studying time.

Le Kim Hoang Pham

TABLE OF CONTENTS

	Page
ABSTRACT	(1)
ACKNOWLEDGEMENTS	(3)
LIST OF CONTENTS	(4)
LIST OF TABLES	(8)
LIST OF FIGURES	(9)
LIST OF SCHEMES	(12)
LIST OF ABBREVIATIONS	(13)
CHAPTER 1 INTRODUCTION	1
1.1 Thesis motivation	1
1.2 Dissertation objectives	4
1.3 Dissertation of instruction	5
CHAPTER 2 INVESTIGATION OF VARIOUS AGRI-FORESIDUE BIOMASS TO PRODUCE HIGH VALUE CHEMICAL VIA FAST PYROLYSIS	6
2.1 Background	6
2.2 Material and method	10
2.2.1 Material	10
2.2.2 Method	11

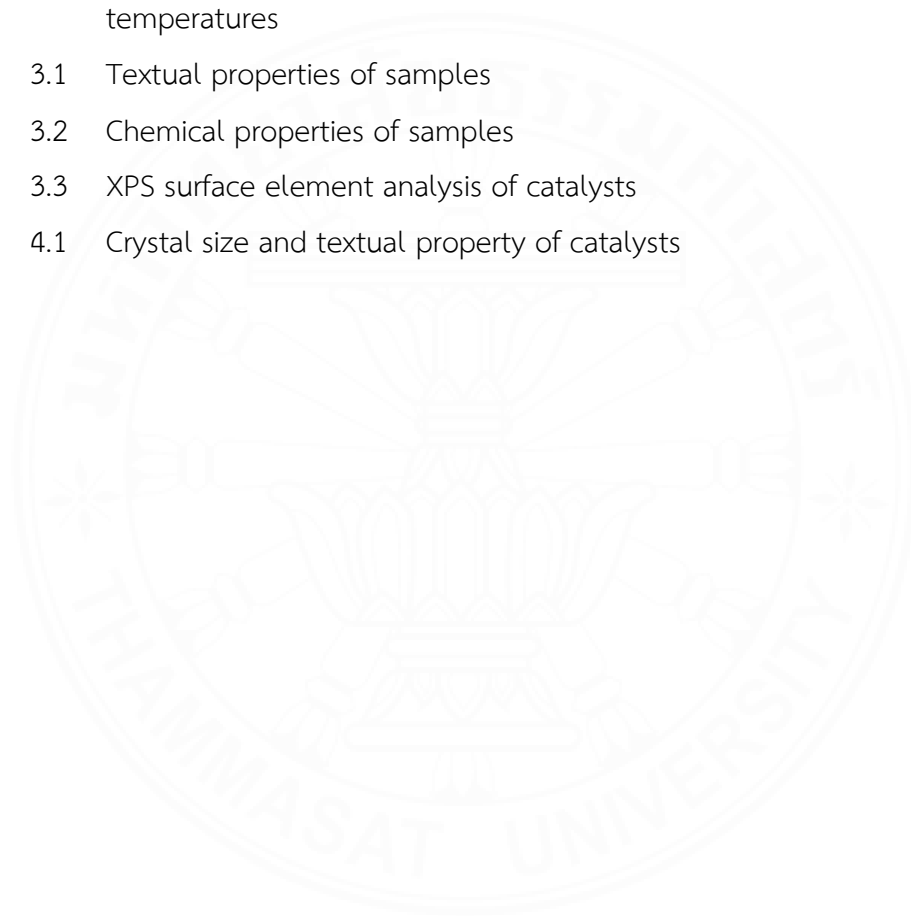
2.2.2.1 Fiber analysis of lignocellulosic biomass analysis	11
2.2.2.2 Thermal pyrolysis of various biomass samples	12
2.2.2.3 Statistical analysis	14
2.3 Results and discussion	15
2.3.1 The relationship between proximate analysis results and heating value	15
2.3.2 Effect of reaction temperature on distribution of pyrolysis product	20
2.3.3 Effect of lignin and hemicellulose on pyrolysis oil composition	22
CHAPTER 3 STUDY OF NICKEL PHOPHIDE BASED-CARBONEOUS CATALYSTS ON HYDRODEOXYGENATION OF PALM KERNEL SHELL PYROLYSIS VAPOR	31
3.1 Background	31
3.2 Material and method	34
3.2.1 Preparation of Ni ₂ P support on based- carbon	34
3.2.1.1 Preparation of N-doping activated carbon	34
3.2.1.2 Preparation of Ni ₂ P/C and Ni ₂ P/CN _x catalysts	34
3.2.1.3 Characterization of Ni ₂ P/C and Ni ₂ P/CN _x catalyst samples	35
3.2.2 Catalytic integrated deoxygenation of Palm kernel shell	36
3.3 Results and discussion	37
3.3.1 Characterization of the catalysts	37
3.3.1.1 XRD results	37
3.3.1.2 TEM results	39
3.3.1.3 Textual results	43
3.3.1.4 H ₂ -TPR results	43
3.3.1.5 NH ₃ -TPD results	45

3.3.1.6 XPS results	46
3.3.2 Catalytic ability	49
3.3.2.1 Effect of various catalysts on the upgrading performance	49
3.3.2.2 Effect of temperature on the upgrading performance	51
3.3.2.3 Effect of catalyst loading on the upgrading performance	52
3.3.2.4 Generation	54
3.3.2.5 Propose the mechanism	55
CHAPTER 4 BIMETALIC Ni-Ce/CN50 CATALYST FOR IN-SITU HYDRODEOXYGENATION OF PALM KERNEL SHELL PYROLYSIS VAPOR	57
4.1 Background	57
4.2 Material and method	60
4.2.1 Preparation of Bimetallic Ni-Ce support on N-doping activated carbon	60
4.2.2 Catalytic integrated deoxygenation of Palm kernel shell	60
4.3 Results and discussions	62
4.3.1 Effect of Ce loading on catalytic upgrading performance under N ₂ carrier gas	62
4.3.2 Effect of Ce loading on catalytic upgrading performance under CO ₂ carrier gas	63
4.3.3 Effect of (N ₂ : H ₂) ratio gas feeding on upgrading performance	65
4.3.4 Effect of gas feeding on upgrading performance	67
4.3.5 Effect of Ni loading on upgrading performance	68
4.3.6 XRD results	69

	(7)
4.3.7 XPS results	71
4.3.8 Textual property results	72
CHAPTER 5 CONCLUSIONS AND RECOMMENDATIONS	74
5.1 Conclusions	74
5.2 Recommendations	75
5.2.1 Thermal pyrolysis of various biomass	75
5.2.2 Catalytic upgrading	75
REFERENCES	77
APPENDICES	84
APPENDIX A	85
APPENDIX B	87
BIOGRAPHY	88

LIST OF TABLES

Tables	Page
2.1 The completed composition analysis of 20 biomass samples	17
2.2 ANOVA table for the model and the model term	23
2.3 The response of target compounds at different pyrolysis temperatures	25
3.1 Textual properties of samples	41
3.2 Chemical properties of samples	42
3.3 XPS surface element analysis of catalysts	48
4.1 Crystal size and textual property of catalysts	70



LIST OF FIGURES

Figures	Page
2.1 Structure of three main components of lignocellulosic biomass	7
2.2 Structure of three main components of lignocellulosic biomass.	9
2.3 Chemical extraction method to analyze biomass's structural analysis	11
2.4 Schematic diagram of pyrolysis system	12
2.5 Pyrolysis product of 20 biomass with different pyrolysis temperature	20
2.6 Effect of lignin and temperature on distribution of phenolic, alkyl phenolic, hydrocarbon and aromatic hydrocarbon in organic oil	26
2.7 Effect of hemicellulose and temperature on distribution of phenolic, alkyl phenolic, hydrocarbon and aromatic hydrocarbon in organic oil	27
2.8 Effect of lignin and hemicellulose ratio of biomass on distribution of phenolic, alkyl phenolic, hydrocarbon and aromatic hydrocarbon in organic oil	28
2.9 Pareto diagrams present the significant effects to produce of (a) phenolic compounds; (b) alkyl phenol compounds; (c) hydrocarbon compounds; and (d) aromatic hydrocarbon compounds	29
2.10 Propose pyrolysis pathways of lignin and hemicellulose to produce phenolic, alkyl phenol, hydrocarbon, and aromatic hydrocarbon compounds	30
3.1 XRD pattern of Ni ₂ P/C and Ni ₂ P/CN _x samples	38
3.2 TEM images, partial distribution, and SAED patterns of Ni ₂ P/C, Ni ₂ P/CN25, Ni ₂ P/CN50, Ni ₂ P/CN75, and Ni ₂ P/CN100 samples.	40
3.3 H ₂ -TPR patterns of samples	44
3.4 NH ₃ -TPD patterns of samples	45

3.5	XPS profile of (i) Ni ₂ P/C, (ii) Ni ₂ P/CN25, (iii) Ni ₂ P/CN50, (iv) Ni ₂ P/CN75, and (v) Ni ₂ P/CN100 samples in wide range (a), Ni _{2p} (b), P _{2p} (c), O _{1s} (d), C _{1s} (e), and N _{1s} (f) spectra.	47
3.6	The pyrolysis products (a), and chemical distribution in liquid product (b) by catalytic upgrading using Ni ₂ P catalysts with and without N-doping.	50
3.7	The pyrolysis products (a, c), and chemical distribution in liquid product (b, d) by catalytic upgrading using Ni ₂ P/CN25 and Ni ₂ P/CN50 catalysts.	51
3.8	The pyrolysis products (a, c), and chemical distribution in liquid product (b, d) by catalytic upgrading using Ni ₂ P/CN25 and Ni ₂ P/CN50 catalysts.	53
3.9	The pyrolysis products (a), and chemical distribution in liquid product (b) by catalytic upgrading using Ni ₂ P/C and Ni ₂ P/CN50 catalysts.	54
3.10	The propose of mechanism	55
4.1	The pyrolysis products (a), and chemical distribution in liquid product (b) by catalytic upgrading using 10Ni _x Ce/CN50 catalysts.	62
4.2	The pyrolysis products (a), and chemical distribution in liquid product (b) by catalytic upgrading using 10Ni _x Ce/CN50 catalysts.	64
4.3	The pyrolysis products (a), and chemical distribution in liquid product (b) by catalytic upgrading using 10Ni ₅ Ce/CN50 catalysts.	66
4.4	The pyrolysis products (a), and chemical distribution in liquid product (b) by catalytic upgrading using 10Ni _x Ce/CN50 catalysts.	67
4.5	The pyrolysis products (a), and chemical distribution in liquid product (b) by catalytic upgrading using 10Ni _x Ce/CN50 catalysts.	68
4.6	XRD patterns of (a) different Ce level doping, (b) different Ni level doping	69
4.7	XPS patterns of (a) different Ce level doping samples, (b) different Ni level doping samples	71

A.1	N ₂ adsorption-desorption Isothermal samples of (a) activated carbon with and without N-doping support, and (a') Ni ₂ P doping on activated carbon with and without N-doping support	85
A.2	Pore distribution of (b) activated carbon with and without N-doping support, and (b') Ni ₂ P doping on activated carbon with and without N-doping support	86
B.1	N ₂ adsorption-desorption Isothermal fresh and spent	87



LIST OF SCHEMES

Schemes	Page
3.1 Presentation of Ni crystals of tetrahedron Ni(1) and pyramid Ni(2) phases in Ni ₂ P unit cell	32
4.1 Cerium in 59transfer-state Ce ⁴⁺ and Ce ³⁺	59
4.2 The role of metallic active in deoxygenation	59
4.3 Describe deoxygenation over Ni and Ce active sites	65



LIST OF ABBREVIATIONS

Symbols/Abbreviations	Terms
%	Percentage
°C	Celsius
AC	Activated carbon
A_i	Area of compound i
Al_2O_3	Alumina
ANOVA	Analysis of Variance
ASTM	American Society for Testing and Materials
A_T	Total Area
BET	Brunauer–Emmett–Teller
C	Carbon
Ce	Cerium
CN	Nitrogen doping Carbon
CO	Carbon monoxide
CO_2	Carbon dioxide
Eq.	Equation
FC	Fixed carbon
$g-C_3N_4$	Graphitic carbon nitride
GC	Gas chromatography
GC-MS	Gas chromatography - mass spectrometry
GHSV	Gas hourly space velocity
h	Hour
H_2 -TPR	Temperature program reduction of hydrogen
HDN	Hydrodenitrogenation
HDO	Hydrodeoxygenation

Symbols/Abbreviations	Terms
HDS	Hydrodesulfurization
HHV	High heating value
Ir	Iridium
m	Mass
min	Minute
mmol	Millimolar
ml	Milliliter
MJ/kg	Megajoules per kilogram
Mg	Magnesium
Mo	Molybdenum
N	Nitrogen
N ₂	Nitrogen gas
NH ₃ -TPD	Temperature program desorption of ammonia
Ni	Nickel
Ni ₂ P	Nickel phosphide
Ni ₁₂ P ₅	Nickel phosphide
NIST	National Institute of Standards and Technology
NREL	The National Renewable Energy Laboratory
O	Oxygen atom
OH	Hydroxyl group
Os	Osmium
P	Phosphorus
Pd	Palladium
Pt	Platinum
Py-GC/MS	Pyrolysis-gas chromatograph-mass spectrometry

Symbols/Abbreviations	Terms
Ru	Ruthenium
SAED	Selected Area Electron Diffraction
SiO ₂	Silicon dioxide
TAPPI	Technical Association of the Pulp and Paper Industry
TCD	Thermal Conductivity Detector
TEM	Transmission electron microscopy
TGA-IR	Thermogravimetric analysis coupled Infrared spectroscopy
TPD	Temperature programmed desorption
TPR	Temperature programmed reduction
VM	Volatile matters
Wt.	Weight
XPS	X-ray photoelectron spectroscopy
XRD	X-ray diffraction
Y	Yield
ZrO ₂	Zirconium oxide

CHAPTER 1

INTRODUCTION

1.1 Thesis motivation

Recently, the non-fossil energy has received grown up considerable scholarly attention to alternative limited source. Among clean and green solutions, bio-fuel derivative from lignocellulosic biomass has seen increasing rapid advances in abundance resources and carbon dioxide recovery that can be helpful in environmental and sustainable energy concepts [1]. Recent developments in the field of biomass feedstock, the lignocellulosic material, which originated from residue of agriculture and forestry economy have led to a potential resource to liquification due to its available and low-cost material [1–3].

Fast pyrolysis is a thermal-conversion and non-oxygen technique generally applied in fragmentation of lignocellulosic biomass to achieve the highest liquid yield and possibly applied in industrial scale [4]. However, the issue of fast pyrolysis has received considerable critical attention by the primary organic oxy-compounds content, which fragmented from which fragmented from lignin, hemicellulose, and cellulose-three main components of lignocellulosic biomass at high temperature and short residence time [5]. The high oxygen content has been noted decreasing ignition ability and unstable storage of fuel. Therefore, the elimination of oxygen and selective to target compounds via deoxygenation plays a crucial role in improvement bio-fuel properties.

Several studies have reported the deoxygenation pathways can be through cracking-deoxygenation and hydrodeoxygenation can be coupled with fast pyrolysis process [6–8]. Research of literature revealed studies of cracking deoxygenation upgrading commonly using the zeolite or noble metal dope- zeolite catalysts. The advantage of this process does not require hydrogen as co-feeding reagents, therefore, can be operated at atmospheric pressure. However, it needs quiet elevated temperatures in the range above 500 °C to significant increasable cracking rate of C-O

and C-C linkages corresponded to form the smaller volatile compounds production, hence decreasing of oil yield and an increasing in the gas yield [8, 9]. It is crucial to control the degree of cracking needed to remove oxygen at high temperature, but if the rate of cracking becomes too high, at increased temperatures, degradation of the bio-oil to form light gases and carbon will occur instead [5]. Moreover, the key to cracking is catalyst required to acidity and porosity properties has been a vital designed factor to linked with selective C-O, C-C cleavage, or coking formation as by-product of further repolymerization. The challenge of cracking-deoxygenation has grown in importance considering recent is control selective deoxygenation to formation the target product as well as prevent the coking formation.

So far, the hydrodeoxygenation technique has been agreement on the precise nature of hydrogen can be deal with complexed mixture substances in bio-oil consisted of acid, ketone, phenolic, furan, alcohol, ... to refers to the removal oxygen by water and to keep same carbon number in backbone of organic oxy-compounds with low coke formation [10, 11]. In case of conditions, it can be carried out at high-pressure operation and moderate temperature. The oxygenate compounds could be reacted with high-pressure hydrogen in the presence of a heterogeneous catalyst to form water and saturated carbon-carbon bonds using heterogeneous catalyst such noble metals, sulfides, phosphides, carbides, nitrides, nonprecious metals, metal oxides, bimetallic amorphous boron-based catalysts, and reduced metal oxides[12–16]. From that point, hydrodeoxygenation has been more interested than cracking-deoxygenation in case of discard oxygen in bio-oil. However, the challenge of this process is how to reduce the hydrogen operation pressure as well as hydrogen co-feeding donor due to the case safety and cost operation.

The designed hydrodeoxygenation catalyst should be multifunctional active site presents not only acid site to assisted C-O cleavage, but also remaining metallic site to further active hydro active site to balance C-O cracking and hydrodeoxygenation performance. Furthermore, the selectivity of deoxygenation has been concerned regarding to obtain the desired compounds. They are corresponded to the absorb ability and hydrogen coupled to reject oxygen. In the detail, it was carried

out through two steps: first, the oxygen from oxygenates can be absorbed on coordinatively unsaturated metal sites by oxygen vacancies (from metal oxide supports through Lewis's acid/base interaction by oxophilicity, or on H in single bond OH that is attached to nonmetal oxides such as SiO₂) [6, 7]. The metal sites such as noble metals played role as activation of hydrogen gas by H spillover or provide single bond H donation available directly from phosphides, carbides, nitrides, or Brønsted acid single bond OH groups. The second, the activated H species then reacts with organics and give deoxygenated products as hydrocarbon and release water [5, 7].

The development catalyst with non-noble metal and low-cost carbon-based support material has been more attention because they can be utilized of by-product of pyrolysis product and, less expensive compared to alumina and silica supports, high thermal stability and various oxygenated functional groups which enhances metal adsorption and catalyst dispersion. Hence, the activated carbon, which derivatives from biomass resources is quite interesting to generate the novel HDO support catalyst used to strengthen the function of N-containing biochar to promote their applications [17, 18]. Nitrogen containing functional groups of biochar can increase the hydrophilicity, therefore, it has a wide range of applications, such as adsorption of pollutants, catalysis, and energy storage. The N-doped carbon-supported metal catalysts have received widespread attention since N dopants can enhance the electronic interaction between metal and carbon support [19, 20], alter the acid–base properties of the support surface, and increase the catalytic activity [17, 21, 22]. prepared a N-functionalized mesoporous carbon-supported Pd catalyst used in the hydrogenation of phenol, a ~80% conversion of phenol and a ~100% selectivity to cyclohexanone were obtained. The superior selectivity may be attributed by the synergetic effect between the N-doped carbon and the highly dispersed Pd nanoparticle. Similarly, Hu *et al.* [23] prepared a Ru–Ni bimetallic catalyst supported on N-doped activated carbon (Ru–Ni-AC/N) by heating phenanthroline sulfonate and activated carbon under N₂ atmosphere. When the 1%Ru-5% Ni-AC/N catalyst was used in the hydrogenolysis of guaiacol, the yield of aromatics reached 57%. While N-doped carbon supported metal-catalysts exhibited enhanced performance for many

reactions, the applications of this kind of catalyst in the conversion of lignin are rarely reported specially with Ni_2P .

In this research, we investigated the fast pyrolysis of biomass to produce the target produce can be applied in jet fuel. This work can be divided to three main parts including: Part 1 focus on investigation thermal fast pyrolysis of biomass feedstocks without catalyst to product phenolic compounds as aromatic hydrocarbon-precursor in deoxygenation. These reactions were performed with twenty biomass feedstocks available in Thailand at four different pyrolysis temperatures. The relationship between the biomass components and pyrolysis temperature were statistical estimate via a central composite design with three factors. Part 2 and 3 were relative to preparation and characterization of designed hydrodeoxygenation catalysts, which could be applied in fast catalytic pyrolysis of the chosen biomass in part 1 under integrated two fixed bed reactors and atmospheric operation pressure with and without hydrogen gas, respectively.

Part 1. Thermal fast pyrolysis of 20 biomass samples in order to find the suitable biomass to produce fine as-precursor chemical such alkyl phenol to apply deoxygenation produce aromatic hydrocarbons

Part 2. Prepare the Nickel phosphide-support on N-doping activated charcoal catalysts and apply in HDO of pyrolysis oil

Part 3. Prepare the Bi-metal functional (Ni-Ce) support on N-doping activated charcoal catalysts and apply in cracking deoxygenation of pyrolysis oil

1.2 Dissertation objectives

1.2.1 To predict the data of 20 biomass samples in thermal pyrolysis to produce phenolic and aromatic hydrocarbons compounds: effected of biomass types and pyrolysis temperatures

1.2.2 To study N doping-activated charcoal to prepare novel support catalyst to prepare catalyst in deoxygenation of pyrolysis oil

1.2.3 To study the catalytic activity of Ni₂P/N-doping activated charcoal for HDO pyrolysis oil from selected biomass (which find in the first objective) under rich hydrogen environment.

1.2.4 To study the catalytic activity Ni-Ce/N-doping activated charcoal catalyst for HDO of pyrolysis oil from selected biomass (which find in the first objective) without hydrogen feeding (hydrogen regenerated by *in-situ* pyrolysis from splitting reaction)

1.3 Dissertation of instruction

The dissertation is divided into five chapters, in which Chapters 2, 3 and 4 are each manuscript that has either been published in or prepared for submission to scholarly journals. The detailed of the dissertation organization is shown below.

Chapter 1 gives the motivations of the research and organization of the dissertation as well as the objectives of the research

Chapter 2 provides an introduction of pyrolysis lignocellulosic background. It also includes a briefly introduction to the mechanism interactive of each lignocellulosic component to as-obtained product and the method for analysis. Finally, a brief discussion about estimated regression equation from data analysis.

Chapter 3 involves preparation with a series of N-doping activated carbon supports and Ni₂P doping catalysts. The effect of reaction conditions (such as catalysts, temperature, catalyst loading, and regeneration catalyst) toward both activity and selectivity were investigated and discussed in detail.

Chapter 4 including synthesis of bimetallic Ni-Ce support on the chosen N-doping support in part and applied in the limited hydrogen gas co-feeding with biomass feedstocks. The effect of reaction conditions (such as catalyst types, gas feeding, metal loading) toward both activity and selectivity were investigated and discussed in detail.

Chapter 5 provides general conclusions and suggestions of future works.

CHAPTER 2

INVESTIGATION OF VARIOUS AGRI-FORESIDUE BIOMASS TO PRODUCE HIGH VALUE CHEMICAL VIA FAST PYROLYSIS

2.1 Background

Lignocellulosic biomass, which is derived from agriculture and forestry residues can be expected as an abundance and low-cost feedstock to replacement of fossil resources. The commercial thermal conversion techniques were used to produce valuable products via torrefaction, pyrolysis, liquefaction, and gasification including biochar, bio-oil, or biogas as the target product. Therein, fast pyrolysis is the most powerful process to produce liquid -biofuel due to achieve high bio-oil yield (up to 70%), which the bio-oil can be applied in industry possibly liquid fossil fuel replacement in the coming future [24]. In fast pyrolysis, the reaction was carried out under a few seconds with the reaction temperature of 400 – 600 °C; resulting formation of liquid product containing various oxygenated compounds from fragmentation of lignocellulosic constituents. Lignocellulose structure is a complex biopolymer mixture of cellulose, hemicellulose, lignin (Figure 2.1), which those compositions were corresponded to the specific biomass types. Cellulose is a linear biopolymer of glucose connected by β -1,4-glycoside linkage, which forms the framework of the biomass cell walls [25]. Most of them are highly crystalline in nature with the polymeric degree frequently more than 9000 with crystalline and amorphous forms [26]. Hemicellulose is structurally amorphous and possesses a heterogeneous composition formed by copolymers of five different C₅ and C₆ sugars, namely glucose, galactose, mannose, xylose, and arabinose [27]. Lignin even plays as the main component in the plant cell but has been received a less considerate in the real application since it is a by-product of cellulose fractionation in bio-ethanol and pulp and paper industry [28].

However, lignin has been predicted in the short future as a sustainable bio-aromatic resources that can be converted to bio-aromatic hydrocarbon rich fuel such as jet fuel.

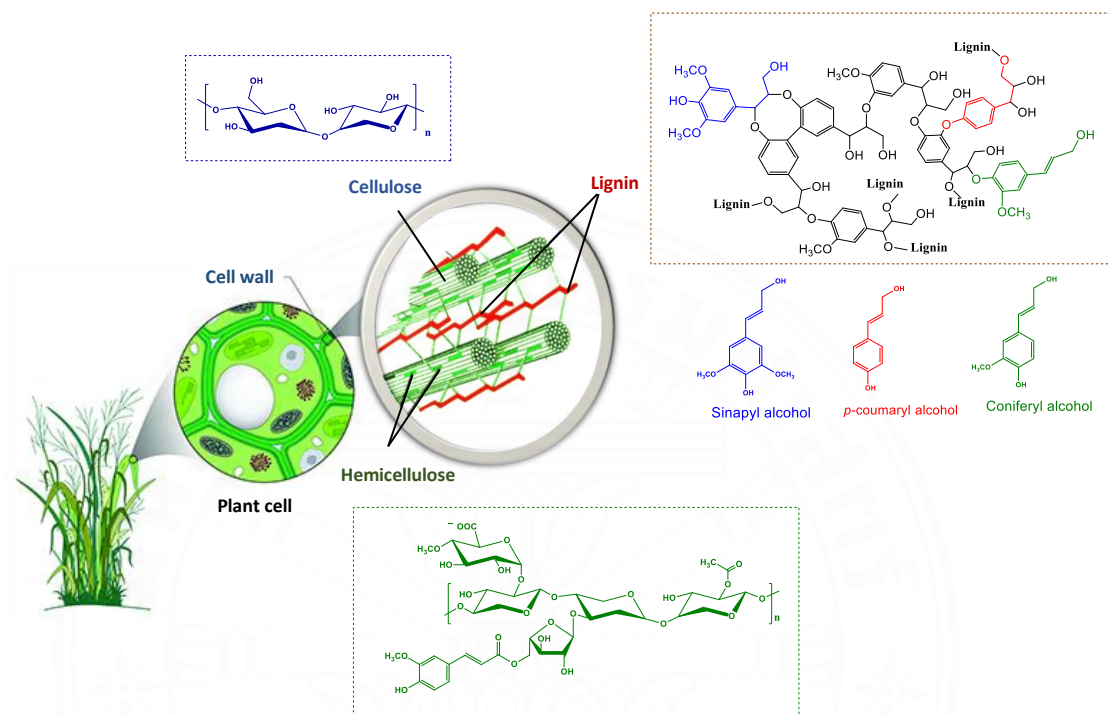


Figure 2.1 Structure of three main components of lignocellulosic biomass

Maturely, lignin's chemical structure is formed by the polyphenolic establishment of the aromatic backbone organization from three units of p-coumaryl/p-hydroxyphenyl, coniferyl/ guaiacyl, and sinapyl/syringyl alcohol together by ether linkages, carbon-carbon bond, and the carbon-oxygen bond [29] (Figure 2.2). The interaction of lignin, cellulose, and hemicellulose molecules are still a challenge topic in fast pyrolysis [30, 31]. According to some studies, no matter their interactions exist, and pyrolysis can be thought of as a simple superposition of the three components [32]. However, the pure cellulose and hemicellulose were decomposed at lower temperatures than woody biomass (mainly contain cellulose and hemicellulose) [33]. This evident may

be the effect of other components in the wood to decompose during the pyrolysis. In the other study [33–36], the char yield increased for cellulose-lignin and cellulose-hemicellulose blends but did not observe for hemicellulose-lignin blends, indicating that only cellulose molecule interacted with the others. It was also noted that the possibility that the interactions were simply from inorganic catalyzed pyrolysis of cellulose when blended.



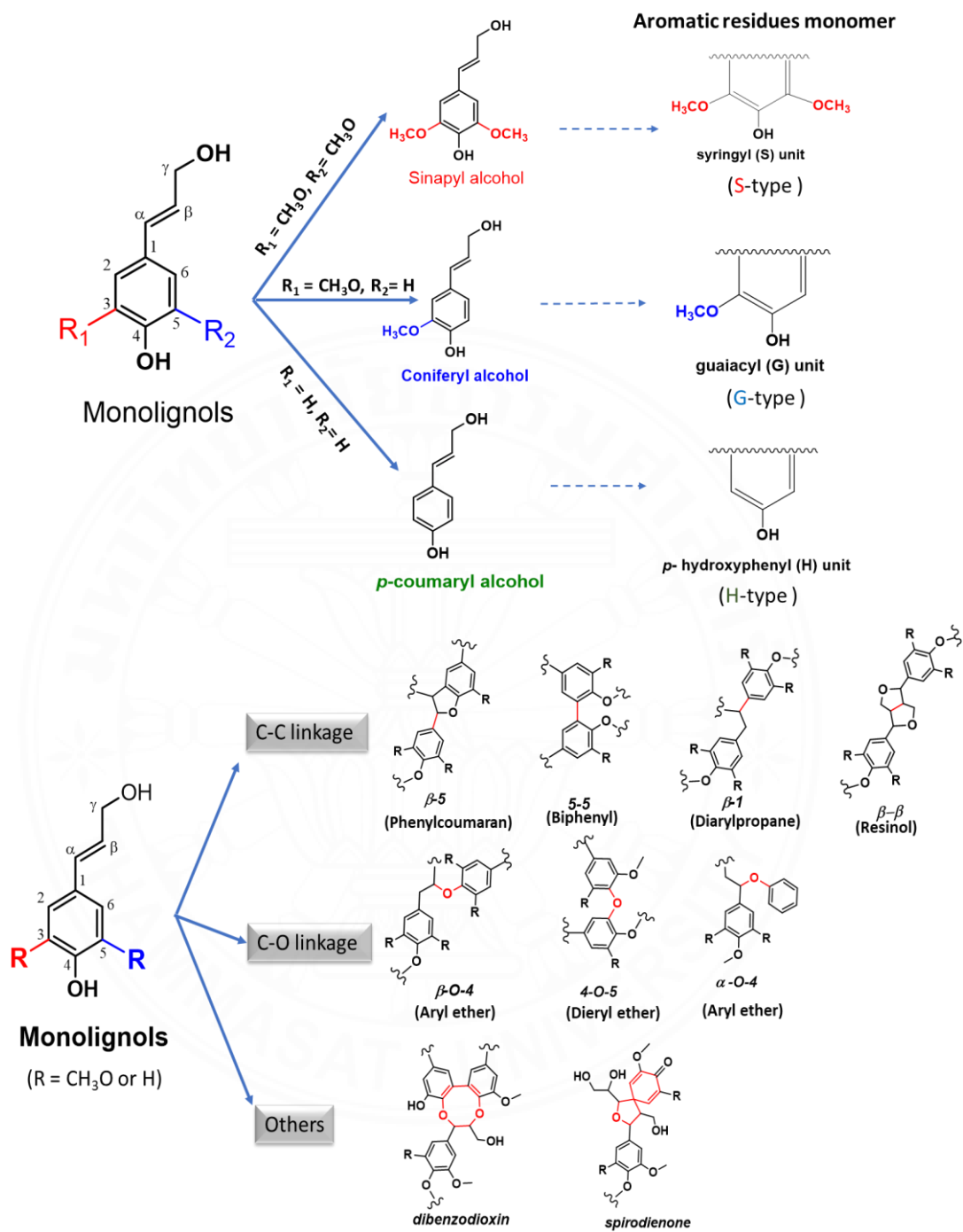


Figure 2.2 Structure of three main components of lignocellulosic biomass.

Hosoya et al. [37] studied the cellulose-lignin interactions were more severe than cellulose-hemicellulose interactions and cellulose may be able to suppress char formation from lignin, while lignin can enhance levoglucosan yield from cellulose by inhibiting further decomposition reactions. However, the rare study focused on the real biomass with mature lignocellulose chemical structure affect with the temperature to produce the desired product in liquid fuel.

In this chapter, we determined the relationship between the various biomass feedstocks and their correlated pyrolysis temperature behavior to produce phenolic and hydrocarbon as the desired products due to valuable compounds. Among of them, the phenol particularly was more attractive precursor aromatic oxy-compounds product, which it could be deoxygenated to aromatic hydrocarbon via catalyst upgrading. The catalyst development for upgrading of pyrolysis products will be discussed in later chapters.

2.2 Material and method

2.2.1 Material

The 20 biomass samples were collected around local area which could be divided to agriculture wastes (rice straw, rice husk, maize stalk and leaves, corn cob, cassava trunk, palm empty fruit bunch, palm kernel shell, palm fiber, durian peel, coconut shell, coconut coir, coconut fond), aquatic plants (water lettuce, water hyacinth), wood-based biomass (wood sawdust, eucalyptus sawdust), and energy plants crops (Napier grass, bamboo, sugarcane bagasse, sugarcane leaves). All biomass samples were air-dried (moisture content < 5%), ground and sieved until particle size within the range of 0.2 – 2.0 mm as a pre-treatment to sort and isolate the analyzed fractions.

Other chemicals used in lignocellulosic fiber analysis were sodium chlorite (NaClO_2 , >80.0%), acetic glacial acid (CH_3COOH , > 99.0%), sulfuric acid (H_2SO_4 , 98.0%), sodium hydroxide (NaOH , > 98.5%).

2.2.2 Method

2.2.2.1 Fiber analysis of lignocellulosic biomass analysis

Briefly, the composition of biomass (Napier grass as an example) was analyzed by the chemical extraction was shown in Figure. 2.3

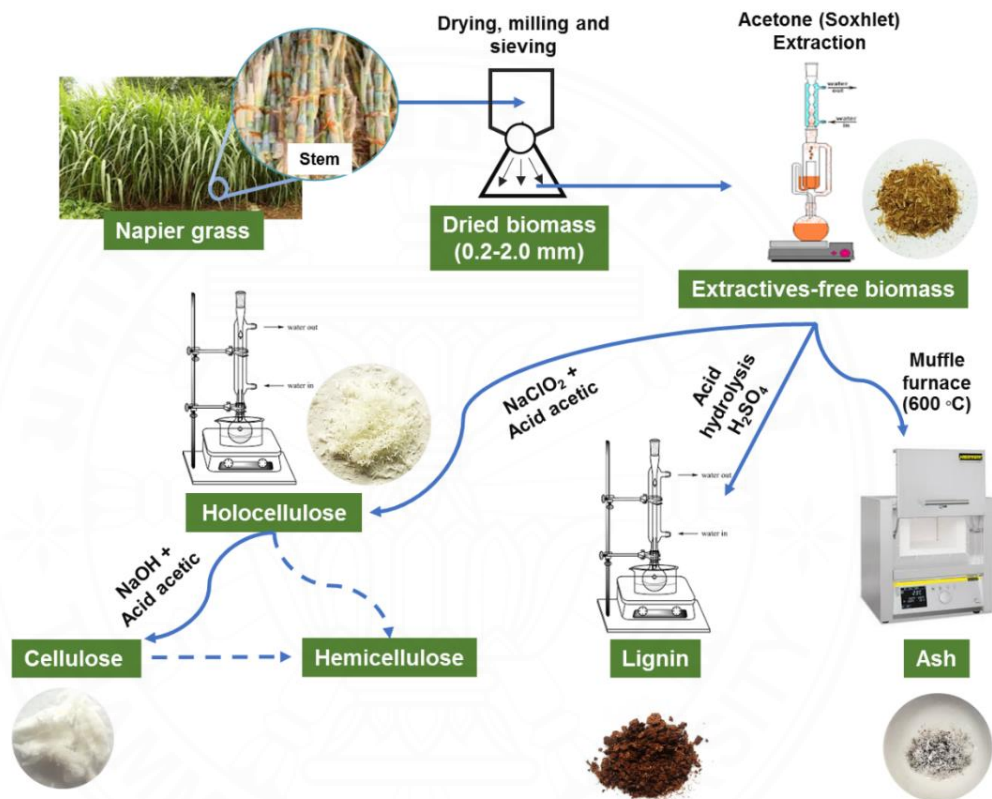


Figure 2.3 Chemical extraction method to analyze biomass's structural analysis

The extractives (resins, waxes, sterols, and fatty acids) from biomass samples were removed during a 24-hour stage extraction process using acetone and the Soxhlet method. Then free-extractives biomass was air-dried for 24 h to reduce the moisture content less than 10% for further analysis. According to ASTM D-1104. The

cellulose and hemicellulose fraction were analyzed according to TAPPI T 212 standard method [38], following treated as-received holocellulose with sodium hydroxide and acetic acid to find out the remaining-solid cellulose content. The hemicellulose content was obtained by the difference weight of holocellulose and cellulose. In the lignin quantification was subjected to a two-step acid hydrolysis according to NREL/TP-510-42618 method [38]. The concentrated sulfuric acid (72 wt.%) and then diluted sulfuric acid at high temperature were treated the biomass sample to yield the lignin in remaining solid sample. Ash quantification was carried out according to NREL/TP-510-42622 method [39]. This procedure consists in a thermal treatment at 600 °C in air.

2.2.2.2 Thermal pyrolysis of various biomass samples

The pyrolysis of sample was performed in two fixed-bed reactors as shown in Figure 2.4.

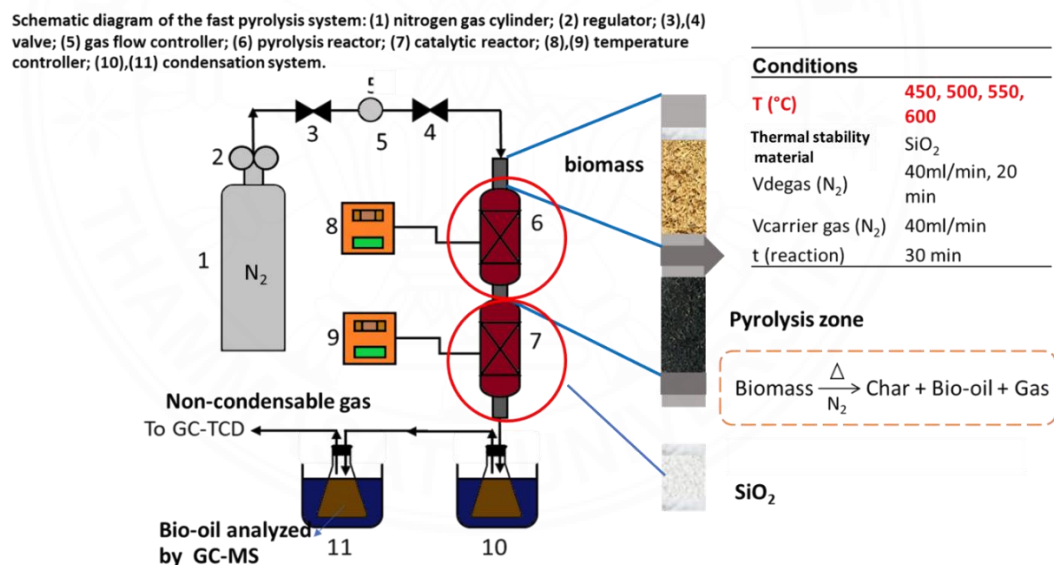


Figure 2.4 Schematic diagram of pyrolysis system

The carrier gas in pyrolysis system was controlled by mass flow controller (Brooks, USA). Two tubular reactors were made by stainless steel with diameter of 1/2 inch, and 24 cm length for pyrolysis zone, and 3/8 inch of diameter for catalyst zone. In the addition, the second tubular reactor contained 1cm of silica bed over the quartz wool to prevent the loss of silica during the reaction. Both tubular reactors were placed in electric furnace (Suan Luang Engineering Company, Thailand). The typical run of the 20 biomass samples (moisture content < 5 wt.%) with 0.2–2 mm particles was investigated by fast pyrolysis (residence time of 5s) with different temperatures (450 - 600 °C) under nitrogen atmosphere (40 ml min⁻¹). In each run, SiO₂ (5 wt.% of dried biomass sample) was packed in the second reactor over a quartz wool layers. Prior to the experiment, the system was purged by N₂ to remove O₂ in air for 20 min. Then, the biomass sample, in the hopper, was falling under the N₂ gas carrier into the pyrolysis reactor, which already reached pyrolysis temperature (450 - 600 °C). The pyrolysis vapor was continuously going to second pyrolysis reactor. The leaved vapor products were immediately condensed to liquid by two trapped condensers connecting in series (cooled by ice-cooling mixed with sodium chloride). The moisture free liquid product was obtained by treated with anhydrous sodium sulfate. The organic oil layer was analyzed by Gas chromatography–mass spectrometry (GC-MS, Agilent technology-7890A) equipped with an HP-5MS capillary column (0.25 mm ID, 30 m length, 0.25 mm film thickness), using He at a flow rate of 1 ml min⁻¹ as the carrier gas. The oven temperature was programmed to remain at 50 °C for 3 min, ramp at 10 °C min⁻¹ to 280 °C, and stay at 280 °C for 5 min. The injector split ratio was set to 50:1 using acetone as solvent to dilute the samples. The non-condensed gas was collected and chemically characterized online by gas chromatography coupled with thermal conductivity detector (GC-TCD, Shimadzu GC-8A, Shin carbon column) at 50 °C. Yield (Y) of pyrolysis products were calculated follow:

$$Y_{bio-char} = \frac{m_{solid_product}}{m_{biomass}} \cdot 100\% \quad (2.1)$$

$$Y_{liquid} = \frac{m_{liquid_product}}{m_{biomass}} \cdot 100\% \quad (2.2)$$

$$Y_{non-condensable_gas} = 100\% - Y_{bio-char} - Y_{liquid_product} \quad (2.3)$$

2.2.2.3 Statistical analysis

A statistic design known as a two-factor factorial collects data for all potential levels of the two factors of interest. The design is a balanced two-factor factorial design with a levels of factor A, b levels of factor B, and n independent replications taken for each of the axb treatment combinations if equal sample sizes are chosen for each of the potential factor combinations. Design size is given by $N = abn$. The average change in response resulting from a change in the level of a factor is considered the effect of that factor. Typically, this is referred to as a major impact. There is an interaction between the factors if the average change in response across all levels of one component is different from all levels of the other factor.

The composition of the biomass, namely its hemicellulose and lignin, is crucial for the production of aromatic-rich bio-oils [28, 40]. In this study, we focused on find out the relationship of lignin, hemicellulose factors (factor A, B) and their interaction based on a two-factor central composite design related to pyrolysis temperature (factor C) to determine how phenolic, alkyl phenol, hydrocarbon, and aromatic hydrocarbon chemicals formation.

In this study, the predicted results based on Contour plot by distance method works well in a wide range of circumstances was investigated by interpolated yield value (z value- the desired product compounds) at the interactions of a regular 20 by 4 mesh with the same x- and y-ranges (interaction from factors of A, B) following the distance method based on saddle function[41].

$$z = \frac{\left(\frac{x}{a}\right)^2 - \left(\frac{y}{b}\right)^2}{c} \quad (2.4)$$

The responses results related to factors and the levels selections were based on results obtained in experiment using the statistical software MINITAB 18 It was employed to assess the analysis of variance in order to establish the importance of each term in the model equation and to estimate the best appropriate model in each situation.

2.3 Results and discussion

2.3.1 The relationship between proximate analysis results and heating value

The 20 biomass samples were analyzed the proximate analysis and fiber analysis as shown in Table 2.1. As the diverse resources, the features of the biomass samples showed diversity in the amount of volatile matter, fixed carbon, and ash, as well as the composition of the fibers. The product yield was considerably impacted by the fixed carbon and volatile matter, which were in the range of 8% to 28% and 50% to 79%, respectively. Meanwhile, ash content and moisture were less than 20%. High ash content could be observed in herbaceous plant (18.32 wt.% in rice straw, 17.01 wt.% in rice husk and aquatic plant contain around 16 wt.%). The lignin, cellulose and hemicellulose contents were shown in Table 2.1. High lignocellulose (lignin, hemicellulose, and cellulose) content mostly observed in wood resource and seed shell. The difference among biomass samples was greatly varied from low lignin content (less than 10 wt.%) in water plant to greater than 54 wt.% in palm kernel shell. While the contents of cellulose exhibited minor differences, the amounts of hemicellulose were largely similar to those of lignin (ranging from 20% to 45%). Water hyacinth had the least amount of lignin (7.84 wt.%), whereas palm kernel shell had the most (54.84 wt.%). Aquatic plants had the highest extractives content, which included sugar, fat, terpenoids, starch, and protein (46.64 wt.% in water hyacinth and 55.15 wt.% in water lettuce, respectively). According the complicate of relationship between the proximate analysis and product yield, the

proximate analysis would be formulated in term of high heating value (HHV) [42], using Eq. 2.5.

$$\text{HHV} = 0.3536\text{FC} + 0.1559\text{VM} - 0.0078\text{Ash} \text{ (MJ/kg)} \quad (2.5)$$

To characterize the energy content and decide how effectively to use these fuels, the high heating value (HHV) was derived based on the proximate analysis [42]. High ash-biomass would be associated with lower HHV than high fixed carbon and volatile matter. The proximate analysis data and product yield connection would be determined using the HHV.



Table 2.1

The completed composition analysis of 20 biomass samples

No.	Feedstock	Proximate analysis, wt.%				Fiber analysis, wt.%*				Total
		Moisture	Ash	Volatile matter	Fixed carbon	Lignin	α -Cellulose	Hemicellulose	Others**	
<i>Agricultural wastes</i>										
1	Rice straw	18.76	18.32	49.93	12.99	22.42 ± 0.05	24.10 ± 0.16	37.60 ± 0.12	15.89 ± 0.24	100 ± 0.02
2	Rice husk	3.40	17.01	61.37	18.22	28.75 ± 0.05	34.32 ± 0.02	34.21 ± 0.04	2.72 ± 0.02	100 ± 0.04
3	Maize stalk and leaves	7.39	7.24	67.69	17.68	14.52 ± 0.16	27.28 ± 0.08	37.64 ± 0.07	20.56 ± 0.29	100 ± 0.09
4	Corn cob	4.32	2.62	71.97	21.09	20.30 ± 0.14	31.62 ± 0.10	45.11 ± 0.05	2.97 ± 0.29	100 ± 0.04
5	Cassava trunk	3.66	3.21	67.59	25.53	24.12 ± 0.25	31.26 ± 0.04	34.12 ± 0.03	10.51 ± 0.26	100 ± 0.13
6	Palm empty fruit bunch	4.49	8.91	65.69	20.92	25.37 ± 0.48	37.31 ± 0.16	22.81 ± 0.20	14.51 ± 0.08	100 ± 0.27
7	Palm kernel shell	7.21	4.15	60.48	28.15	54.84 ± 0.01	7.24 ± 0.04	28.45 ± 0.30	9.46 ± 0.31	100 ± 0.16
8	Palm fiber	7.87	6.11	66.49	19.54	24.77 ± 0.06	31.73 ± 0.08	31.60 ± 0.07	11.90 ± 0.03	100 ± 0.04

Table 2.2

The completed composition analysis of 20 biomass samples (*cont.*)

No.	Feedstock	Proximate analysis, wt.%				Fiber analysis, wt.%*				
		Moisture	Ash	Volatile matter	Fixed carbon	Lignin	α -Cellulose	Hemicellulose	Others**	Total
9	Durian peel	3.09	5.12	69.89	21.90	23.17 ± 0.49	34.83 ± 0.03	31.92 ± 1.07	10.08 ± 0.21	100 ± 0.81
10	Coconut shell	3.33	1.15	70.69	24.84	41.04 ± 0.33	18.82 ± 0.19	38.99 ± 0.17	1.15 ± 0.03	100 ± 0.18
11	Coconut coir	6.96	2.54	63.21	27.28	36.17 ± 0.01	31.39 ± 0.22	23.22 ± 0.14	9.21 ± 0.07	100 ± 0.04
12	Coconut fond	8.37	7.70	68.36	15.57	18.40 ± 0.02	33.31 ± 0.10	32.33 ± 0.20	15.96 ± 0.04	100 ± 0.07
<i>Aquatic plants</i>										
13	Water lettuce	17.01	16.95	58.18	7.87	9.59 ± 0.21	15.93 ± 0.28	19.32 ± 0.30	55.15 ± 0.02	100 ± 0.07
14	Water hyacinth	15.32	16.31	53.38	14.98	7.84 ± 0.02	24.67 ± 0.11	20.85 ± 0.05	46.64 ± 0.03	100 ± 0.06
<i>Wood based biomass</i>										
15	Wood sawdust	0.91	4.62	79.04	15.43	26.14 ± 0.60	40.48 ± 0.12	25.64 ± 0.26	7.74 ± 0.22	100 ± 0.52

Table 2.3

The completed composition analysis of 20 biomass samples (*cont.*)

No.	Feedstock	Proximate analysis, wt.%				Fiber analysis, wt.%*				
		Moisture	Ash	Volatile matter	Fixed carbon	Lignin	α -Cellulose	Hemicellulose	Others**	Total
16	Eucalyptus sawdust	13.68	2.15	64.94	19.23	22.17 \pm 0.11	35.02 \pm 0.07	28.34 \pm 0.16	14.47 \pm 0.11	100 \pm 0.10
	<i>Energy crops</i>									
17	Napier grass	8.84	6.87	68.91	15.39	20.93 \pm 0.06	27.32 \pm 0.03	35.78 \pm 0.29	15.96 \pm 0.29	100 \pm 0.23
18	Bamboo	3.89	5.69	70.94	19.48	28.77 \pm 0.01	38.71 \pm 0.77	23.52 \pm 0.29	9.01 \pm 0.13	100 \pm 0.24
19	Sugarcane bagasse	6.52	1.67	73.01	18.80	12.76 \pm 0.11	32.43 \pm 0.33	29.09 \pm 0.39	25.72 \pm 0.14	100 \pm 0.06
20	Sugarcane leaves	9.58	15.92	60.10	14.40	15.03 \pm 0.08	28.96 \pm 0.31	32.77 \pm 0.20	23.24 \pm 0.05	100 \pm 0.09

*wt.% based on dry and ash-free basis

**Others include sugar, fats, phenol, terpenoids, protein, or starch

2.3.2 Effect of reaction temperature on distribution of pyrolysis product

The pyrolysis of lignocellulose mainly produced three different products including biochar, bio-oil, and non-condensable gases. There were numerous factors affected on product yield and chemical composition of bio-oil such as particle size, residence time and reaction temperature [20]. In this study, the particle size of biomass (0.2-2 mm) and short residence time (5 seconds) were controlled due to their optimum conditions for good heat transfer and typically to achieve maximum bio-oil yields [43]. Meanwhile, reaction temperature would be varied within the range of 450 °C to 600 °C. The pyrolysis temperature and proximate analysis data of biomasses in term of HHV were investigated the effects on product yields. Figure 2.5 presents the effect of pyrolysis temperature on product yield.

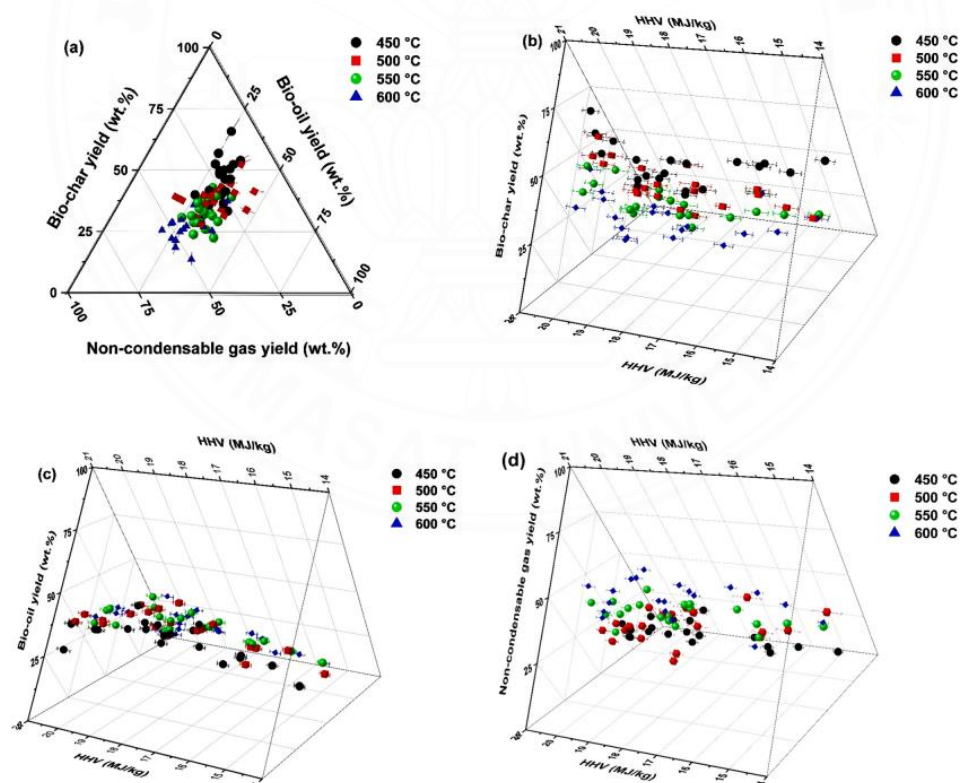


Figure 2.5 Pyrolysis product of 20 biomass with different pyrolysis temperature [44].

The biochar yield significantly decreased when the pyrolysis temperature was increased from 450 °C to 600 °C (Figure 5(a)).

Pyrolysis products (biochar, liquid and gaseous) obtained through complicated process via thermochemical conversion at different temperature, which described below:

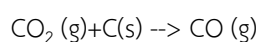
Step 1: Raw biomass → moisture + unreactive residues

Step 2: Unreactive residues → (volatile + gas) + primary biochar

Step 3: Primary biochar → (volatile + gas) + secondary biochar

The biochar was derived by thermal decomposition of biomass corresponding to temperature undergo the step one to step three. Moisture is lost at low temperatures, and the second stage results in the synthesis of primary biochar. Repolymerization of reactive intermediates cracked at moderate and high temperatures regulated the secondary biochar as well as volatiles and gases, therefore, the concentration of reactive intermediates played the important factor on biochar yield.

As the amount of bio-char decline corresponding to the increasing output of bio-oil, and the amount of non-condensable gas would tend to rise as the pyrolysis temperature increased because of the cracking process. The step three entails decomposition of primary biochar to produce carbon-rich solid residue usually undergo at high temperature. In addition, a primary product at a high pyrolysis temperature of 600 °C would be the non-condensable gas. This outcome was consistent with the subsequent Boudouard reaction, in which solid biochar was subjected to a high reaction temperature and the biochar was transformed into carbon monoxide.



From this study, the pyrolysis temperature played the important effect on product yield. Three simultaneous processes, including the Boudouard reaction, repolymerization, and cracking reaction, which were all highly influenced by the pyrolysis temperature, could be used to characterize the reaction pathway.

The product yield was impacted by the proximate analytical parameters of fixed carbon, volatile matter, and ash, but there were also some interactions between them. Consequently, the link between fixed carbon, volatile matter, and ash was represented by the HHV. The HHV would be used as representative to study the effect of proximate analysis data of biomass on product yield. From equation 1, the HHV was mostly depended on fixed carbon and inverse with ash content. In addition, the volatile matter also played the positive effect on HHV. The high bio-oil yield was obtained from the biomass containing HHV range from 18 MJ/kg to 20 MJ/kg which were affected by volatile matter. Meanwhile, the HHV over than 20 MJ/kg trended to large bio-char yield as shown in Figure 2.5 (b) and (c). The non-condensable gas was not affected by HHV as shown in Figure 2.5 (d). The bio-oil was mainly derived from volatile matter fraction which this fraction could be decomposed to small molecules in bio-oil liquid and non-condensable gas. Whereas fixed carbon content strongly affected biochar yield. The yield of non-condensable gas, on the other hand, was unaffected by the results of the proximate analysis since the non-condensable gas was produced by the Boudouard reaction, which was influenced by reaction temperature.

2.3.3 Effect of lignin and hemicellulose on pyrolysis oil composition

To create high-quality gasoline and petrochemical fuel, the single ring bio-aromatic was a valuable resource. The chemical routes toward aromatic compounds required to be studied since the single aromatic may be extracted from bio-oil. The composition of biomass especially hemicellulose and lignin content played the important factor for the aromatic rich bio-oil [40, 45]. The experimental data was statistically processed mathematical equation to represent the relationship between biomass composition including lignin and hemicellulose and the composition of bio-oil including the percentages of phenol, alkylphenol, hydrocarbon and aromatic hydrocarbon with different pyrolysis temperatures as shown in equations (7)-(22) in Table 2.3. Analysis of Variance (ANOVA) was presented in Table 2.2

Table 2.4

ANOVA table for the model and the model term

Source	Degree of freedom	Sum square	Mean square	F-value	P-value
Distribution of phenolics					
Model	14	14056.00	1004.00	5.14	0.000000
A	1	1727.50	1727.52	8.84	0.004000
B	1	456.10	456.10	2.33	0.131000
C	3	1510.20	503.39	2.58	0.061000
A ²	1	4556.20	4556.23	23.31	0.000000
B ²	1	199.80	199.77	1.02	0.316000
AB	1	12.70	12.65	0.06	0.800000
AC	3	2488.30	829.43	4.24	0.008000
BC	3	692.60	230.86	1.18	0.324000
Error	65	12705.10	195.46		
Distribution of alkyl phenolics					
Model	14	13755.40	982.53	3.27	0.001000
A	1	3025.00	3025.04	10.06	0.002000
B	1	1113.60	1113.56	3.70	0.059000
C	3	1291.30	430.42	1.43	0.242000
A ²	1	1752.20	1752.22	5.83	0.019000
B ²	1	2.50	2.52	0.01	0.927000
AB	1	690.60	690.61	2.30	0.134000
AC	3	2131.90	710.62	2.36	0.079000
BC	3	922.00	307.32	1.02	0.389000
Error	65	19543.60	300.67		

Table 2.5ANOVA table for the model and the model term (*cont.*)

Source	Degree of freedom	Sum square	Mean square	F-value	P-value
Distribution of hydrocarbons					
Model	14	8037.50	574.11	5.01	0.000000
A	1	0.30	0.26	0.00	0.962000
B	1	141.80	141.84	1.24	0.270000
C	3	5305.80	1768.61	15.44	0.000000
A ²	1	879.10	879.08	7.68	0.007000
B ²	1	77.60	77.61	0.68	0.413000
AB	1	6.80	6.76	0.06	0.809000
AC	3	359.50	119.82	1.05	0.378000
BC	3	24.00	7.99	0.07	0.976000
Error	65	7444.80	114.54		
Distribution of aromatic hydrocarbons					
Model	14	9896.70	706.91	7.46	0.000000
A	1	87.90	87.89	0.93	0.339000
B	1	111.80	111.79	1.18	0.281000
C	3	5721.40	1907.15	20.13	0.000000
A ²	1	810.30	810.31	8.55	0.005000
B ²	1	339.30	339.26	3.58	0.063000
AB	1	41.60	41.59	0.44	0.510000
AC	3	125.50	41.83	0.44	0.724000
BC	3	85.00	28.35	0.30	0.826000
Error	65	6158.90	94.75		

A: Lignin (wt.%)

B: Hemicellulose (wt.%)

C: Pyrolysis temperature (°C)

Table 2.6

The response of target compounds at different pyrolysis temperatures

Temp (°C)	Equations
Responds phenolics with each temperature	
450	Phenolics = $36.2 + 4.126*A - 2.50*B - 0.04777*AA + 0.0330*BB + 0.0068*AB$ (7)
500	Phenolics = $32.5 + 3.348*A - 1.85*B - 0.04777*AA + 0.0330*BB + 0.0068*AB$ (8)
550	Phenolics = $31.1 + 2.868*A - 1.25*B - 0.04777*AA + 0.0330*BB + 0.0068*AB$ (9)
600	Phenolics = $35.3 + 2.818*A - 1.65*B - 0.04777*AA + 0.0330*BB + 0.0068*AB$ (10)
Responds alkyl phenolics with each temperature	
450	Alkyl phenolics = $31.4 + 1.65*A - 1.70*B - 0.0296*AA + 0.0037*BB + 0.0501*AB$ (11)
500	Alkyl phenolics = $39.2 + 1.08*A - 1.21*B - 0.0296*AA + 0.0037*BB + 0.0501*AB$ (12)
550	Alkyl phenolics = $36.3 + 0.51*A - 0.32*B - 0.0296*AA + 0.0037*BB + 0.0501*AB$ (13)
600	Alkyl phenolics = $45.9 + 0.45*A - 0.73*B - 0.0296*AA + 0.0037*BB + 0.0501*AB$ (14)
Responds hydrocarbons with each temperature	
450	Hydrocarbons = $11.0 - 1.448*A + 1.31*B + 0.02098*AA - 0.0206*BB - 0.0050*AB$ (15)
500	Hydrocarbons = $12.3 - 1.247*A + 1.22*B + 0.02098*AA - 0.0206*BB - 0.0050*AB$ (16)
550	Hydrocarbons = $15.0 - 1.001*A + 1.08*B + 0.02098*AA - 0.0206*BB - 0.0050*AB$ (17)
600	Hydrocarbons = $27.2 - 0.951*A + 1.15*B + 0.02098*AA - 0.0206*BB - 0.0050*AB$ (18)
Responds aromatic hydrocarbons with each temperature	
450	Aromatic hydrocarbons = $-34.3 - 0.927*A + 3.09*B + 0.02015*AA - 0.0430*BB - 0.0123*AB$ (19)
500	Aromatic hydrocarbons = $-32.4 - 0.754*A + 2.99*B + 0.02015*AA - 0.0430*BB - 0.0123*AB$ (20)
550	Aromatic hydrocarbons = $-21.2 - 0.595*A + 2.68*B + 0.02015*AA - 0.0430*BB - 0.0123*AB$ (21)
600	Aromatic hydrocarbons = $-4.4 - 0.727*A + 2.82*B + 0.02015*AA - 0.0430*BB - 0.0123*AB$ (22)

A: Lignin (wt.%), B: Hemicellulose (wt.%) in biomass (dry basis)

The response surface was built using these equations. The impact of lignin on bio-oil composition at various pyrolysis temperatures is shown in Figure 2.6. At pyrolysis temperatures lower than 480 °C, the substantial lignin fraction produced high phenol content (> 70%) and alkyl-phenol content (> 40%) (Figure 6(a) and (b)). Thermal fragmentation of the alkoxy phenolic macromolecule lignin resulted in the formation of single-ring phenolic and alkyl phenolic chemicals, whereas the low hydrocarbon content especially aromatic hydrocarbon was obtained. On the other

hand, the hydrocarbon and aromatic hydrocarbon become significant products at the temperature higher than 550 °C and derived from biomass containing large lignin fraction (> 50%) as shown in Figure 2.6 (c) and (d). Figure 2.7 illustrates how the composition of bio-oil was also impacted by the hemicellulose concentration.

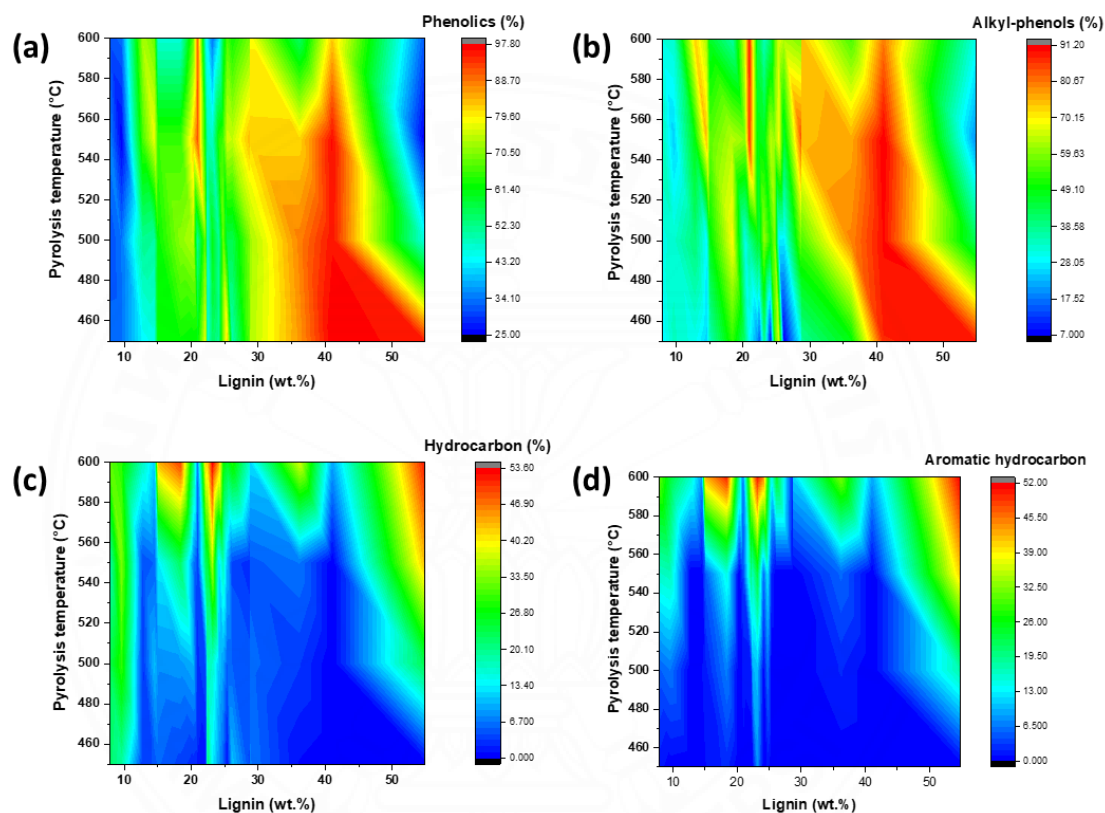


Figure 2.6 Effect of lignin and temperature on distribution of phenolic, alkyl phenolic, hydrocarbon and aromatic hydrocarbon in organic oil [44].

Although the considerable portion of hemicellulose tended to enhance phenolic and alkylphenol compounds, the composition of the bio-oil was unaffected by the pyrolysis temperature. According to the findings, phenolic compounds were the only reactions that the hemicellulose underwent before reacting with hydrocarbon and aromatic hydrocarbon. Figure 2.8 illustrates the impact of the biomass content and the lignin to hemicellulose ratio on the composition of bio-oil.

The phenolic and alkylphenol were the highest yield at all pyrolysis temperatures and the ratio of 1.1 while the hydrocarbon and aromatic hydrocarbon was trace amount.

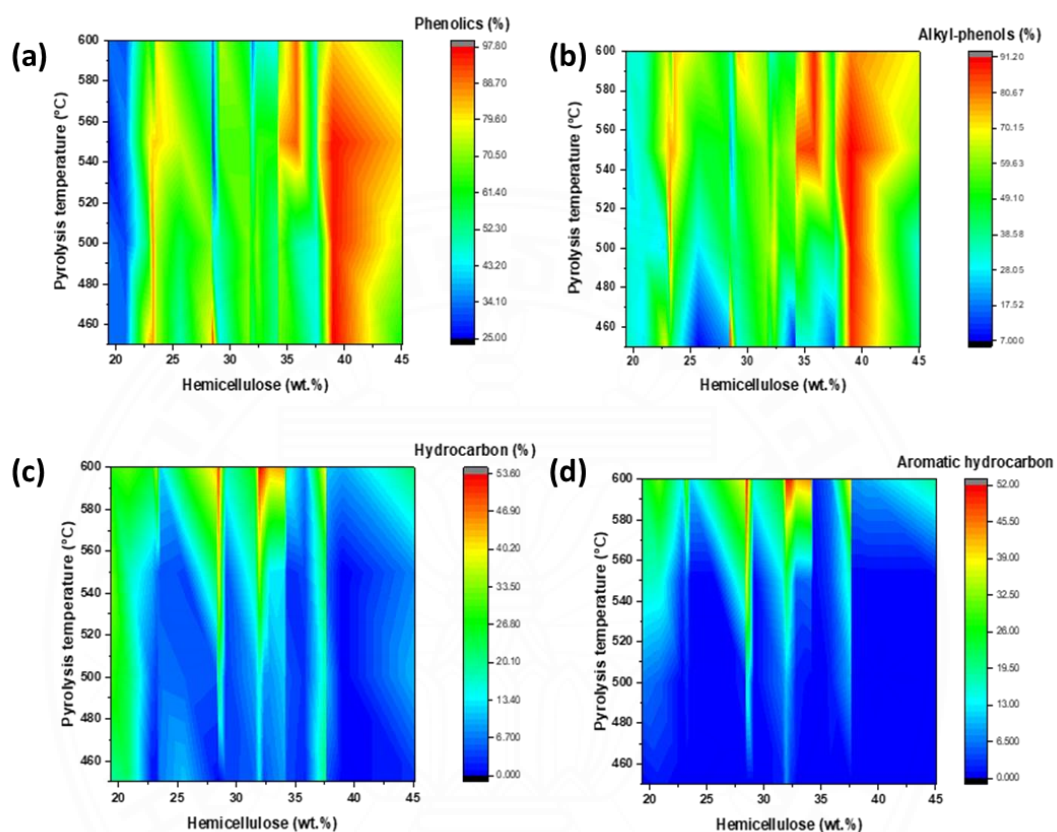


Figure 2.7 Effect of hemicellulose and temperature on distribution of phenolic, alkyl phenolic, hydrocarbon and aromatic hydrocarbon in organic oil [44].

Hemicellulose and lignin interacted to prevent the conversion of phenolic chemicals to hydrocarbons. Meanwhile, low lignin concentration detected the synthesis of hydrocarbon and aromatic at high pyrolysis temperatures. Therefore, the lignin was synergized by hemicellulose for further reaction of hydrocarbon formation. A Pareto chart showing the effect of experimental factors at an 80% confidence level was confirmed (Figure 2.9). The lignin content, pyrolysis temperature, and hemicellulose content were the main effects on phenolic formation. The interaction between lignin content and pyrolysis temperature strongly affected the

phenolic content. Therefore, the phenolic content would not only depend on lignin content, but the pyrolysis temperature was also considered. Meanwhile, the alkylphenol content was affected by lignin and hemicellulose contents on the other hand, the pyrolysis temperature did not significant affect.

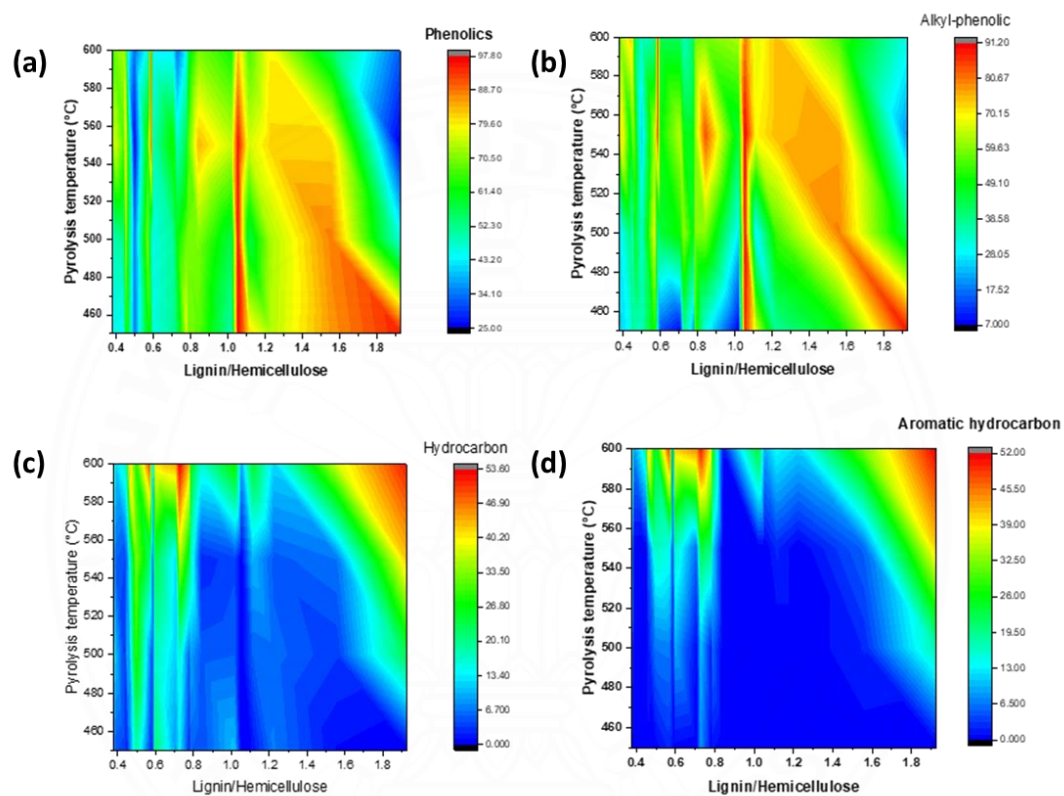


Figure 2.8 Effect of lignin and hemicellulose (wt./wt.) ratio of biomass on distribution of phenolic, alkyl phenolic, hydrocarbon and aromatic hydrocarbon in organic oil [44].

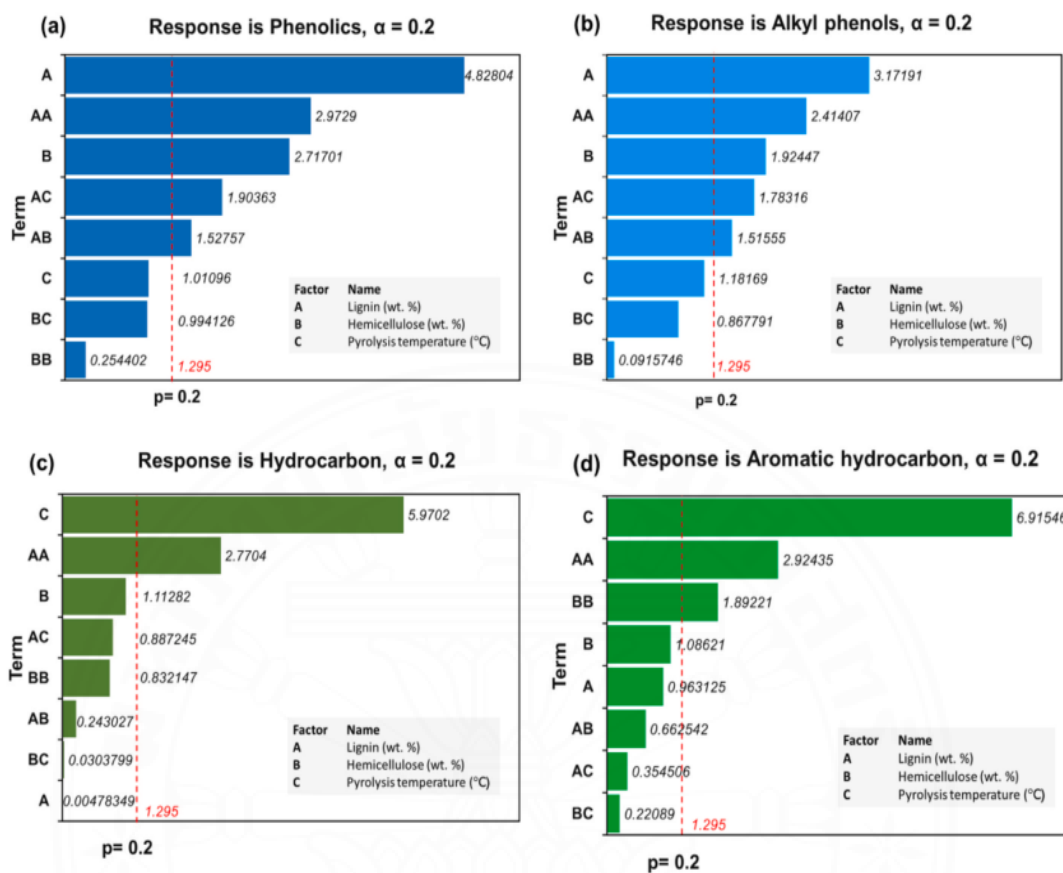


Figure 2.9 Pareto diagrams present the significant effects to produce of (a) phenolic compounds; (b) alkyl phenol compounds; (c) hydrocarbon compounds; and (d) aromatic hydrocarbon compounds (validated at an 80% confidence level) [44]

Alkylphenol content was not only affected by the interaction between lignin content and pyrolysis temperature but the interaction between lignin and hemicellulose also played the influence. This result supported the high content of alkylphenol at the ratio of 1.1 due to the different pathways of phenolic formation between lignin and hemicellulose. The lignin fragmentation and aromatization of furan-based intermediates from the breakdown of hemicellulose were the sources of the phenolic chemicals. The intermediates of both reactions inhibited further deoxygenation. In the case of hydrocarbon and aromatic hydrocarbon, pyrolysis

temperature was a main effect however, hydrocarbon and aromatic hydrocarbon were depended on phenol contents.

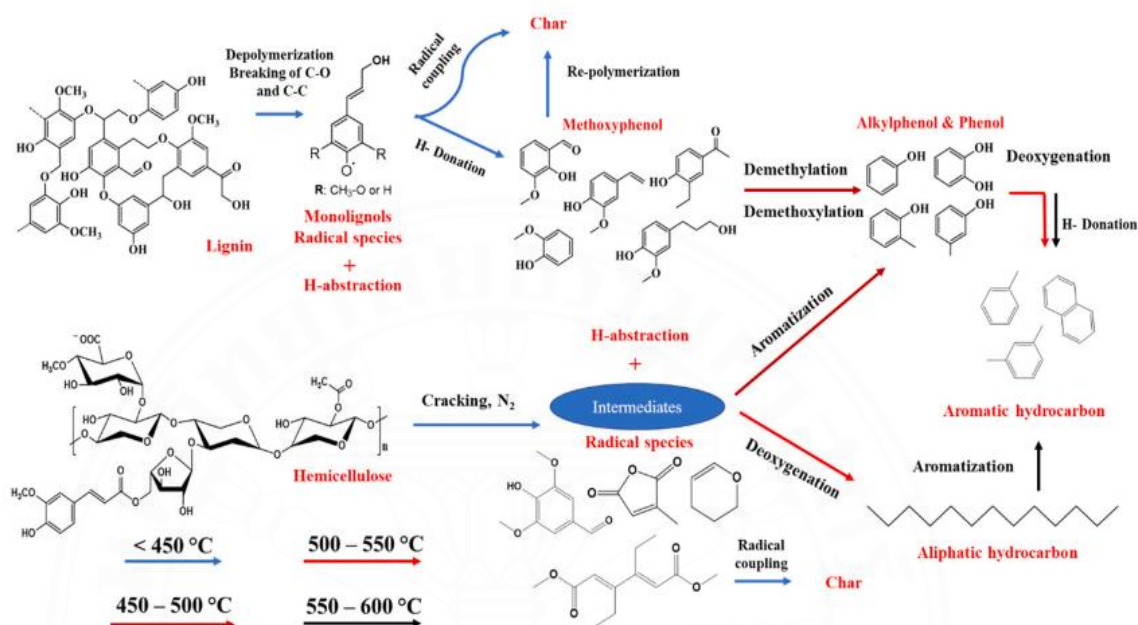


Figure 2.10 Propose pyrolysis pathways of lignin and hemicellulose to produce phenolic, alkyl phenol, hydrocarbon, and aromatic hydrocarbon compounds [44].

Figure 2.10 illustrates the proposed biomass pyrolysis reaction routes toward phenolic chemicals and aromatic hydrocarbons. Lignin's C-C and C-O bonds were thermally broken down, forming the intermediate alkoxyphenol. When reached to a high temperature, the alkoxyphenol was going to undergo demethoxylation and demethylation, forming phenolic and alkylphenol molecules. Meanwhile, the hemicellulose was cracked to furan compounds which could undergo to two different temperature dependent pathways. Furan compounds were aromatized to generate phenolic compounds at pyrolysis temperatures below $500\text{ }^\circ\text{C}$, whereas furan compounds were decomposed to tiny alkene and then further oligomerized and aromatized to paraffinic hydrocarbon and aromatic hydrocarbon, respectively.

CHAPTER 3

STUDY OF NICKEL PHOSPHIDE BASED-CARBONEOUS CATALYSTS ON HYDRODEOXYGENATION OF PALM KERNEL SHELL PYROLYSIS VAPOR

3.1 Background

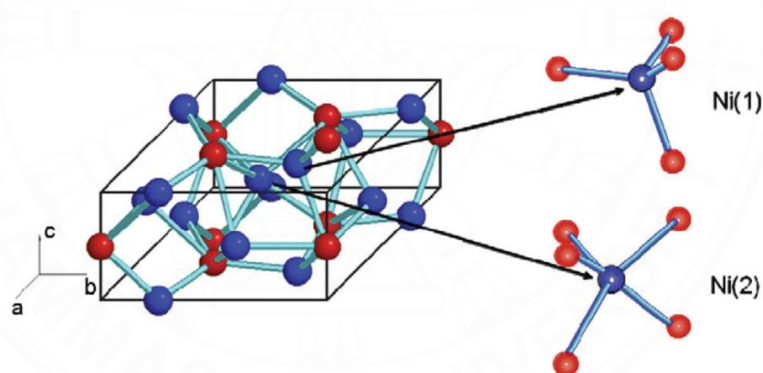
Biofuel from fast pyrolysis of biomass is attracting consideration of sustainable and green energy due to vital links with the replacement fossil fuel and abundance resources. However, the quality bio-oil is limited by its high oxygenated compounds, which can be extremely harmful to low stability, high viscosity, and poor calorific value of fuel. To date, researchers have noted that the upgrading bio-oil with eliminating oxygen via deoxygenation is essential to gain the high-quality fuel [46].

Studies over the past two decades have provided the important deoxygenation under hydrotreatment method, that can deal with a large and tenacious oxygenated compounds in bio-oil such ketones, acids, phenols, and furans to obtain hydrocarbon containing same carbon number with bio-oil and water as byproduct via hydrodeoxygenation (HDO) [47]. Relatively research carried out on heterogeneous catalysts, the noble metals (Pt, Pd) supported on the acidic support like alumina, or a high-surface-area carrier (carbon-based support) achieved the excellent deoxygenation performance [48]. However, the high-cost precious metal and coking were affected by acid-support. Therefore, the current research has been attentive published on low-cost material and development anti-coke catalyst, but still significantly succeed in HDO performance.

The noble metal performed excellent catalyst deoxygenation. The trend of these ability metallic active site follows: Pd > Pt > Ni > Rh > Ir > Ru > Os [49]. So that, the non-noble metal such Ni-based catalysts could be a candidate for HDO catalyst due to low cost and high hydrogenolysis- metallic active site. Transition metal phosphides, especially nickel phosphide, have recently been shown to have excellent activity not only in hydrodesulfurization (HDS), and hydrodenitrogenation (HDN), but also hydrodeoxygenation (HDO) [50]. The metal phosphide was bifunctional catalyst

including acidic and metallic properties like noble metals supported on acidic support has been attracted due to its cheap and presence good HDO performance. The main active phases for nickel phosphide during HDO are $\text{Ni}^{\delta+}$ and Brønsted sites [10, 51, 52]. $\text{Ni}^{\delta+}$ acted as Lewis acid sites and embarked in hydrogenation, hydrogenolysis and demethylation reactions. Brønsted sites (PO-H) donated active hydrogen species, but they was less active than metal sites due to incomplete reduction of phosphate species. The trend catalytic HDO performance presented following: $\text{Ni}_2\text{P}/\text{ZrO}_2 < \text{Ni}_2\text{P}/\text{Al}_2\text{O}_3 < \text{Ni}_2\text{P}/\text{SiO}_2$ was reported by Shin-Kuan Wu and his co-operators [53] for HDO of Guaiacol.

Moreover, the conversion of oxygenated compounds over Ni_2P catalyst is also influenced by Ni-P surface sites in crystal structure and electron density and ligand effect for DO activity and selectivity [54, 55]. The unit cell of Ni_2P consists of two types of Ni sites



Scheme 3.1 Presentation of Ni crystals of tetrahedron Ni(1) and pyramid Ni(2) phases in Ni_2P unit cell [56]

A Ni(1) site with four P atoms next to it in a nearly tetragonal structure and a Ni(2) site with five P atoms next to it in a square pyramidal arrangement [56]. The bulk structure of Ni_2P has an equal amount of Ni(1) sites and Ni(2) sites. However, it was discovered that Ni(2) sites existed at the surface of Ni_2P , and the fraction of these sites grew as the size of the Ni_2P particles shrank (a greater proportion of Ni(2) sites

with a larger surface area) [56]. It was also suggested that the Ni(2) site was mostly in charge of HDO activity, whilst the Ni(1) site was in charge of DCO via activation of the $C_{\text{carbonyl}}-C_{\text{alkyl}}$ bond [55]. Therefore, by adjusting the particle size, it would be able to adjust the HDO performance of Ni₂P catalysts. In the deoxygenation of 4-methylphenol, smaller Ni₂P particles favored the HDO pathway for the synthesis of methylcyclohexane whereas bigger Ni₂P particles prefer the DDO pathway for the production of toluene [57]. After examining the intrinsic electronic characteristics of Ni₂P, Liu et al. hypothesized that the structure's Ni significant HDS activity affected from a weak ligand effect from the Ni-P bonds, which only slightly stabilized Ni 3d levels and resulted in a tiny electrostatic interaction from Ni to P [58]. Ni sites suddenly contain just little positive electrical charge (i.e., Ni^{δ+}), as a result of the charge transfer from Ni to P, creating Lewis acid site. For additional metal phosphides, a similar Lewis acid site was discovered. High catalytic activity in Ni₂P was thought to be caused by its greater d-electron density compared to MoP and Ni_xMo_yP, however Lewis acid concentration changes with the electronic configuration of metals and their binding to P [54].

In the other researches, the co-ordination of N-function and metal have received widespread attention in deoxygenation due to N dopants to improve the electronic interaction between metal and carbon support [17, 19–22]. Li *et al.* [18] prepared a N-functionalized mesoporous carbon-supported, which formed pyridinic-N, pyrrolic-N, quaternary-N, pyridinic-N-oxide, graphitic-N can be synergetic with highly dispersed Pd nanoparticle assisted on hydrogenation of phenol, with 80% conversion of phenol and 100% selectivity to cyclohexanone. Similarly, Hu *et al.* [23] fused phenanthroline sulfonate and activated carbon in the presence of N₂, results in the formation of a Ru–Ni bimetallic catalyst supported by N–doped carbon (Ru–Ni–AC/N). The yield of aromatics reached 57% when the hydrogenolysis of guaiacol was conducted using the 1%Ru5%Ni-AC/N catalyst. Even though N-doped carbon functionalized shown improved performance for a range of processes, applications of this kind of catalyst in the conversion of lignin are rare, particularly as Ni₂P is involved.

The hypothesis is supported by a comparative study using with and without N-doping activated carbon to examine the crystal size of Ni₂P. Our previous study, we applied catalytic upgrading napier grass pyrolysis vapor using Ni₂P/C catalyst, and found out the Ni₂P even presented the great HDO performance however, large particle size was significantly affected deoxygenation performance [59, 60].

The aim of this research is critically examining the claim that effect of coordination C-N with Ni in N-doping activated carbon and pure activated carbon on formation of Ni₂P particle (reduction from nickel phosphate) and qualified in upgrading fast pyrolysis of rich- lignin biomass (palm kernel shell) under atmospheric in integrated two fixed bed reactors. The desirable target catalyst is high performance in oxygen removal and obtained high selectivity of valuable chemical in liquid product.

3.2 Material and method

3.2.1 Preparation of Ni₂P support on based- carbon

3.2.1.1 Preparation of N-doping activated carbon

The marketable grade activated charcoal (AC), from Xilong Scientific Co., Ltd, China, served as raw support material with a carbon basis material. The AC was first pretreated with hot solution nitric acid (5M) for 4 h and washed thereafter with distilled water until neutralization to remove the impurity and oven-dried at 105 °C overnight. The as-pretreated carbon was combined with a hot solution of melamine (HIMEDIA, India) to add N-containing groups to the structure of the carbon with investigated weight ratio of melamine to AC and stirred at 90 °C for 5 h. The resulting suspension was heated to 120 °C for drying after boiling to remove the water. The impregnated carbon was then loaded into ceramic boats, positioned in the middle of an electric furnace quartz tube, and calcined for two hours at 900 °C (5 °C min⁻¹) with a low rate of 100 ml min⁻¹.

3.2.1.2 Preparation of Ni₂P/C and Ni₂P/CN_x catalysts

The Ni₂P catalyst support on pure activated carbon and N-doping activated carbon samples named Ni₂P/C and Ni₂P/CN_x, (x = 25 wt.%-100 wt.%)

of melamine in activated carbon) respectively, were prepared by temperature program reduction (TPR). First, 1 g of support was wet-impregnated with a mixed solution of $(\text{NH}_4)_2\text{HPO}_4$ and $\text{Ni}(\text{NO}_3)_2$ at Ni/P molar ratio of 1.5 and Ni loading levels 5.37 mmol g^{-1} support. The samples were then aged for 12 h at ambient temperature, vacuum dried at $110 \text{ }^\circ\text{C}$ for 12 h. After that, the catalyst precursors were calcinated under nitrogen atmosphere at temperature of $600 \text{ }^\circ\text{C}$ for 1h and subsequently switched to hydrogen atmosphere at the same temperature. The as-reduced catalyst was finally cooled to the required reaction temperature or to room temperature under nitrogen gas for further catalyst characterization.

3.2.1.3 Characterization of $\text{Ni}_2\text{P/C}$ and $\text{Ni}_2\text{P/CN}_x$ catalyst samples

The crystal phases of $\text{Ni}_2\text{P/C}$ and $\text{Ni}_2\text{P/CN}_x$ ($x = 25, 50, 75, 100$) catalysts were examined by X-ray powder diffraction (XRD; D8 ADVANCE, Bruker) in the 2θ range of 5° – 80° using Cu $K\alpha$ radiation ($\lambda = 0.154 \text{ nm}$), operating at 40 kV and 40 mA with a scan speed of 0.1 s step^{-1} . The crystallite sizes were calculated using Scherrer's equation. The reducibility of each catalyst sample was investigated by Hydrogen temperature-programmed reduction (H_2 -TPR), which was performed in a quartz reactor by loading 0.05 g of the test catalyst in the presence of 10% (v/v) H_2 in Argon at a flow rate of 30 ml min^{-1} and heating the sample from 100 to $900 \text{ }^\circ\text{C}$ at $10 \text{ }^\circ\text{C min}^{-1}$. The amount of H_2 consumption was determined using a thermal conductivity detector. The acidic properties were characterized using ammonia (NH_3)-temperature programmed desorption (TPD), which was recorded by the thermal conductivity sensor of the gas chromatograph (GOW MAC 69-350, USA) system. The number of acid sites corresponded to the amount of desorbed NH_3 over temperatures of 100 – $600 \text{ }^\circ\text{C}$. The catalyst textural was characterized by nitrogen (N_2) sorption measurement at $-196 \text{ }^\circ\text{C}$ using autosorb-iQ-C analyzer (Quantachrome, USA) instrument. The specific surface areas and pore diameter were analyzed by the Brunauer-Emmett-Teller (BET) combined with t- plot, and Barrett-Joyner-Halenda (BJH) methods, respectively. The morphology of both catalysts was investigated by transmission (TEM) electron microscopy (JEM-2010, JEOL Ltd., Japan) at an accelerating voltage of 200 kV. The surface chemical composition was analyzed by X-ray photoelectron spectroscopy

(XPS) performed by an ULVAC-PHI, PHI 5000 VersaProbe II (Physical Electronics USA) system using Al K α radiation.

3.2.2 Catalytic integrated deoxygenation of Palm kernel shell

Biomass used as the feedstock for pyrolysis was palm kernel shell, which was by-product in palm oil industrial obtained from local community. First, palm kernel shell was washed several times with distill water to remove the impurities, milled and sieved within the range of 0.2 – 2.0 mm, dried at 105 °C for 24 h, and stored in a desiccator. The lignocellulosic content of biomass was determined based on our previous work with lignin content of 54.84 wt.%, hemicellulose content of 28.45 wt.%, and cellulose content of 7.24 wt.%. In a typical run, the calculated biomass and catalyst were separately packed with quartz wool into the two different fixed bed reactors. Prior to the run reaction, the reactor was purged with N₂ gas at 50 ml min⁻¹ for 20 min to remove air. Next, a nitrogen- calcination and then hydrogen-reduction of precursor to form nickel phosphide catalyst was performed at the second reactor with flow rate of 100 ml min⁻¹, 600 °C for 2 h. The temperature of the second reactor was cooled to target upgrading temperature, while the temperature of pyrolysis zone heated fixed at 550 °C. After reach terminated temperatures, biomass from biomass hoper was crewed and dropped following the hydrogen carrier gas. The residence time of the process was 5 seconds, while the operation pressure was 1 atm. The detected bio-oil main components in this study were the light bio-oil compounds was collected in acetone-ice cool trap condensers. The bio- oil produced in no-catalyst and catalytic upgrading was water-free absorbed by sodium sulfate before identified by GC–MS (GC-Agilent 7890B, MS-Agilent 5973) equipped with an BD-5MS capillary column (0.25 mm ID, 30 m length, 0.25 mm film thickness) and using He at a flow rate of 1 ml min⁻¹ as the carrier gas. The oven temperature was programmed to remain at 50 °C for 3 min, ramp at 10 °C min⁻¹ to 280 °C, and stay at 280 °C for 5 min. The injector split ratio was set to 50:1 using methanol as solvent to dilute the samples. The chemical compositions of the oil phase were identified based on the NIST Mass Spectral Library and literature. The relative peak area of each compound was calculated by regulation with the total peak area in the GC–MS using Eq. (3.1):

$$C_i = \frac{A_i}{A_T} \times 100 \% \quad (3.1)$$

Where, C_i is the relative area of each compound i ; A_i symbolizes the peak area of compound i , and A_T represents the total peak area of all compounds present in the GC-MS data of the oil phase.

The oxygen removal rate was calculated based on the GC-MS results as follows:

$$\text{Oxygen removal} = \left[\frac{T_{\text{no-catalyst}} - T_{\text{catalytic upgrading oil}}}{T_{\text{no-catalyst}}} \right] \times 100 \% \quad (3.2)$$

where, $T_{\text{no-catalyst}}$ and $T_{\text{catalytic upgrading oil}}$ are the total oxygen relative-mole percentage in all the oxygenated compounds as determined by the GC-MS analyses of the pyrolysis oil and upgraded oil, respectively.

3.3 Results and discussion

3.3.1 Characterization of the catalysts

3.3.1.1 XRD results

To investigate the effect of the growth of nickel phosphide species on surface of activated carbon, the treated support with and without N-doping were performed. As shown in Figure 3.1, the N-doping had significant influences on the formation of Ni_2P species demonstrated by XRD patterns.

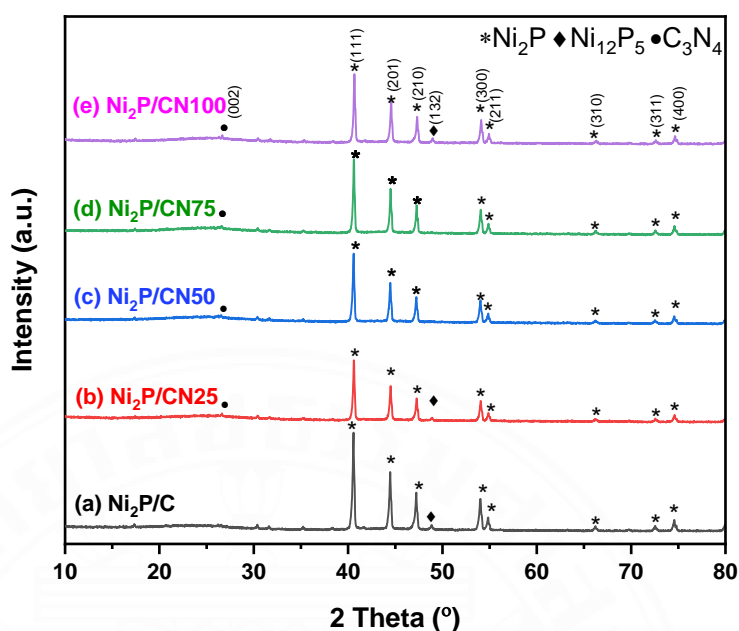


Figure 3.1 XRD pattern of $\text{Ni}_2\text{P}/\text{C}$ and $\text{Ni}_2\text{P}/\text{CN}_x$ samples

The strong diffraction peaks of 2θ values 40.7° , 44.6° , 47.4° , 54.2° , 54.5° , and 74.4° corresponding to (111), (201), (210), (300), (211), and (400) crystal planes, presented on both $\text{Ni}_2\text{P}/\text{C}$ and $\text{Ni}_2\text{P}/\text{CN}_x$ samples, respectively, indicate formation of the hexagonal crystal structure of Ni_2P crystals. Without N-doping, the dominant Ni_2P phase accompanied with Ni_{12}P_5 , which assigned at 2θ of 35.4° , 38.3° , 41.6° , and 48.9° corresponding to (002), (112), (231) and (312) crystal planes on $\text{Ni}_2\text{P}/\text{C}$ sample. On the contrary, presence of N-doping led to form weakening intensity of pure Ni_2P and almost disappearance of Ni_{12}P_5 phase in $\text{Ni}_2\text{P}/\text{CN}_x$ doping sample, while the crystallite size of Ni_2P decreased from 51.16 nm on $\text{Ni}_2\text{P}/\text{C}$ to 47.87 nm on $\text{Ni}_2\text{P}/\text{C}-\text{N}25$ samples (Table 3.1).

Moreover, the crystalline peak of g- C_3N_4 , which can be formed by thermal condensation of melamine below 600°C disappears at 2θ of 27.0° and 38.3° [61] agrees with the exfoliation of the graphite (turbostratic) like carbon nitrides after calcination [62]. However, all wide broaden peaks of Ni_2P with less intense in $\text{Ni}_2\text{P}/\text{CN}_x$ sample are observed, suggesting that its crystal structure can be annealed around and interleaved with the destroyed-multilayers of graphite carbon nitride,

which possessed an amorphous and stacked ordering degree of different C-N graphite layers.

3.3.1.2 TEM results

The morphology and microstructure of Ni_2P before and after nitrogen doping on activated carbon were investigated by scanning electron microscopy (TEM) as shown in Figure 3.2

The uniform black dots disperse on the carbon-based material are Ni_{12}P_5 particles, while the dark dots belong to Ni_2P particles. The simultaneous formation of Ni_2P and Ni_{12}P_5 nanoparticles were homogeneously dispersed on the pure-activated carbon, while Ni_2P interface nanosheet structures N-doping graphite carbon in CN_x samples. The uniform porous morphology of $\text{Ni}_2\text{P}/\text{CN}_x$ in Figure 3.2 (d, g, j, m) gives direct evidence that Ni_2P were doped in crumpled mono- or few-layer sheets of N-doping graphite carbon, rather than the formation of Ni_2P or Ni_{12}P_5 particles. Moreover, the smaller particle size of Ni_2P was determined in N-doping support in Figure 3.2 (b, e, h, k, n), implies a chemical interaction between Ni_2P - N-doping graphite assisted reducing particle size of metal than pure activated carbon. A close electronic coupling could be obtained at the interfaces of Ni and P with carbon nitride /graphene sheets promote decreasing mean size of Ni_2P from 28.91 nm to 10.85 nm correspond to $\text{Ni}_2\text{P}/\text{C}$ and $\text{Ni}_2\text{P}/\text{CN}_{25}$, respectively. The interact between Ni_2P and graphitic carbon was observed with interface is helpful to reducing particle of Ni_2P nanoparticles avoid aggregation Ni_2P and form Ni-rich like Ni_{12}P_5 during phosphidation of nickel phosphate precursors at high temperature [63] by the support of nitrogen atoms, which contain lone pairs of electrons could serve as sites for the nucleation of Ni_2P nanoparticles and stabilize the Ni_2P nanoparticles [64, 65]

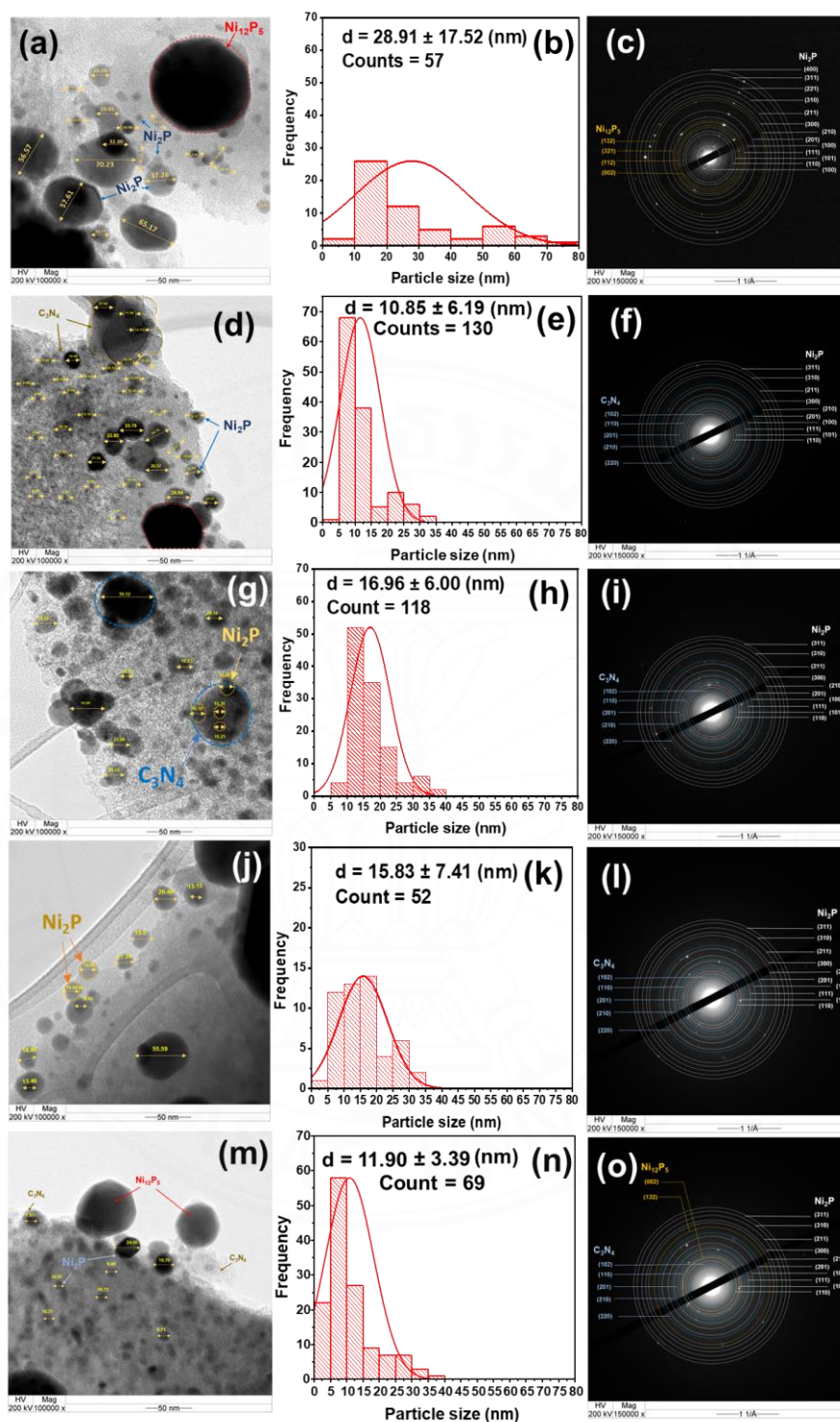


Figure 3.2 TEM images (a, d, g, j, m), partial distribution (b, e, h, k, n), and SAED (c, f, i, l, o) patterns of $\text{Ni}_2\text{P}/\text{C}$, $\text{Ni}_2\text{P}/\text{CN}_{25}$, $\text{Ni}_2\text{P}/\text{CN}_{50}$, $\text{Ni}_2\text{P}/\text{CN}_{75}$, and $\text{Ni}_2\text{P}/\text{CN}_{100}$ samples, respectively.

Table 3.1

Textual properties of samples

Sample	BET area (m ² .g ⁻¹)	t-Plot method micropore analysis			BJH method analysis		Ni ₂ P crystalline size (nm)*	Acidity (μmol NH ₃ m ⁻²)
		Micropore area (m ² .g ⁻¹)	External surface area (m ² .g ⁻¹)	Micropore volume (mL.g ⁻¹)	Pore volume (mL.g ⁻¹)	Pore diameter (nm)		
C	461.068	153.893	307.175	0.059	0.249	3.059	-	-
CN25	471.512	144.646	326.867	0.071	0.119	3.410	-	-
CN50	441.449	117.476	323.972	0.060	0.118	3.411	-	-
CN75	406.702	107.622	299.080	0.055	0.128	3.408	-	-
CN100	387.162	132.195	254.968	0.056	0.130	3.405	-	-
Ni ₂ P/C	440.360	102.260	338.101	0.050	0.137	3.415	51.16	1.428
Ni ₂ P/CN25	407.611	55.084	352.527	0.044	0.127	3.415	47.87	5.348
Ni ₂ P/CN50	397.275	106.779	290.496	0.051	0.123	3.057	49.03	5.462
Ni ₂ P/CN75	337.025	4.130	332.895	0.027	0.093	3.057	49.54	5.875
Ni ₂ P/CN100	247.634	0	247.634	0	0.129	3.420	51.24	10.459

*Calculation from XRD pattern

Table 3.2

Chemical properties of samples

Sample	Reducibility								Acidity				
	Reduction peak temperature (°C)								NH ₃ desorption peak temperature (°C)				
	Peak (I)	Peak (II)	Peak (III)	Peak (IV)	Peak (V)	Peak (VI)	Peak (VII)	Total	Weak acid (150-250 °C)	Medium acid (300-400 °C)	Strong acid (450-550 °C)	Total	
Ni ₂ P/C	%	7.37	50.85	33.95	7.83	0	0	-	100	4.32	46.60	49.08	100
	Value	17.421	120.195	80.248	18.508	0	0	-	236.372 ^a	0.027	0.293	0.309	0.629 ^b
Ni ₂ P/CN25	%	3.89	25.98	5.92	23.83	29.11	11.28	-	100	28.46	49.13	22.41	100
	Value	26.52	177.13	40.36	162.47	198.47	76.91	-	681.79 ^a	0.62	1.07	0.49	2.18 ^b
Ni ₂ P/CN50	%	1.90	28.30	8.74	23.90	23.52	12.44	-	100	17.89	58.19	23.92	100
	Value	10.31	153.22	47.31	129.39	127.33	67.35	-	541.46 ^a	0.39	1.26	0.52	2.17 ^b
Ni ₂ P/CN75	%	3.36	27.58	9.23	11.86	28.78	14.02	5.17	100	13.49	50.70	35.80	100
	Value	20.75	170.30	56.98	73.22	177.68	86.54	31.94	617.41 ^a	0.27	1.00	0.71	1.98 ^b
Ni ₂ P/CN100	%	3.03	24.83	14.29	17.61	22.46	11.52	6.26	100	8.37	64.04	27.59	100
	Value	19.84	162.77	93.67	115.47	147.23	75.49	41.05	655.51 ^a	0.22	1.66	0.71	2.59 ^b

^a $\mu\text{mol H}_2 \text{ g}^{-1}$

^b $\text{mmol NH}_3 \text{ g}^{-1}$

The selected area electron diffraction pattern (SEAD) of the Ni₂P/C in Figure 3.2c with polycrystalline materials show a ring pattern. The SAED pattern demonstrated in results of point-like spots in N-doping represents single crystalline nature of Ni₂P indicated good crystallinity for the metallic nanoparticles in Figure 3.2 (f, i, l, o). Furthermore, the crystalline diffraction rings located at the d-spacing values of 2.39, 2.061, 1.473, 1.286 and 1.207 Å, which are corresponded to (201), (210), (311), (320) and (002) lattice planes of amorphous graphite carbon nitride appearance. It is simultaneously supporting the XRD results the formation Ni₂P crystalline effected by N-doping.

3.3.1.3 Textual results

The texture characteristics and pore size distributions of N-doping carbon, nickel phosphide on carbon -based support calculated from nitrogen adsorption-desorption isotherms are presented in Table 3.1.

It is worth to mention that the external surface area of pure activated carbon (461.068 m² g⁻¹) is higher than N-doping samples (352.537 m² g⁻¹) and decreasing of micropore following with metal doping (from 440.360 to 247.634 m² g⁻¹) agreed that the C-N from melamine and metal were successful engaged supports. The exfoliation of multi-layered graphitic carbon nitride (g-C₃N₄) to obtained well-wrinkled mesoporous graphitic carbon with doped nitrogen atoms were formed after the pyrolysis at 900 °C. The pore volume and the pore diameter likely did not change. The textural parameters and TEM results evidence that the Ni₂P/CN_x samples containing narrow slit and parallel plate shape pores like hybrid.

3.3.1.4 H₂-TPR results

Even the crystalline of carbon nitride disappeared by XRD result, the presence of N-doping on activated carbon convinced by temperature-programmed reduction (TPR) shown in Figure 3.3 and Table 3.2.

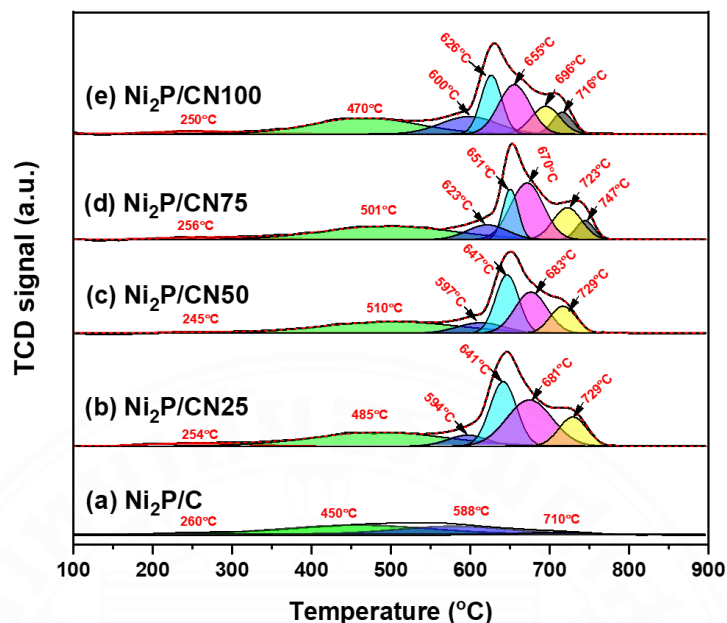


Figure 3.3 H₂-TPR patterns of samples

The reduction peaks were observed on the Ni₂P/C and Ni₂P/CN_x samples over the reduction temperature range of 250 to 727 °C. In the detail, the reduction peaks at 250, 450, 598 and 727 °C appeared on all samples and H₂ consumption of reduction peak on the Ni₂P/CN_x samples were the higher than Ni₂P/C (Table 2). The very small peak at 250 °C is due to the reduction of Ni²⁺ in NiO [11, 66]. The reduction peaks at 450 °C might assigns as reduction of Ni oxidized of Ni₂P in air, while reduction peaks at 588 °C is reduction of P-O bond in P-O-C=O group or P-O-H, which was bonded P (electron withdrawing group) with the -O-C=O or O-H group on activated carbon surface, respectively [66]. The high reduction peak at 727 °C may be belonged to the reduction of nickel polyphosphates [Ni₂P₄O₁₂, Ni₂P₂O₇, Ni(PO₃)₂] [66] and P-O bond during transformed nickel phosphate by passivation in air, respectively [63, 67]. Generally, a certain number of the oxygen atoms are shared between PO₄ groups in polyphosphates, and the reduction of polyphosphates were realized by breaking of P-O_{4-x} linkages in phosphate, which is more difficult as compared with the P-O-H linkages [68]. The low distribution of reduction peak of 727 °C and shifting lower reduction temperature also agrees with XRD results in complete reduction of PO₄

group to form nickel phosphide during hydrogen reduction. Interestingly, the major reduction peak at 641 °C, 675 °C and 727 °C still significantly appear in the Ni₂P/CN_x samples even its successful Ni₂P formation. As the literatures, the reduction peak at higher 700 °C belonged to decomposition of graphitic N-doping carbon [69]. In the result, appearance of the reduction peak at 641 °C and 675 °C and shift higher reduction temperature of Ni compounds (from 450 to 485 °C, and 588 to 598 °C), in the case of the modified-support catalysts is relevant by interaction between nickel-nitrogen bond and P with the modified carbon support [70, 71]. Evidence thus indicates that the magnitude of the interaction between the nickel phosphide component and support's nitrogen content in results in the growing of the reduction temperature.

3.3.1.5 NH₃-TPD results

Figure 3.4 shows the NH₃-TPD profiles of all catalysts, and the amounts of surface acids are listed in Table 3.2.

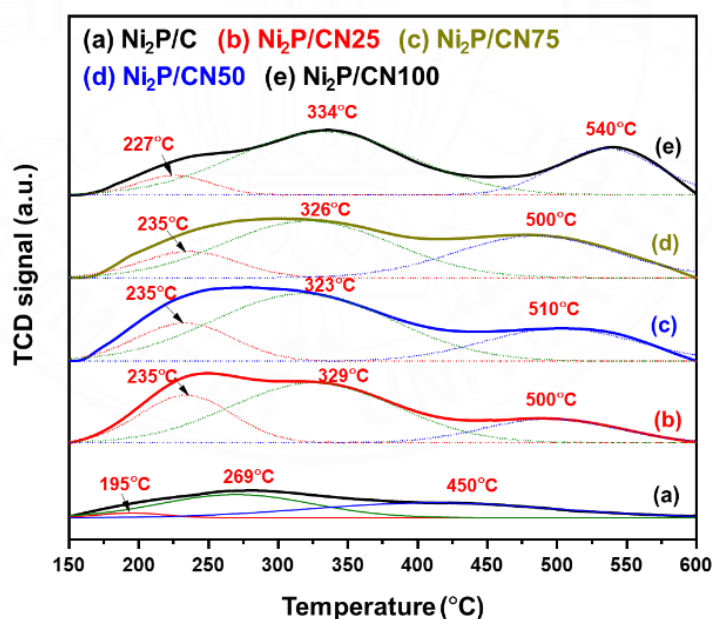


Figure 3.4 NH₃-TPD patterns of samples

The NH₃-TPD profiles of Ni₂P/C consisted of less intense peak at approximately 200 °C (low temperature) and strong peak at 280 °C (high temperature), which corresponded to the weak Brønsted acid sites and strong Lewis

acid sites, respectively. The Brønsted acid sites were attributed to the surface P-O, P-O-C=O groups, and the high-temperature shoulder at approximately 280 °C corresponded to NH₃ absorption by Ni^{δ+} (0 < δ < 1) ions in the nickel phosphide phase. The strong adsorption of NH₃ molecules by the was observed at high temperature (350 °C) owing to the reduction of the nickel phosphate, which passivated in air of Ni₂P during the catalyst synthesis step.

The normalized increment of absorption quantity of Ni₂P/CN_x is much larger and shift to higher temperature than that of Ni₂P/C. This result indicates the introduction of Ni₂P endows more acidity sites of N-doping carbon in comparison to pure activated carbon, which may could be ascribed to the substitution effect that resulted from introduction of the foreign atom Ni₂P into N-graphitic carbon. In fact, nitrogen atoms in the support, exist various functional groups of the terminal -NH_x or CN have been to act as Lewis basic useful to doping the Ni and P on surfaces. Amount of P and Ni in N-doping carbon are higher than pure activated carbon attributed the higher surface Lewis acidity of CN, which can be attributed to the NH₃ adsorbed on the Lewis acidic Ni and P atoms with different chemical statuses.

3.3.1.6 XPS results

To determine the elemental chemical composition in Ni₂P/C and Ni₂P/CN_x (x= 25- 100 %), XPS was carried out and the results are shown in Figure 3.5 and Table 3.3

In the Ni₂P/C sample, the high-resolution XPS reveals that the binding energies of Ni_{2p} located at 852.5 and 853.5 eV correspond to Ni_{2p1/2} in Ni₁₂P₅ and Ni₂P, respectively (Figure 3.6b). The peaks at 856.79, and 874.75 eV can be assigned to the oxidized Ni species (Ni²⁺). In addition, the peaks at 862.3 and 881.02 eV correspond to the satellite of the Ni_{2p1/2} and Ni_{2p3/2}, while the peak at 870.54 eV is ascribed to Ni_{2p3/2} in Ni₂P. In the P_{2p} spectrum (Figure 3.5b), peaks at 129.50, 130.0 eV correspond to the P_{2p3/2} in Ni₁₂P₅ and Ni₂P, while peaks at 133.53, and 134.34 eV indicate to P in Ni₂P passivation in air and surface nickel phosphate species, respectively. The observation of peak at 131.80 eV, and 532.10 eV might be ascribed to the P and O in in P-O-C=O group in P_{2p} and O_{1s} (Figure 3.5(b), and (d)).

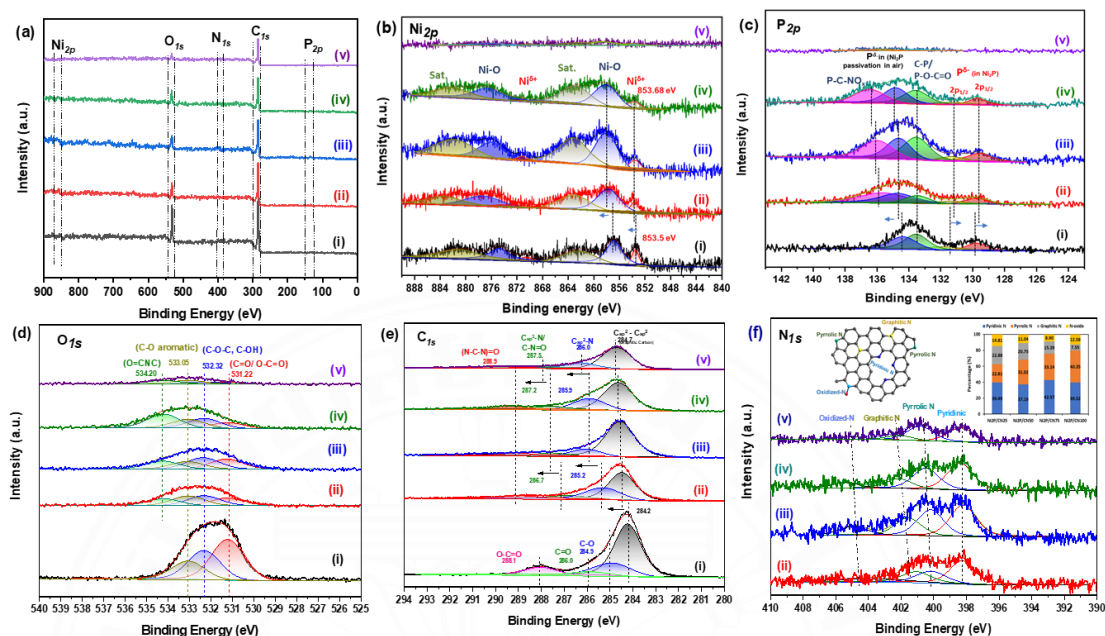


Figure 3.5 XPS profile of (i) Ni₂P/C, (ii) Ni₂P/CN25, (iii) Ni₂P/CN50, (iv) Ni₂P/CN75, and (v) Ni₂P/CN100 samples in wide range (a), Ni_{2p} (b), P_{2p} (c), O_{1s} (d), C_{1s} (e), and N_{1s} (f) spectra.

The presence of lactonic groups on surface of activated carbon caused by acid pretreatment and proved by temperature-programmed reduction (TPR) for presence of P-O-C=O group.

In the C_{1s} spectrum of Ni₂P/C sample (Figure 3.5(e)), the main peak at 284.93 eV belonged to the C-C bond in the carbon network. Two binding energy peaks at 284.7 and 288.10 eV were assigned to C-O and O=C-O bond, respectively. After N-doping, C-C and C-O shift to more positive due to interact between C-C with sp² hybridized carbon in (N-(C)₃) tertiary N groups and sp³ hybridized carbon in aromatic ring with terminal N group (-NH₂). Appearance of peaks at 285.97 eV and 289.17 eV belonged to C-N or C=N bonds and N-C=N from N-doping graphite carbon nitride.

The O_{1s} region in Ni_2P/C sample (Figure 3.5(c)) showed a dominant peak at 533.06 eV, a broad shoulder at 532.10 eV and 533.06 eV, which are assigned to phenolic oxygen, $-O-C=O$, and $C=O$ groups, respectively.

Table 3.3

XPS surface element analysis of catalysts

Sample	Element (at. %)					
	C	O	N	P	Ni	C/(C+N)
Ni_2P/C	79.25	19.01	0	0.91	0.83	1
Ni_2P/CN_{25}	80.75	12.93	2.82	1.94	1.56	0.966
Ni_2P/CN_{50}	77.05	14.55	3.33	2.99	2.09	0.959
Ni_2P/CN_{75}	79.78	13.98	2.46	2.06	1.72	0.970
Ni_2P/CN_{100}	90.07	7.35	2.23	0.3	0.06	0.976

The N_{1s} XPS spectrum showed that there were three types of N in CN_x samples (Figure 3.5(f)). The main peak at 398.04, 400.00 and 401.15 eV correspond to the aromatic N atoms bonded to two C atoms ($C=N-C$) in the pyridine-N (44.65%), sp^2 tertiary N groups ($N-(C)_3$) in pyrrolic-N (18.62%) and sp_3 terminal N group ($H-N-H$) in graphitic-N (32.68%), and π -excitation (4.03%) respectively. It is noteworthy that the Ni_{2p} in Ni_2P/CN_x sample (Figure 3.6b (ii- vi)) peaks all shift toward the positive binding energy, while the binding energy of graphitic-N (22.88%) and π -excitation (14.81%) shift to more negative correspond to 401.07eV, and 403.78 eV, respectively, indicating the chemical coupling between Ni in Ni_2P and graphitic carbon nitride in the form of a Ni-N bond. Interestingly, the P peak in Ni_2P at has positive shift at 134.63 eV and 135.63 (Figure 3.5c) combination with the trend of negative shift of the C_{1s} peak in N-CN 288.57 eV (Figure 3.6(e)) are observed due to electron delocalization between N and Ni atoms. In the addition, the new form P_{2p} in Ni_2P at 136.48 eV belonged P-N=O bonding was obtained by P-C-N linkage, which C_{1s} in were

positive shifted in 284.99 eV and 286.35 eV and negative shift N_{1s} peak of pyridine-N (39.49%) and pyridine-N (22.81%).

Such chemical interaction will result in a decreased electron density in Ni atoms along with an increased electron density in N atoms, forming covalent $Ni(\delta^+)-N(\delta^-)$ bonding states between Ni_2P and graphitic N in the carbon host, while pyridinic or pyrrolic N atoms conjugated with $P(\delta^-)$ on the graphitic carbon support could not only homogeneously disperse and stabilize the Ni-P nanoparticles but also create the defect-rich carbon structure.

The XPS elemental surface analysis was shown in Table 3.3. The increasing amount of melamine doping 25% to 100% consulted that C content increasing contrast of decreasing O content, while $C/(C+N)$ no significant changed. Differences in Ni and P content were observed with various melamine doping level. What stands out in this table is the remarkedly the dominance of replacement of C-N to C-O functional groups assisted engaged the level of Ni and P content. In case that, CN50 with 50% melamine doping present the highest Ni, P elemental surface content according to the high N-doping level.

Combined with the growth results XRD, TEM, TPR, N_2 absorption- desorption and XPS of samples, we can indicate that the formation of nickel phosphide species was strong affected by N-doping due to the difference in the contents of surface groups. N-doping could be used to tune the interfacial group distribution, hereby providing a strategy to rationally design transition metal phosphide supported catalysts carbon and nitrogen from exfoliation $g-C_3N_4$ diffused into carbon support.

3.3.2 Catalytic ability

3.3.2.1 Effect of various catalysts on the upgrading performance

The catalytic hydrodeoxygenation activity of the Ni_2P/C and Ni_2P/CN_x catalysts were tested in the two joined fixed- reactors (atmosphere's pressure and pyrolysis's constant temperature of 550 °C). To upgrading liquid oil, catalytic upgrading reactor was investigated at various catalyst, at 350 °C shown in Figure 3.6.

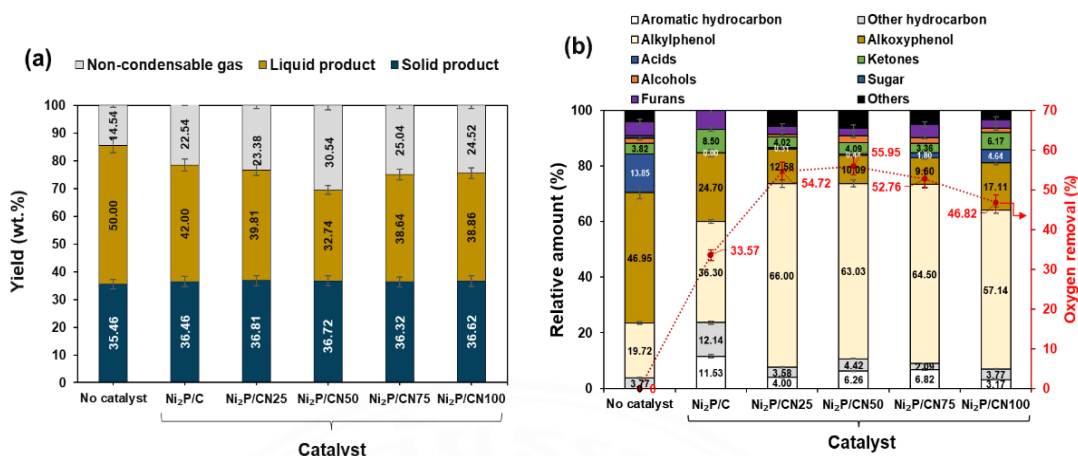


Figure 3.6 The pyrolysis products (a), and chemical distribution in liquid product (b) by catalytic upgrading using Ni₂P catalysts with and without N-doping, respectively. Conditions: T= 350 °C, P = 1 atm, Biomass: catalyst = 4 : 1 (wt.), GHSV of 1.44 (1/s).

The catalyst had a great effect on both of relative content in chemical composition in the liquid products, and pyrolysis products distribution. The decreasing yield of liquid product was due to the cracking reaction, which had a greater effect at hydrolysis couples with catalytic deoxygenation reaction of the pyrolysis vapor to give lighter molecular belong to non-condensable gas. Furthermore, the chemical composition of high oxygenated compound in raw oil (pyrolysis without catalyst) such alkoxyphenols (46.95%), alkylphenols (19.72%), acids (13.85%), furans (4.99%), ... obtained from fragmentation of high lignin-content of palm kernel shell would be deoxygenated to form low oxy-compounds like hydrocarbon and alkyl phenol. The fraction of alkylphenol compounds (> 57%) increasing after catalytic upgrading was observed in Ni₂P/CN_x catalysts. Interestingly, Ni₂P/CN_x present high acid site but unfavored to cracking C-C to form more aliphatic hydrocarbon and further aromatization to form aromatic hydrocarbon, even achieve high oxygen removal (> 46.82%) compared to Ni₂P/C (33.57%).

3.2.2.2 Effect of temperature on the upgrading performance

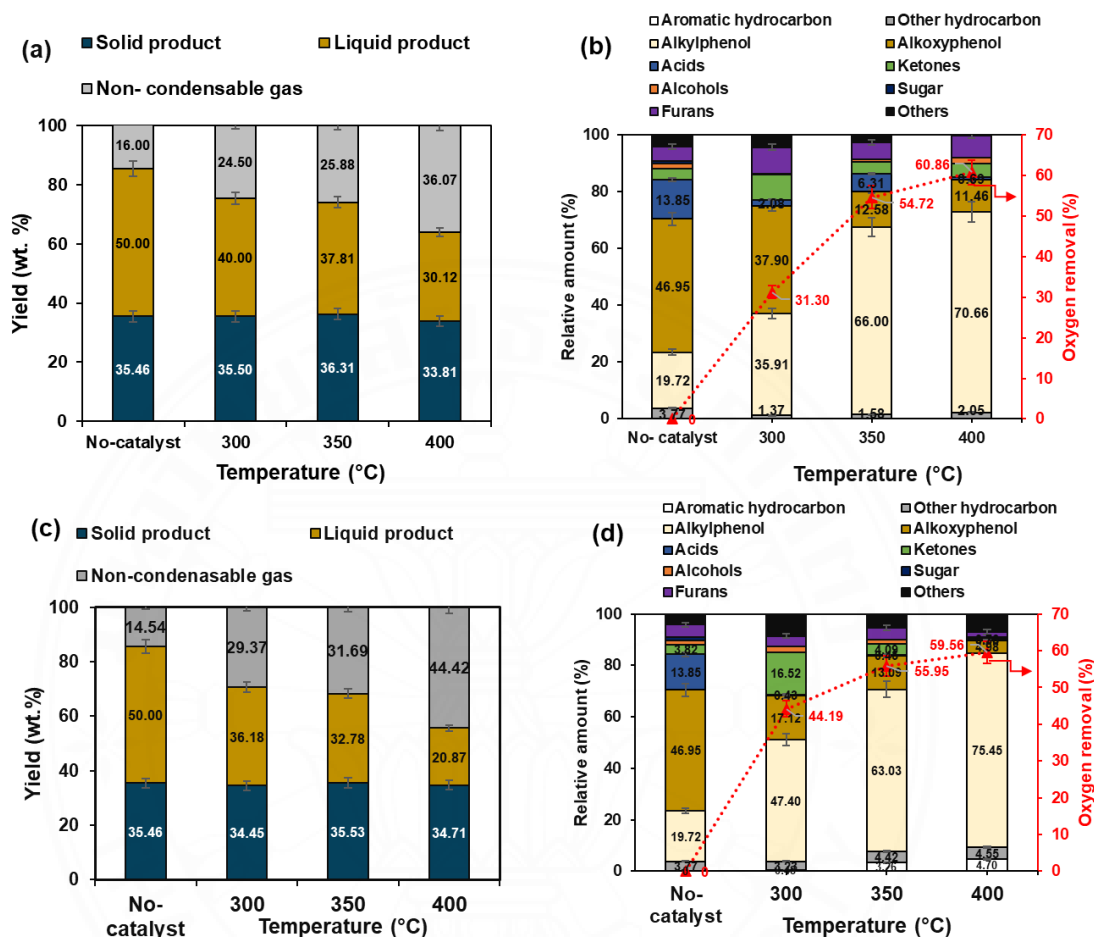


Figure 3.7 The pyrolysis products (a, c), and chemical distribution in liquid product (b, d) by catalytic upgrading using Ni₂P/CN25 and Ni₂P/CN50 catalysts, respectively. Conditions: P = 1 atm, biomass : catalyst = 4 : 1 (wt.), GHSV (1/s) of 1.44 (for Ni₂P/CN50) and 0.96 (for Ni₂P/CN25).

The catalytic temperature was significant effect on cracking and deoxygenation of alkoxyphenol to form alkyl phenol. Figure 3.7 shown the chemical composition of the products, whereby a decrease in yield of the liquid phase products using the Ni₂P/CN25 catalyst. The results of correlational analysis of phenol faction can be compared with different distribution of multiple-hydroxyl phenol and

single-hydroxyl phenol. The highest alkylphenol (75.45% compared to 19.72% without catalyst) regarding to the lowest oxy-phenol (from 46.95% without catalyst to 4.98%), following increasing yield of aromatic hydrocarbon improved that under atmospheric pressure and fixed bed reactor, the high temperature is essentials to cracking from hug lignin-oligomer fragment to form monomer-phenolic and further deoxygenation by hydrogen-extracted oxygen to form aromatic hydrocarbon. This was significant in cracking reaction under mild condition, which had a greater effect at hydrolysis couples with catalytic deoxygenation reaction of the pyrolysis vapor to give lighter molecular.

3.2.2.3 Effect of catalyst loading on the upgrading performance

In the other factor-catalyst loading is remarkably influence to the catalytic performance was displayed in Figure 3.8. In case of N-doping, the $\text{Ni}_2\text{P}/\text{CN}25$ and $\text{Ni}_2\text{P}/\text{CN}50$ catalyst were selected to comparison different type of Ni_2P and Ni_{12}P_5 to catalytic performance via the pure Ni_2P formation in 50% melamine level doping and 25% melamine doping with presence both phase Ni_2P and Ni_{12}P_5 . This was a remarkable outcome results with superior selective alkylphenol in all catalysts. The only significant factor different between the two conditions is the GHSV. The pure Ni_2P phase in $\text{Ni}_2\text{P}/\text{CN}50$ catalyst in fact of short residence time condition was observed similarity performance in deoxygenation degree and selectivity of alkylphenol competitive with presence both Ni_2P and Ni_{12}P_5 in $\text{Ni}_2\text{P}/\text{CN}25$ sample. It could be speculated that it was possible to obtain different ratio of Ni_{12}P_5 to Ni_2P species and control crystalline size by tuning the carbon support surface properties with N-doping corresponding to hydrodeoxygenation reaction. The pure Ni_2P with small particle size associated with high performance under light condition contrasted to the mixed Ni_{12}P_5 to Ni_2P phase with rich metallic active site.

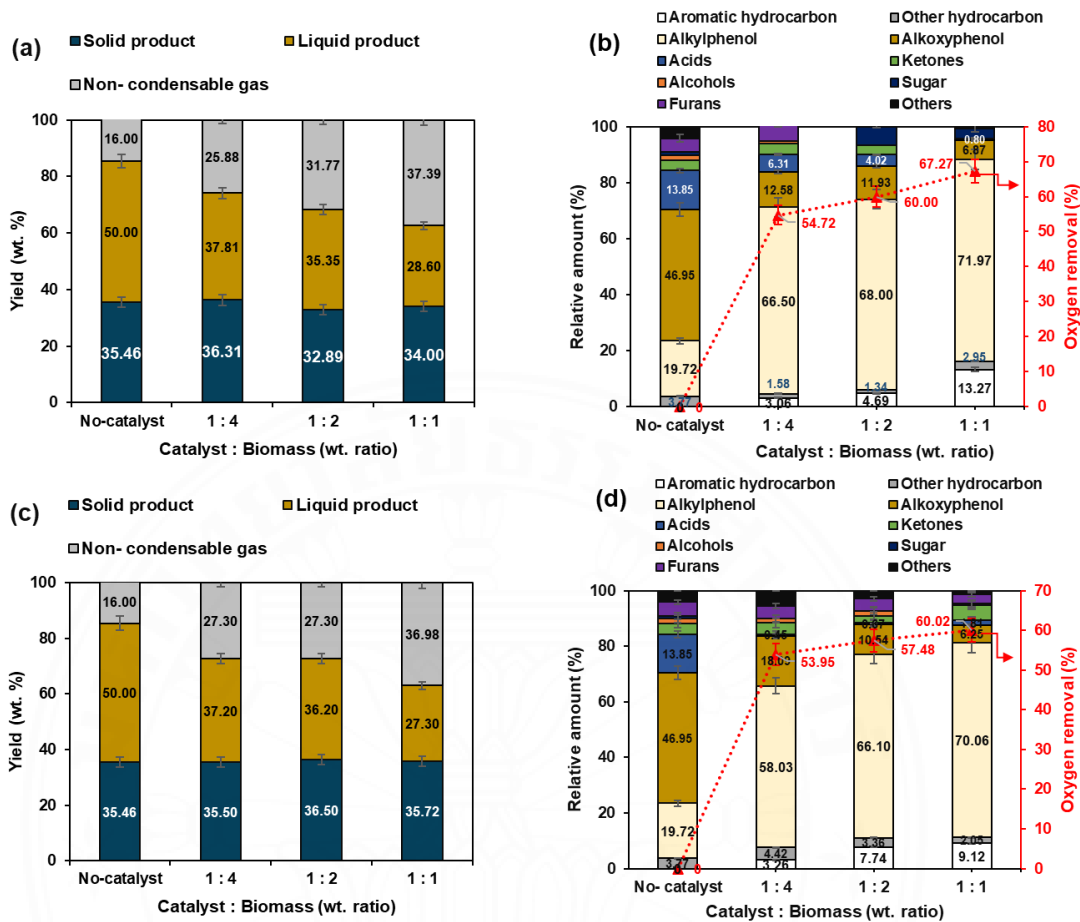


Figure 3.8 The pyrolysis products (a, c), and chemical distribution in liquid product (b, d) by catalytic upgrading using Ni₂P/CN25 and Ni₂P/CN50 catalysts, respectively. Conditions: T= 350 °C, P = 1 atm, GHSV (1/s) of 1.44 (for Ni₂P/CN50) and 0.96 (for Ni₂P/CN25).

3.2.2.4 Generation

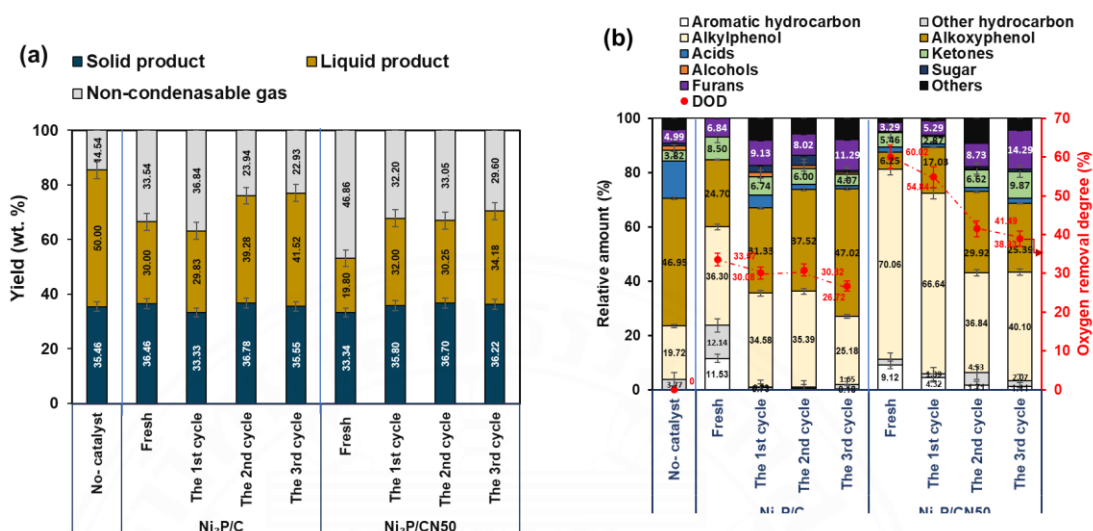


Figure 3.9 The pyrolysis products (a), and chemical distribution in liquid product (b) by catalytic upgrading using Ni₂P/C and Ni₂P/CN50 catalysts. Conditions: T = 350 °C, P = 1 atm, GHSV of 1.44 (1/s), biomass : catalyst = 1 : 1 (wt.)

Figure 3.9 provides the three cycles of run Ni₂P/CN25 and Ni₂P/CN50 catalysts without treatment. The recovery of a catalyst is important from both the economic and the environmental point of view. Typically, a catalyst has been recycled several times with deactivation is inevitable for most catalytic processes. However, the catalysts with N-doping can be cycle three times and still assisted to lifetime of catalyst based on controlling the particle size and deoxygenation performance. The results obtained from three cycle are set out even catalytic performance of Ni₂P/CN50 decreasing but still be better than without catalytic upgrading and Ni₂P/C without N-doping. These results suggest that N-doping is helpful not only to high selectivity, but also improvement of lifetime of catalyst.

3.2.2.5 Propose the mechanism

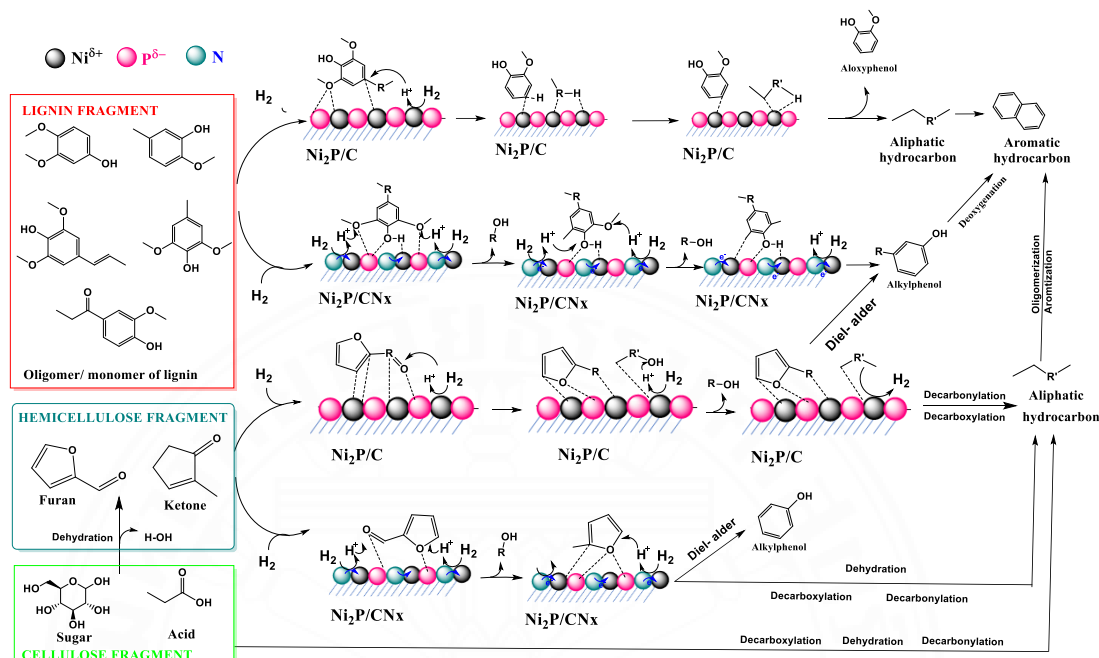


Figure 3.10 The propose of mechanism

The deoxygenation reaction could be performed by various pathways depending on the reaction conditions supported by decarboxylation and dehydration process in the presence of the Ni_2P with presence of N-doping supports.

The major differences between $\text{Ni}_2\text{P}/\text{C}$ catalyst and $\text{Ni}_2\text{P}/\text{CN}_x$ catalysts are Ni_2P crystalline form structure and nitrogen content. In this circumstance, the electrical connection between nitrogen atoms and Ni_2P nanoparticles increased the catalytic activity, which improved the adsorption of the substrates and promoted the heterolytic cleavage of H_2 . It is well acknowledged that the active species for the reduction of polar bonds like $\text{C}=\text{O}$ and $\text{C}=\text{N}$ bonds are the proton (H^+) and the hydride (H^-), which are produced by the heterolytic cleavage of H_2 . The $\text{Ni}_2\text{P}/\text{CN}_x$ catalyst's nitrogen atoms would function as Lewis bases to encourage the heterolytic cleavage of H_2 . In actuality, nitrogen atoms in transition metal complexes or the external addition of organic amines have been to operate as Lewis base for the heterolytic cleavage of

H₂, generating NH⁺ and Ni-hydride (Ni-H⁻). Therefore, the presence of N-doping support for active site in cleavage of H₂ to form H species helpful to Ni in Ni₂P in hydro-transfer favor dehydrogenation of the -OH group than C-O cleavage. Therefore, it prefers to reject O in hydroxyl group (OH) in polyphenol to form alkylphenol and then final to aromatic hydrocarbon. In the Ni₂P/C, presence of large particle of Ni₂P polycrystalline and Ni-rich like Ni₁₂P₅ with higher Lewis acid site prefer C-O and C-C cleavage, thus, deoxygenation prefer to cracking and re-conjured like higher aromatic hydrocarbon.



CHAPTER 4

BIMETALIC Ni-Ce/CN50 CATALYST FOR IN-SITU HYDRODEOXYGENATION OF PALM KERNEL SHELL PYROLYSIS VAPOR

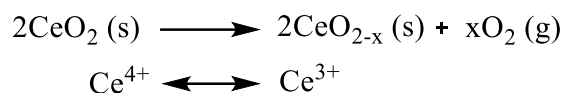
4.1 Background

The HDO process is typically operated at high hydrogen pressure (4-20 MPa) and relatively low reaction temperatures (200–400 °C) [72]. In this regard, the high-pressure H₂ supply limits the general adoption of HDO. On the one hand, commercial H₂ is a costly energy resource that is primarily generated by steam reforming of fossil fuels (natural gas, oil, and coal) [73] or water electrolysis [74]. To address this safety in H₂ storage, the catalysis community has interested in the development of innovative techniques to reduce the supply of H₂ from external source. To date, numerous ways have been proposed to achieve the deoxygenation process with in-situ hydrogen production such catalytic transfer hydrogenation or reforming followed by HDO, the combination of metal oxidation with water and HDO, or nonthermal plasma technology [75]. First, hydrogen is created in the catalytic transfer hydrogenation process by dehydrogenating a hydrogen donor solvent (formic acid) [76]. Then, HDO process is proceeded with the production of hydrogen through a metal hydride pathway [77]. In general, the catalytic transfer hydrogenation technique is advantageous for successful phenolic partial deoxygenation. The disposition of byproducts created by dehydrogenation of a hydrogen donor, on the other hand, it cannot be overlooked. Furthermore, undesirable side reactions (such as dehydration) give a negative impact on the catalyst. In comparison, tandem reforming (e.g., methane or alcohols) [78, 79] followed by HDO to give the great efficiency for complete deoxygenation. Lee et al.[80] created a new MgNiMo/activated charcoal (AC) catalyst and employed it in the catalytic upgrading of biotar under supercritical ethanol conditions. Pyrolytic oil over MgNiMo/AC yielded more than 70.1 wt.% with negligible coke [81].

The HDO process is carried out by hydrogenolysis of CO bonds across heterogeneous catalyst, with subsequent oxygen removal to form a water. During the HDO process, many processes such as decarboxylation, hydrogenation, hydrogenolysis, hydrocracking, and dehydration are concurrently occurred. As a result, controllable selective a reaction to produce a desirable product is critical and difficult. Selective deoxygenation of phenolics to aromatics is particularly fascinating since it uses the least amount of hydrogen compared to other reactions and the aromatics product are useful in fuel components. As a result, adsorption of oxygen atom on the surface necessitates overcoming a high barrier, resulting in a high total barrier for C–O cleavage. From this perspective, it's reasonable to assume that a method that favors O adsorption on the surface can improve deoxygenation activity.

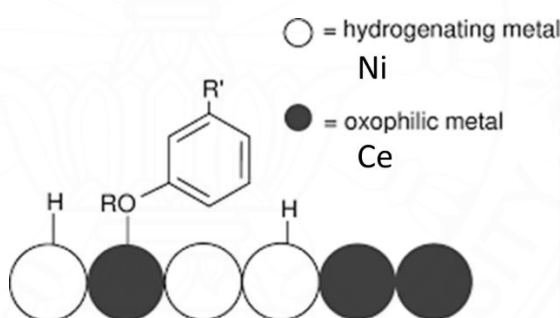
Recent studies have more attention on Cerium due to its water-resistant ceria containing redox and acid-base synergistic catalytic sites. The presence of oxygen vacancies and reversible $\text{Ce}^{3+}/\text{Ce}^{4+}$ redox couples boost its redox ability and consequently catalytic activity. Furthermore, its acid-base characteristics allow it to be used in acid-base catalytic processes. W. Jin *et al.*, studied the series of Ni-based catalysts supported on carbon/ceria-based for HDO of guaiacol. This study using water as the hydrogen source during the in situ HDO process. Accordingly, the novel HDO method to conduct HDO with generation of without H_2 supply was proposed. It was observed that water would undergo a splitting process on the catalytic surface to produce hydrogen. Hence, hydrogen can further participate in the HDO of bio-oil, facilitating the C–O bond breaking and ultimately the oxygen removal from the organic molecules [82]. Weiyang Wang *et al.*, studied the effect of Ce content on Ce–Ni–W–B amorphous catalysts in the hydrodeoxygenation (HDO) of phenols in bio-oil. Adding the promoter Ce could increase the content of Ni active site, therefore, leading to the improvement of the deoxygenation activity [83]. Deboshree Mukherjee *et al.*, studied Ceria (CeO_2) promoted Cu–Ni bimetallic catalyst supported on SiO_2 catalytic hydrodeoxygenation (HDO) of vanillin. The highest conversion of vanillin was achieved with the Cu–Ni/ CeO_2 – SiO_2 catalyst comparison without Ceria promotor [84]. Oxygen

vacancies of Ce (or coordinatively unsaturated metal cations) have a high oxygen affinity in these oxides.



Scheme 4.1 Cerium in transfer-state Ce^{4+} and Ce^{3+}

As a result, they promote O adsorption and increase deoxygenation combination with metal active site of Ni with N-doping activated carbon support as a catalyst for HDO of phenolics has been extensively studied. In general, reducible oxide Ce supported Ni catalysts have better activity and selectivity toward aromatic deoxygenation than monometallic catalysts [85].



Scheme 4.2 The role of metallic active in deoxygenation

In this part, we discuss of bi Metallic Ni-Ce/N-doping AC catalyst to improve the activity and selectivity of deoxygenation to aromatics during HDO of phenols by altering the surface structure of Ni-based catalysts. It is especially crucial to reduce selectivity toward C–C hydrogenolysis, in addition to improving deoxygenation. While oxophilic metals of Ce demonstrated to adsorb the O atom of oxygenate compounds. Combining a hydrogenating metal with an oxophilic metal to generate a bimetallic alloy with finely regulated hydrogenation and oxophilicity may increase the activity and selectivity toward aromatic production under mild conditions at fixed bed reactor.

4.2 Material and method

4.2.1 Preparation of Bimetallic Ni-Ce support on N-doping activated carbon.

The bimetallic Ni-Ce catalyst supported on the selected N-doping activated carbon CN50 support with different metal doping: $15\text{Ni}_x\text{Ce}/\text{CN50}$ ($x=0, 1, 3, 5, 10$ wt.%, at fixed 15wt.% Ni loading) and $y\text{Ni}5\text{Ce}/\text{CN50}$, ($y=5, 15$ wt.%, at fixed 5 wt.% Ce loading) were prepared by wetness impregnation method. First, the of CN50 support was prepared following in synthesized N-doping in the chapter 3 was dried overnight for 12 h before impregnation. The calculated amount of Ce and Ni from $\text{Ce}(\text{NO}_3)_3 \cdot 6\text{H}_2\text{O}$ (99.99 %, Merck) and $\text{Ni}(\text{NO}_3)_2 \cdot 6\text{H}_2\text{O}$ (99.98 %, Xi Long) were homogeneously diluted in initial amount of acetone solution, then impregnated with of CN50 support coupled ultrasounds assisted for 1 h. The samples were then aged for 2 h at ambient temperature, then dried at 100 °C for 12 h. After that, the catalyst precursors were nitrogen-calcinated at 400 °C for 2 h and then hydrogen-reduced in tubular reactor to 500 °C (3 °C min^{-1} from room temperature) to obtain the fresh catalysts. The as-reduced catalyst was finally cooled to the required reaction temperature or to room temperature under nitrogen gas for further catalyst characterization.

4.2.2. Catalytic integrated deoxygenation of Palm kernel shell

The rich lignin-palm kernel shell biomass content (lignin content of 54.84 wt. %, hemicellulose content of 28.45 wt.%, and cellulose content of 7.24 wt%) used as a feedstock in catalytic fast pyrolysis was investigated to examine the catalyst performance deoxygenation. The biomass and catalyst were fixed at weight ratio 1 :1. Prior to the run reaction, the reactor was purged with N_2 gas at 50 ml min^{-1} for 20 min to remove air. Next, the reduction of catalyst was performed to reactive metal site under H_2/N_2 (20 v./v) gas with flow rate of 50 ml min^{-1} , 500 °C for 2 h. The temperature of the second reactor was cooled to target upgrading temperature, while the temperature of pyrolysis zone heated fixed at 550 °C. After reach terminated temperatures, palm kernel shell powder from biomass hoper was crewed and dropped following the carrier gas. The residence time of the process was 5 s, while the operation

pressure was 1 atm. The detected bio-oil main components in this study were the light bio-oil compounds was collected in acetone-ice cool trap condensers. The bio-oil produced in no-catalyst and catalytic upgrading was water-free absorbed by sodium sulfate before identified by GC–MS (GC–Agilent 7890B, MS–Agilent 5973) equipped with an BD-5MS capillary column (0.25 mm ID, 30 m length, 0.25 mm film thickness) and using He at a flow rate of 1 ml min⁻¹ as the carrier gas. The oven temperature was programmed to remain at 50 °C for 3 min, ramp at 10 °C min⁻¹ to 280 °C, and stay at 280 °C for 5 min. The injector split ratio was set to 50:1 using methanol as solvent to dilute the samples. The chemical compositions of the oil phase were identified based on the NIST Mass Spectral Library and literature. The relative peak area of each compound was calculated by regulation with the total peak area in the GC–MS using Eq. (1):

$$C_i = \frac{A_i}{A_T} \times 100 \% \quad (4.1)$$

Where, C_i is the relative area of each compound i ; A_i symbolizes the peak area of compound i , and A_T represents the total peak area of all compounds present in the GC–MS data of the oil phase.

The oxygen removal rate was calculated based on the GC–MS results as follows:

$$\text{Oxygen removal} = \left[\frac{T_{\text{no-catalyst}} - T_{\text{catalytic upgrading oil}}}{T_{\text{no-catalyst}}} \right] \times 100 \% \quad (4.2)$$

where, $T_{\text{no-catalyst}}$ and $T_{\text{catalytic upgrading oil}}$ are the total oxygen relative-mole percentage in all the oxygenated compounds as determined by the GC–MS analyses of the pyrolysis oil and upgraded oil, respectively.

4.3 Results and discussions

4.3.1 Effect of Ce loading on catalytic upgrading performance under N₂ carrier gas

The catalytic deoxygenation activity of the 10NiCe/CN50 catalysts was tested in the integrated fixed bed pyrolysis and upgrading reactors (atmospheric pressure and constant pyrolysis temperature at 550 °C and upgrading temperature at 400 °C) in terms of liquid yield and liquid product composition as shown in Figure 4.1. As can be seen from the Figure 4.1.a, the fraction of liquid yield of catalytic upgrading is lower than without catalyst applied.

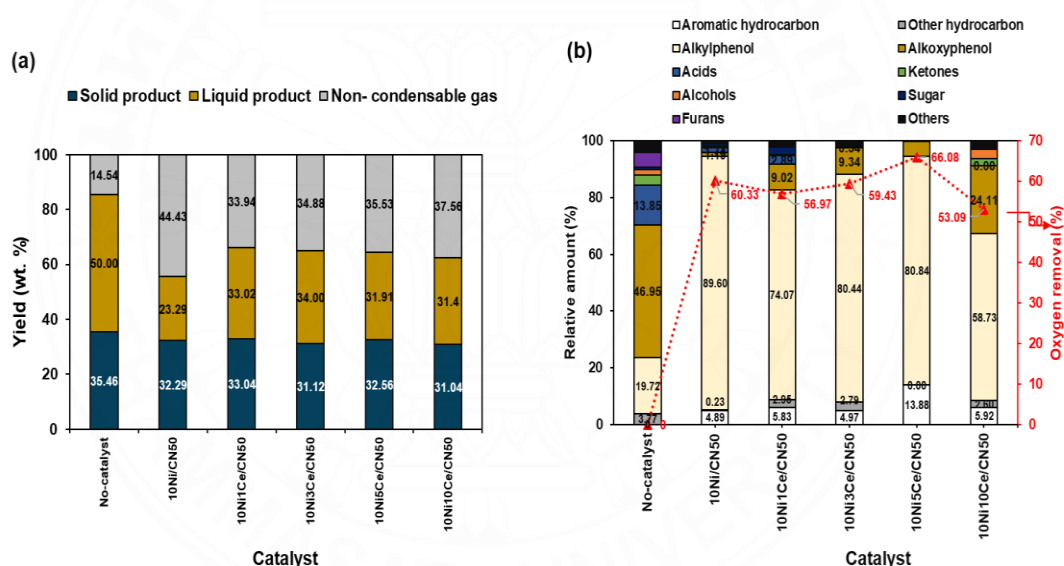


Figure 4.1 The pyrolysis products (a), and chemical distribution in liquid product (b) by catalytic upgrading using 10NiCe/CN50 catalysts. Conditions: $T_{\text{pyrolysis}} = 550\text{ °C}$, $T_{\text{upgrading}} = 400\text{ °C}$, $P = 1\text{ atm}$, Biomass : catalyst = 1 : 1 (wt.), N₂ carrier gas with GHSV of 0.96 (1/s).

The decreasing of liquid yield following increasing non-condensable gas proved that the catalyst assisted to cracking high-molecular weight of oligomer of lignocellulose, special is rich lignin to light molecular. There was no significant different

between solid yield associated with completely vaporized of palm kernel shell at pyrolysis zone fixed at 500 °C. Moreover, the results obtained from analysis of chemical distribution in Figure 4.1b shown the alkylphenol groups with successive increase in intensity, the alkoxyphenol moved further formation of simple phenol via demethoxylation to cleavage methoxy groups. Noteworthy that under inert gas, and mild condition the bimetallic Ni-Ce and mono metallic Ni presented high deoxygenation performance due to well dispersion of Ni with support metallic and high acid-metal site. However, at high level of Ce doping at 10wt.% may be controlled metal acidity, then reducing cracking.

4.3.2 Effect of Ce loading on catalytic upgrading performance under CO₂ carrier gas

Cerium has the oxygen vacancy nature due to reversible state of Ce³⁺ and Ce⁴⁺ by redox reaction, therefore it contained unique acid–base characteristics and strong oxophilicity. which may be suitable for deoxygenation of oxygenates in biomass to obtain high-grade bio-oils with low oxygen content. The hypothesis is the basic Ce properties may be usefully assisted to dry reforming of bio-oil vapor for in-situ generation of hydrogen, which coupled with hydrodeoxygenation. We characterized the catalytic deoxygenation activity of the 10Ni_xCe/CN50 catalysts under CO₂/N₂ (1:1) gas mixture presented in Figure 4.2 in terms of liquid yield and product composition.

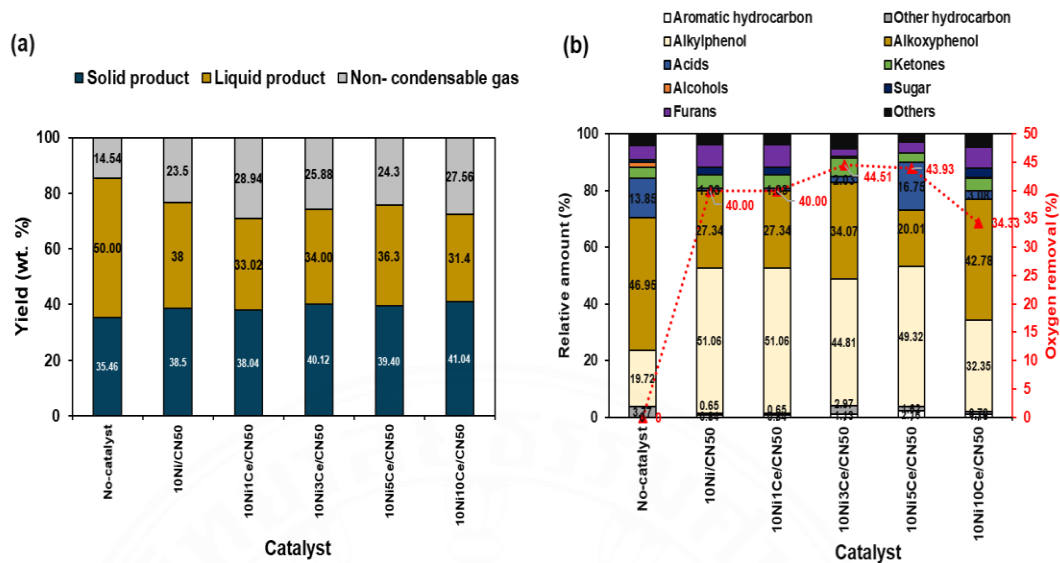
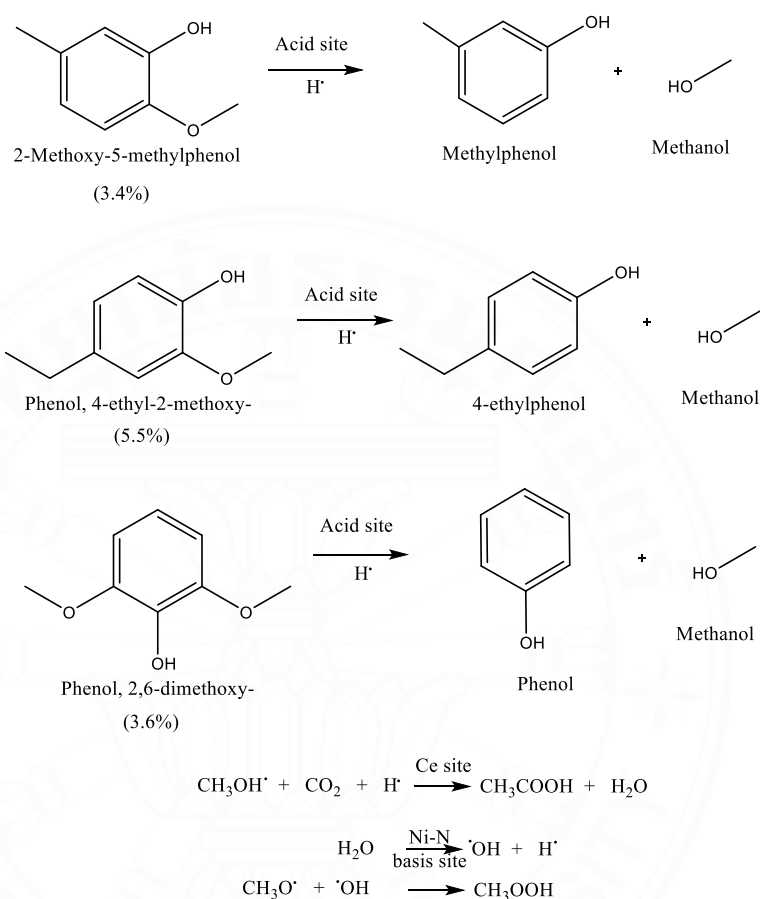


Figure 4.2 The pyrolysis products (a), and chemical distribution in liquid product (b) by catalytic upgrading using 10Ni_xCe/CN50 catalysts. Conditions: $T_{\text{pyrolysis}} = 550\text{ }^{\circ}\text{C}$, $T_{\text{upgrading}} = 400\text{ }^{\circ}\text{C}$, $P = 1\text{ atm}$, Biomass : catalyst = 1 : 1 (wt.), CO_2 carrier gas GHSV of 0.96 (1/s).

Under mild temperature and atmospheric operation pressure, CO_2 as oxidate reagent can be participated in dry reforming, competitive with oxidization of metal Ni active site, which have can reduce acid Ni active site. Figure 4.2 (a, b) provided the fraction of oil and alkyphenol in liquid at all catalyst provides no significant difference, but still higher than without catalyst even decreasing liquid yield. Ce doping in bimetallic Ni-Ce may has the selective absorb oxygen-atom from oxygenated compounds, while Ni can react with hydro atom from C-H molecular in molecular bone and prefer to scission of C-C or C-O by acid site. The reforming may be required more energy at high temperature over bimetallic Ni-Ce due to overcome the energy barrier to extract hydrogen donor[86, 87]. Ce in case may plays as role for catalyze the oxidation of derivative lignocellulosic fragment under rich CO_2 environment. The high fraction of ketone or acid at high Ce doping content in Figure 4.2 (b) conducted with the ketonization. There is a surprising result at 5 wt% of Ce obtained high selective of acetic in acid fraction might be explained by the fact syngenetic of Ni and Ce by

cleavage of methoxyl of aloxyphenol to alkylphenol via acid site then reformed with oxidate CO_2



Scheme 4.3 Describe deoxygenation over Ni and Ce active sites

4.3.3 Effect of (N_2 : H_2) ratio gas feeding on upgrading performance

The reduce gas such H_2 internal also studied to investigate the effect amount of H_2 in feeding gas on the hydrodeoxygenation, which shown in Figure 4.3.

As the results of valuable finding that the reduced gas such H_2 is significant improved deoxygenation performance. Moreover, the increasing H_2 faction in mixed gas can be assisted to generate higher free oxygen compounds such aromatic and aliphatic hydrocarbon. The results shown that the designed catalyst required not

much amount of hydrogen mixing (50%) can be achieved higher deoxygenation performance (68%) under mild conditions

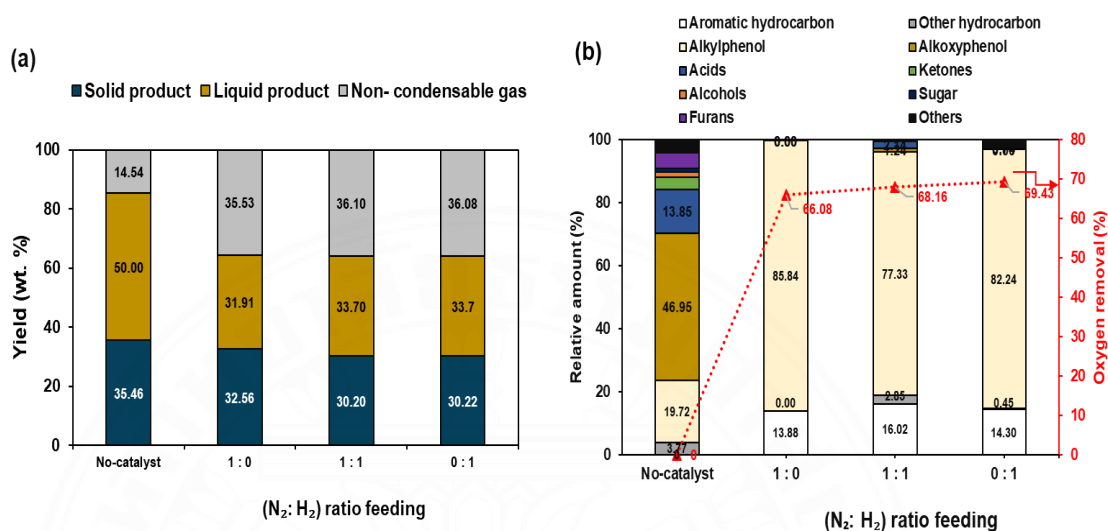


Figure 4.3 The pyrolysis products (a), and chemical distribution in liquid product (b) by catalytic upgrading using 10Ni5Ce/CN50 catalysts. $T_{\text{pyrolysis}} = 550 \text{ }^{\circ}\text{C}$, $T_{\text{upgrading}} = 400 \text{ }^{\circ}\text{C}$, $P = 1 \text{ atm}$, Biomass : catalyst = 1 : 1, GHSV of 0.96 (1/s).

4.3.4 Effect of gas feeding on upgrading performance

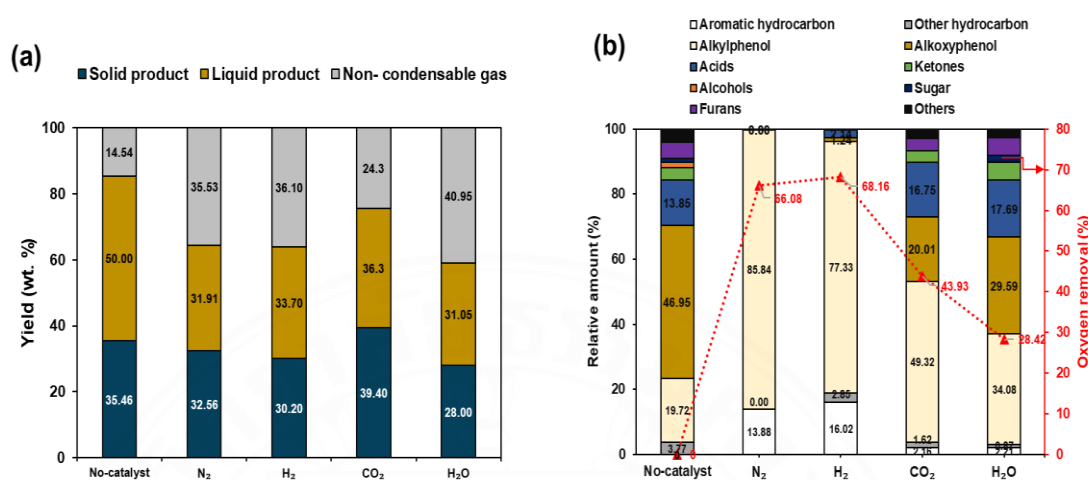


Figure 4.4 The pyrolysis products (a), and chemical distribution in liquid product (b) by catalytic upgrading using 10NixCe/CN50 catalysts. Conditions: $T_{\text{pyrolysis}} = 550$ °C, $T_{\text{upgrading}} = 400$ °C, $P = 1$ atm, Biomass: catalyst = 1 : 1 (wt.), GHSV of 0.96 (1/s).

To summarize all effect of co-gas feeding on catalyst performance, Figure 4 presents in fact of pyrolysis products (a), and chemical distribution in liquid product (b) by using 10Ni5Ce/CN50 catalyst. These are particularly remarkable finding using inert (N₂) or reduced (H₂) gas atmosphere had a significant effect on the quantity and quality of bio-oils produced, while the use of CO₂, water more oxygenated products and lower oxygen content.

The results might be explained by in produce of H species, which content following the trend H₂ > N₂ > CO₂ > H₂O. The 50% H₂ gas mixing was significantly increasing of selective of alkyl phenol product, meanwhile obtained more aromatic hydrocarbon than without H₂ internal. The free H species, which activated from H₂ gas feeding or generation during reforming play as an important a key to led to an increase in the H/C ratio and decreasing O/C content via hydrodeoxygenation. The results suggests that bimetallic Ni-Ce even can reduce the amount of H₂ gas

feeding from (100% to 50%), but for in-situ generation hydrogen and hydrogenation, the mild condition (400 °C and atmospheric operation pressure) did not meet the requirement of H donor.

4.3.5 Effect of Ni loading on upgrading performance

The effect of Ni loading on catalyst performance was investigated under 50% H₂, which shown in Figure 4.5.

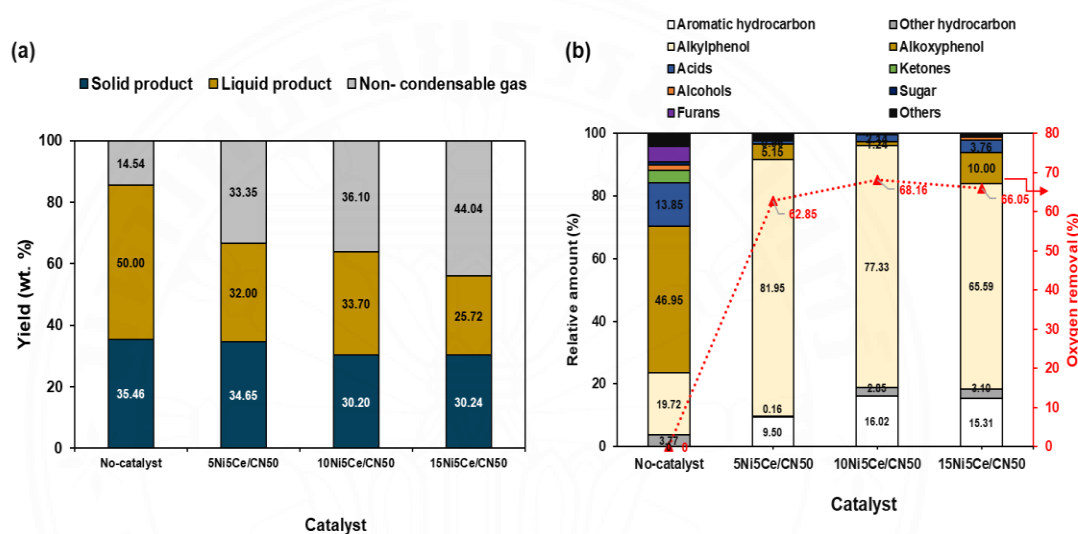


Figure 4.5 The pyrolysis products (a), and chemical distribution in liquid product (b) by catalytic upgrading using 10Ni_xCe/CN50 catalysts. Conditions: $T_{\text{pyrolysis}} = 550$ °C, $T_{\text{upgrading}} = 400$ °C, $P = 1$ atm, Biomass : catalyst = 1 : 1 (wt.), (N₂: H₂ = 1 : 1) carrier gas with GHSV of 0.96 (1/s).

The decrease in liquid yield as non-condensable gas increased demonstrated that the high Ni level doping catalyst aided in breaking high-molecular-weight lignocellulose oligomers, particularly those rich in lignin, to light molecular weight. There was no significant difference in solid yield associated with entirely vaporized palm kernel shell at pyrolysis zone set at 550 °C. Furthermore, the findings of the chemical distribution study in Figure 4.5(b) showed that the alkylphenol groups was main composition. It is worth noting that high Ni level prefer more hydrocarbon than low metal doping in the bimetallic Ni-Ce. The 10Ni₅Ce/CN50 catalyst may the

best catalyst due to present the deoxygenation content, which high aromatic and alkylphenol fractions.

4.3.6 XRD results

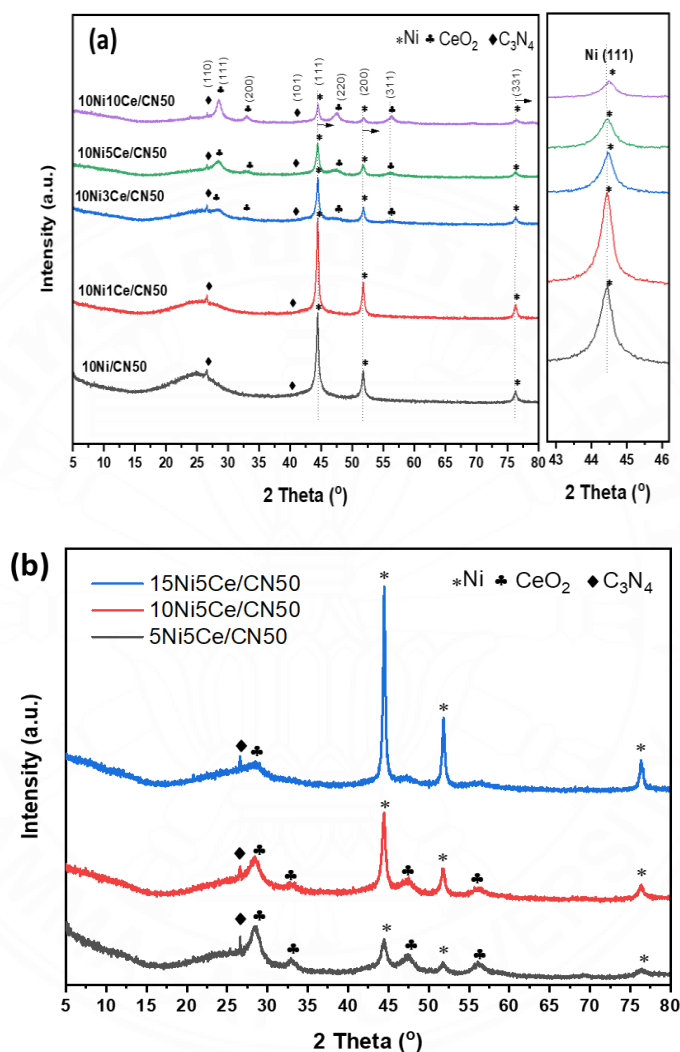


Figure 4.6 XRD patterns of (a) different Ce level doping, (b) different Ni level doping

To investigate the crystallize form of bimetal Ni-Ce species on surface of N-doping activated carbon, the XRD analysis was performed and shown in Figure 4.6. The diffraction peaks at 44.4°, 51.7°, and 76.4° corresponding to (111), (200), (331) of Ni⁰ crystals (ICDD#96-432-0490), while 28.4°, 33.7°, 47.3°, and 56.1° were ascribed to CeO₂ with the planes of (111), (200), (220), and (311) respectively (ICDD# #01-075-0151).

N-doping presented of γ - C_3N_4 accompanied diffraction peaks at 20.9° (110), and 26.5° (101) (ICDD#00-050-1249). The Ce doping altered to the shifting of Ni (111) shown in Figure 4.6 (a). There is no peak of CeO_2 was observed at low Ce doping of 1 and 3 wt.% due to small particle size below the XRD detection. The mean Ni and CeO_2 crystalline sizes were calculated based on Scherrer method, as shown in Table 4.1. Overall, the Ni crystalline size was found in the range from 5.41 to 27.23 nm, proving the well-dispersed Ni over N-doping activated carbon support. The 10Ni/CN50 appeared with Ni^0 crystalline average size of 23.75 nm, while its lower range 19.52 nm to 10.28 nm was observed at Ce dosages of 1 – 10 wt.%. The decreased crystalline size of Ni may be formed by the dilution effect, wherein Ce may create a fortress around the nickel active components and prevent them from sintering. However, an inverted trend seemed at a higher dosage of nickel at 15 wt.% due to cerium oxide may occupy the accessible pore of the N-doping carbon, leading to nickel oxide agglomeration with high Ni doping and, ultimately, a larger grain of particle size formed.

Table 4.1

Crystal size and textual property of catalysts

Samples	Crystal size (nm)*		BET area ($m^2 \cdot g^{-1}$)	BJH method analysis	
	Ni	Ce		Pore volume ($mL \cdot g^{-1}$)	Pore diameter (nm)
Fresh 10Ni/CN50	23.75	n.d.	726.1	0.61	3.38
Fresh 10Ni1Ce/CN50	19.52	n.d.	-	-	-
Fresh 10Ni3Ce/CN50	18.72	7.01	-	-	-
Fresh 10Ni5Ce/CN50	16.05	5.41	524.8	0.65	4.94
Fresh 10Ni10Ce/CN50	15.09	7.76	-	-	-
Fresh 5Ni5Ce/CN50	10.28	5.99	-	-	-
Fresh 15Ni5Ce/CN50	27.23	5.53	-	-	-
Spent 10Ni/CN50	-	-	555.3	0.74	5.36
Spent 10Ni5Ce/CN50	-	-	297.1	0.63	8.58

*Determined by Scherrer equation from XRD analysis

"n.d." not detected, "-" not examined

4.3.7 XPS results

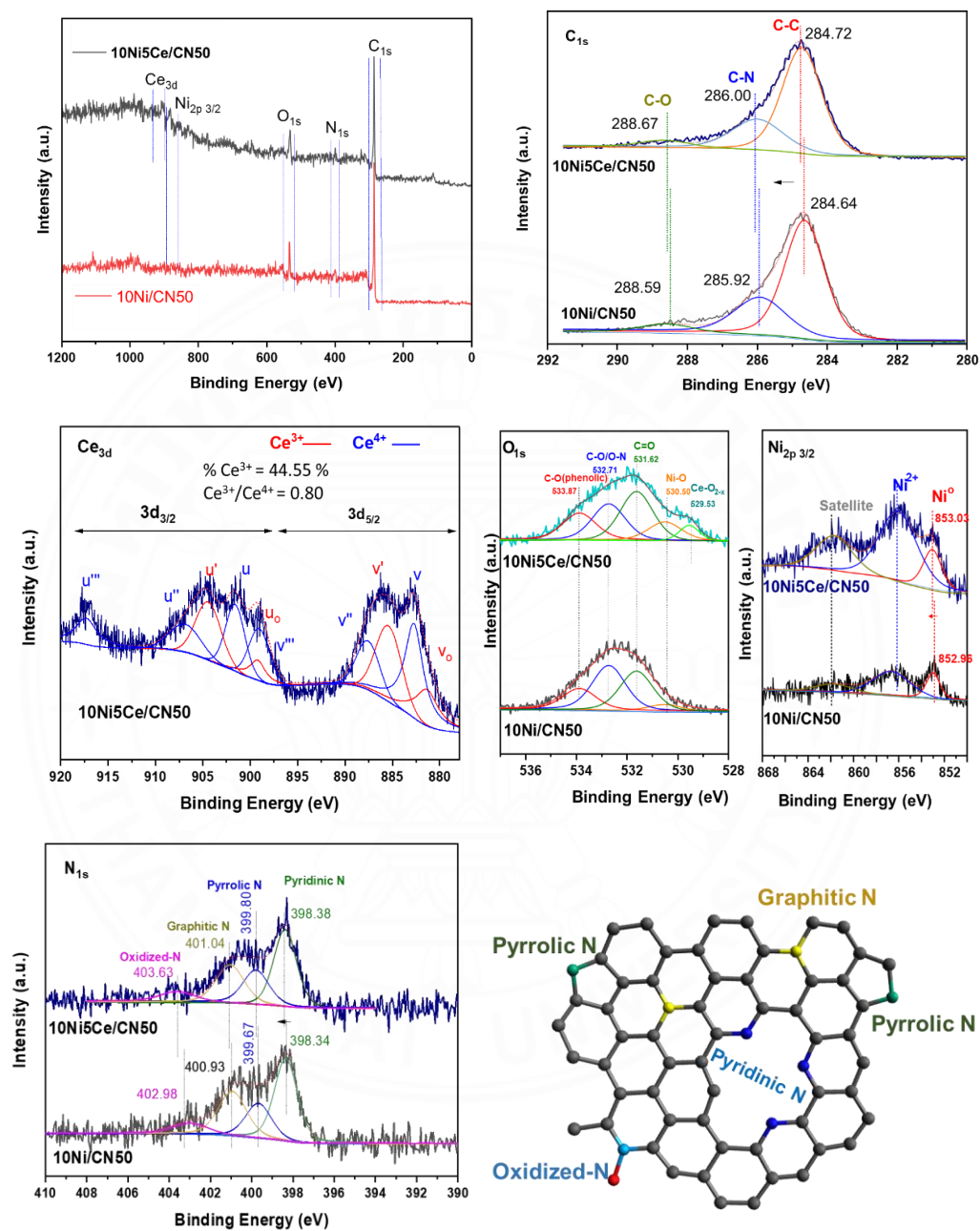


Figure 4.7 XPS patterns of (a) different Ce level doping samples, (b) different Ni level doping samples

XPS analysis was carried out to investigate the influence of Ce doping on Ni chemical surface structure shown in Figure 4.7. In the 10Ni/CN50 sample, the high-resolution XPS reveals that the binding energies of $Ni_{2p_{3/2}}$ located at 852.96 eV and 856.20 eV correspond to Ni^0 and Ni^{2+} , while the peaks at 862.3 eV correspond to the $Ni_{2p_{3/2}}$ satellite. In the C_{1s} spectrum, the three main peaks at 284.634 eV, 285.92 eV, and 288.59 eV regarded to the C–C bond, C–N bond, and C–O bond in the carbon network; while pyridinic N, pyrrolic N, graphitic N, and oxidized N in C–N linkage structure corresponded to 398.34 eV, 399.67 eV, 400.93 eV, and 402.98 eV, respectively. The curious results of Ce doping in 10Ni5Ce/CN50 sample revealed that the higher shift binding energy of Ni (852.96 to 853.03 eV) agreement with the shifting binding energy of both C–N and C–C demonstrated the interaction of Ce on Ni electronic properties. Moreover, the appearance of peaks at 529.53 eV in O_{1s} pattern belonged to O in CeO_{2-x} , whereas Ce^{3+} (v_o, v', u_o, u') combined Ce^{4+} spectra ($v, v'', v''', u, u'', u'''$) presented in Ce_{3d} . There is the ratio Ce^{3+}/Ce^{4+} of 0.8 result in the reducing of Ce^{4+} to Ce^{3+} and the obtained oxygen vacancy of Ce^{3+} assisted Ni state emerged with lower nickel oxide fraction in result of low distribution of O in NiO at 530.50 eV.

4.3.8 Textual property results

The N_2 adsorption-desorption isotherms of fresh and spent catalysts of 10Ni/CN50, and 10Ni5Ce/CN50 are shown in Figure. B1 and Table 4.1. Based on IUPAC classification, all catalysts belong to type I, indicating the micropores material. In case of in without Ce doping, 10Ni/CN50 exhibited H4 hysteresis loops, while presence of Ce doping makes 10Ni5Ce/CN50 displayed H3 hysteresis loops. The outcome results revealed that a wide range of narrow slit-like nanopores of 10Ni/CN50 was filled by Ce -doping particles aggregation giving rise plate-like to slit-shaped pores. Moreover, all spent catalyst presented in type I with H3 hysteresis loops indicated that the pore size of activated carbon may blocked with coke, which lead to decreasing surface area. In addition, BET surface area of 10Ni/CN50 was $726.1 \text{ m}^2 \text{ g}^{-1}$ higher than 10Ni5Ce/CN50 with $524.8 \text{ m}^2 \text{ g}^{-1}$ proved that Ni and Ce were well infused in the carbon support. The Ce-doping assisted to stabilization of pore volume after reaction (0.65 ml g^{-1} from fresh 10Ni5Ce/CN50 to 0.63 ml g^{-1} from spent 10Ni5Ce/CN50); even the pore

diameter of both spent catalysts were higher than both fresh catalysts. The results indicated that Ce doping assisted Ni limited coke formation and absorption on carbon material.



CHAPTER 5

CONCLUSIONS AND RECOMMENDATIONS

5.1 Conclusions

The first part of analyses examined the impact of thermal-fast pyrolysis of 20 various biomass samples to produce the desired compounds in liquid product such as phenolic and hydrocarbon compounds revealed the correlation relationship between lignin and hemicellulose were associated with each pyrolysis temperature. The statistic ANOVA measured the main factor to produce of phenolic influenced by high lignin factor, while the obtained hydrocarbon was significantly affected by pyrolysis temperature. Further analysis yield of pyrolysis products, especially the highest liquid product yield contained high-level of alkylphenol, the rich-lignin biomass content such palm kernel shell was choose at optimized pyrolysis temperature of 550 °C.

The next section of the survey was concerned by designed catalysts applied in catalytic upgrading coupled with fast pyrolysis of palm kernel shell by using N-doping activated carbon support material. The increasing melamine doping on activated carbon presented decreasing the O content in N-doping activated carbon following increasing C content even no- different in N content. In case of well dispersion and catalyst performance, melamine doping at 50% (CN50) was optimized. The develop of N-doping on carbonaceous porous structure enhanced allocation of the miniature Ni active particle since transfer-crossing metallic electron coordinated with C-N in N-doping activated carbon support. Therefore, it accelerated to selective formation of pure Ni₂P phase with small particle site, which enhanced the deoxygenation performance (~ 68%) with high selective alkylphenol production (~ 80%) at mild reaction conditions (350 °C, 1atm). In reaction consideration in fixed bed reactor, the Ni₂P/CN50 catalyst significantly improved selectivity of alkylphenol at ratio 1 : 1 and superior long-life catalyst in three cycles without any treatment.

In the final part of survey, the bimetallic Ni-Ce printed as a bright candidate HDO catalyst to reduce of amount of H₂ external under fixed bed reactor and mild

condition. The 10 wt.% of Ni and 5 wt.% of Ce were optimized with small particle size (16.05 nm for Ni, 5.41 nm for Ce) enhanced deoxygenation performance (~68%) and high selective deoxygenated compounds (~78% alkylphenol and ~20% hydrocarbon) at 400 °C with limited 50% H₂ co-feeding gas. Comparing the different gas feeding including H₂, N₂, CO₂, and H₂O, we observed that the deoxygenation performance following H₂ > N₂ > CO₂, > H₂O. The reduced gas such H₂ is extremely affected on deoxygenation; however, Ce assisted to high-level selective formation of alkylphenol (~ 50%) and acetic acid product (~ 17%) through by pathway of deoxygenation of aloxylphenol to form alkyl phenol and methanol, which further reacted with CO₂ in gas feeding and H active species to obtained methanol at 400 °C and atmospheric operation pressure.

5.2 Recommendations

5.2.1 Thermal pyrolysis of various biomass

The thermal kinetic of pyrolysis of the real biomass feedstock should be clearly identified interactive of cellulose, hemicellulose and lignin by other accurated techniques such TGA-IR or Py-GC/MS. For the selective desired compounds such acid, ketone, furan, ... the further survey should be predicted and optimized via response surface methodology.

5.2.2 Catalytic upgrading

The gas composition should be analyzed to confirm the deoxygenation pathways in catalytic upgrading.

In part 2, the N-doping activated carbon support should be further investigated of the effect of different N-sources on the faction of C-N structure (pyridinic N, pyrrolic N, graphitic N, and oxidized N) as well as the morphology of carbonaceous material. The N-doping content should be investigated with different calcination temperature. The P precursor suggested with other resources such as phosphite to reduce of reduction temperature. To improve the well-dispersion of small metal size may be studied with other catalyst synthesis methods such as sol-gel

method, solvothermal methods, The spent $\text{Ni}_2\text{P}/\text{CN}_x$ should be characterized with TEM, element analysis to confirm the metal leaching and morphology after reaction. Coke formation and water content should be analyzed by TGA analysis and Karl Fischer titration.

In part 3, the bimetallic Ni-Ce supported on N-doping activated carbon support should be further investigated of the effect of different N-sources on the fraction of C-N structure (pyridinic N, pyrrolic N, graphitic N, and oxidized N) as well as the morphology of carbonaceous material. In the reaction parameters, the increasing upgrading pyrolysis temperature to 500 and 600 °C is required to further study of in-situ H_2 generation via dry reforming using CO_2 co-feeding gas. The thermodynamic study also concerns to evaluate the H_2 consumption at different temperature.

In case of catalyst characterization, the TEM, H_2 -TPR, NH_3 -TPD and CO_2 -TPD should further analysis to determine morphology and acid-base properties of Ni-Ce. The well-dispersion of small metal size may be studied with other catalyst synthesis methods such as sol-gel method, solvothermal methods.... The spent $10\text{Ni}5\text{Ce}/\text{CN}50$ should be characterized with BET, element analysis to confirm the metal leaching and morphology after reaction. Coke formation and water content should be analyzed by TGA analysis and Karl Fischer titration.

REFERENCES

- [1] Thermochemical Conversion Processes. Biofuels. 2008 Springer London, p. 261–304
- [2] Altman R., Sustainable Aviation Biofuels. Bioenergy. 2015 Elsevier, p. 443–466
- [3] Dahiya A., Biomass to Liquid Biofuels Service Learning Projects and Case Studies. Bioenergy. 2015 Elsevier, p. 239–257
- [4] Huber, G. W. et al., Synthesis of transportation fuels from biomass: Chemistry, catalysts, and engineering. Chem. Rev., 2006, 106, p. 4044–4098
- [5] Liu C. et al., Catalytic fast pyrolysis of lignocellulosic biomass. Chem. Soc. Rev., 2014, 43, p.7594–7623
- [6] Li X. et al., Heterogeneous sulfur-free hydrodeoxygenation catalysts for selectively upgrading the renewable bio-oils to second generation biofuels. Renew. Sustain. Energy Rev., 2018, 82, p. 3762–3797
- [7] Mortensen, P. M. et al., A review of catalytic upgrading of bio-oil to engine fuels. Appl. Catal. A Gen., 2011, 407, p. 1–19
- [8] Vogt, E. T. C. et al., Fluid catalytic cracking: recent developments on the grand old lady of zeolite catalysis. Chem. Soc. Rev., 2015, 44, p.7342–7370
- [9] Nishu, R. L. et al., A review on the catalytic pyrolysis of biomass for the bio-oil production with ZSM-5: Focus on structure. Fuel Process. Technol., 2020, 199: 106301
- [10] He Z. et al., Hydrodeoxygenation of model compounds and catalytic systems for pyrolysis bio-oils upgrading. Catal Sustain Energy, 2013, 1, p. 28–52.
- [11] Pan Z. et al., Effect of a second metal (Co, Fe, Mo and W) on performance of Ni₂P/SiO₂ for hydrodeoxygenation of methyl laurate. J Energy Chem, 2016, 25, p. 418–426.
- [12] Teles, C. A. et al., Catalytic upgrading of biomass pyrolysis vapors and model compounds using niobia supported Pd catalyst. Appl Catal B Environ, 2018, 238, p. 38–50
- [13] Itthibenchapong V. et al., Deoxygenation of palm kernel oil to jet fuel-like

- hydrocarbons using Ni-MoS₂/γ-Al₂O₃ catalysts. *Energy Convers Manag.*, 2017, 134, p. 188–196.
- [14] Chen J. et al., Regulating product distribution in deoxygenation of methyl laurate on silica-supported Ni-Mo phosphides: Effect of Ni/Mo ratio. *Fuel*, 2014, 129, p. 1–10
- [15] Phimsen S. et al., Nickel sulfide, nickel phosphide and nickel carbide catalysts for bio-hydrotreated fuel production. *Energy Convers Manag.*, 2017, 151, p. 324–333
- [16] Shu R. et al., A review on the catalytic hydrodeoxygenation of lignin-derived phenolic compounds and the conversion of raw lignin to hydrocarbon liquid fuels. *Biomass and Bioenergy*, 2020, 132: 105432
- [17] Zhao Y. et al., Nitrogen-doped carbon nanomaterials as non-metal electrocatalysts for water oxidation. *Nat Commun*, 2013, 4, p. 1–7
- [18] Li Z. et al., Nitrogen-functionalized ordered mesoporous carbons as multifunctional supports of ultrasmall Pd nanoparticles for hydrogenation of phenol. *ACS Catal.*, 2013, 3, p. 2440–2448
- [19] Lv L-B. et al., Mono-Atomic Fe Centers in Nitrogen/Carbon Monolayers for Liquid-Phase Selective Oxidation Reaction. *ChemCatChem*, 2018, 10, p. 3539–3545
- [20] Cao Y. et al., Metal/Porous Carbon Composites for Heterogeneous Catalysis: Old Catalysts with Improved Performance Promoted by N-Doping. *ACS Catal.*, 2017, 7, p. 8090–8112
- [21] Jagadeesh, R. V. et al., Green synthesis of nitriles using non-noble metal oxides-based nanocatalysts. *Nat Commun.*, 2014, 5, p. 1–8
- [22] Liu S. et al., Identifying Active Sites of Nitrogen-Doped Carbon Materials for the CO₂ Reduction Reaction. *Adv Funct Mater.*, 2018, 28: 1800499
- [23] Hu Y. et al., Hydrogenolysis of lignin model compounds into aromatics with bimetallic Ru-Ni supported onto nitrogen-doped activated carbon catalyst. *Mol Catal.*, 2018, 445, p. 316–326
- [24] Isahak, WNRW. et al., A review on bio-oil production from biomass by using pyrolysis method. *Renew Sustain Energy Rev.*, 2012, 16, p. 5910–5923
- [25] Isahak, W. N. R. W. et al., A review on bio-oil production from biomass by using

- pyrolysis method. *Renew Sustain Energy Rev.*, 2012, 16, p. 5910–5923
- [26] Polysaccharides : Structural Diversity and Functional Versatility. Polysaccharides. 2004 CRC Press, p. 1224
- [27] Ma L. et al., A review of thermal–chemical conversion of lignocellulosic biomass in China. *Biotechnol Adv.*, 2012, 30, p. 859–873.
- [28] Xu C. et al., Lignin depolymerisation strategies: towards valuable chemicals and fuels. *Chem Soc Rev.*, 2014, 43, p. 7485–7500
- [29] Calvo-Flores, F. G. et al., Lignin as Renewable Raw Material. *ChemSusChem*, 2010, 3, p. 1227–1235
- [30] Chen W. et al., Co-pyrolysis of lignocellulosic biomass and microalgae: Products characteristics and interaction effect. *Bioresour Technol.*, 2017, 245, p. 860–868
- [31] Fan Y. et al., Effects of the cellulose, xylan and lignin constituents on biomass pyrolysis characteristics and bio-oil composition using the Simplex Lattice Mixture Design method. *Energy Convers Manag.*, 2017, 138, p. 106–118.
- [32] Liu Q. et al., Interactions of biomass components during pyrolysis: A TG-FTIR study. *J Anal Appl Pyrolysis*, 2011, 90, p. 213–218
- [33] Liu C. et al., Catalytic fast pyrolysis of lignocellulosic biomass. *Chem Soc Rev.*, 2014, 43, p. 7594–7623
- [34] Kawamoto H. et al., Secondary decomposition of levoglucosan in pyrolytic production from cellulosic biomass. *J Anal Appl Pyrolysis*, 2009, 85, p. 247–251
- [35] Kawamoto H. et al., Pyrolysis behavior of levoglucosan as an intermediate in cellulose pyrolysis: polymerization into polysaccharide as a key reaction to carbonized product formation. *J Wood Sci.*, 2003, 495 (49), p. 469–473
- [36] Antal, M. J. et al., Cellulose Pyrolysis Kinetics: The Current State of Knowledge. *Ind Eng Chem Res.*, 2002, 34, p. 703–717
- [37] Hosoya T. et al., Cellulose–hemicellulose and cellulose–lignin interactions in wood pyrolysis at gasification temperature. *J Anal Appl Pyrolysis*, 2007, 80, p. 118–125
- [38] Sluiter A. et al., Determination of Structural Carbohydrates and Lignin in Biomass: Laboratory Analytical Procedure (LAP), 2008 (Revised July 2011)

- [39] Sluiter A. et al., Determination of Ash in Biomass: Laboratory Analytical Procedure (LAP), 2008
- [40] Qu T. et al., Experimental Study of Biomass Pyrolysis Based on Three Major Components: Hemicellulose, Cellulose, and Lignin. *Ind Eng Chem Res.*, 2011, 50, p. 10424–10433
- [41] Sun Q. et al., Measuring the distance from saddle points and driving to locate them over quantum control landscapes. *J Phys A Math Theor.*, 2015, 48: 465305
- [42] Parikh J. et al., A correlation for calculating HHV from proximate analysis of solid fuels. *Fuel*, 2005, 84, p. 487–494
- [43] Dinh Ngo S. et al., Catalytic pyrolysis of Napier grass with nickel-copper core-shell bi-functional catalyst. *J Anal Appl Pyrolysis.*, 2020, 145: 104745
- [44] Pham L. K. H. et al., Data-driven prediction of biomass pyrolysis pathways toward phenolic and aromatic products. *J Environ Chem Eng.*, 2021, 9: 104836
- [45] Xiao R. et al., Thermogravimetric analysis and reaction kinetics of lignocellulosic biomass pyrolysis. *Energy*, 2020, 201: 117537
- [46] Chen K. et al., Production of low-oxygenated bio-fuels (hydrocarbons and polymethylphenols) from lignocellulose by a two-stage strategy with non-noble metal catalysts. *Fuel*, 2021, 286: 119401
- [47] Wang Y. et al., Catalytic pyrolysis of lignocellulosic biomass for bio-oil production: A review. *Chemosphere*, 2022, 297: 134181
- [48] Gao D. et al., Conversion of Guaiacol on Noble Metal Catalysts: Reaction Performance and Deactivation Studies. *Ind Eng Chem Res.*, 2014, 53, p. 18658–18667
- [49] Snåre M. et al., Heterogeneous Catalytic Deoxygenation of Stearic Acid for Production of Biodiesel. *Ind Eng Chem Res.*, 2006, 45, p. 5708–5715
- [50] Prins R. et al., Metal phosphides: Preparation, characterization and catalytic reactivity. *Catal. Letters*, 2012, 142, p. 1413–1436
- [51] Prins R. et al., Metal phosphides: Preparation, characterization and catalytic reactivity. *Catal. Letters*, 2012, 142, p. 1413–1436
- [52] Oyama ST. et al., Transition metal phosphide hydroprocessing catalysts: A review.

- Catal. Today, 2009, 143, p. 94–107
- [53] Wu SK. et al., Atmospheric hydrodeoxygenation of guaiacol over alumina-, zirconia-, and silica-supported nickel phosphide catalysts. ACS Sustain Chem Eng., 2013, 1, p. 349–358
- [54] Li K. et al., Hydrodeoxygenation of Anisole over Silica-Supported Ni₂P, MoP, and NiMoP Catalysts. Energy and Fuels, 2011, 25, p. 854–863
- [55] Yang Y., et al., Ni₂P/SBA-15 as a hydrodeoxygenation catalyst with enhanced selectivity for the conversion of methyl oleate into n-octadecane. ACS Catal., 2012, 2, p. 592–598
- [56] Oyama, S. T. et al., The active site of nickel phosphide catalysts for the hydrodesulfurization of 4,6-DMDBT. J Catal., 2008, 258, p. 393–400
- [57] Whiffen, V. M. L. et al., A Comparative Study of 4-Methylphenol Hydrodeoxygenation Over High Surface Area MoP and Ni₂P. Top Catal., 2012 5514(55), p. 981–990
- [58] Liu P. et al., Desulfurization Reactions on Ni₂P(001) and α -Mo₂C(001) Surfaces: Complex Role of P and C Sites. J Phys Chem B, 2005, 109, p. 4575–4583
- [59] Pham, L. K. H. et al., Formation and activity of activated carbon supported Ni₂P catalysts for atmospheric deoxygenation of waste cooking oil. Fuel Process Technol., 2019, 185, p. 117–125
- [60] Pham, L. K. H. et al., Integrated catalytic hydrodeoxygenation of Napier grass pyrolysis vapor using a Ni₂P/C catalyst. J Anal Appl Pyrolysis, 2019, 140, p. 170–178
- [61] Xu J. et al., In situ derived Ni₂P/Ni encapsulated in carbon/g-C₃N₄ hybrids from metal–organic frameworks/g-C₃N₄ for efficient photocatalytic hydrogen evolution. Appl Catal B Environ., 2019, 246, p. 72–81.
- [62] Seredych M. et al., Photoactivity of g-C₃N₄/S-Doped Porous Carbon Composite: Synergistic Effect of Composite Formation. ChemSusChem, 2016, 9, p. 795–799
- [63] Pham, L. K. H. et al., Formation and activity of activated carbon supported Ni₂P catalysts for atmospheric deoxygenation of waste cooking oil. Fuel Process Technol., 2019, 185, p. 117–125
- [64] Wang S. et al., Selective deoxygenation of carbonyl groups at room temperature

- and atmospheric hydrogen pressure over nitrogen-doped carbon supported Pd catalyst. *J Catal.*, 2018, 368, p. 207–216
- [65] Bi, Q. Y. et al., Dehydrogenation of Formic Acid at Room Temperature: Boosting Palladium Nanoparticle Efficiency by Coupling with Pyridinic-Nitrogen-Doped Carbon. *Angew Chemie Int Ed.*, 2016, 55, p. 11849–11853
- [66] Xin H. et al., Controlling the growth of activated carbon supported nickel phosphide catalysts via adjustment of surface group distribution for hydrodeoxygenation of palmitic acid. *Catal Today*, 2019, 319, p. 182–190
- [67] Oyama, S. T. et al., Effect of Phosphorus Content in Nickel Phosphide Catalysts Studied by XAFS and Other Techniques. *J Catal.*, 2002, 210, p. 207–217
- [68] Jiang N. et al., Effect of reduction temperature on the structure and hydrodesulfurization performance of Na doped Ni₂P/MCM-41 catalysts. *RSC Adv.*, 2019, 9, p. 15488–15494
- [69] Chen Z. et al., The texture evolution of g-C₃N₄ nanosheets supported Fe catalyst during Fischer-Tropsch synthesis. *Mol Catal.*, 2018, 444, 90–99
- [70] Xu Z. et al., Ni catalyst supported on nitrogen-doped activated carbon for selective hydrogenation of acetylene with high concentration. *Catal Commun.*, 2021, 149: 106241
- [71] Zhou S. et al., Pd Single-Atom Catalysts on Nitrogen-Doped Graphene for the Highly Selective Photothermal Hydrogenation of Acetylene to Ethylene. *Adv Mater.*, 2019, 31: 1900509
- [72] Elliott D. C. et al., Hydrocarbon Liquid Production via Catalytic Hydroprocessing of Phenolic Oils Fractionated from Fast Pyrolysis of Red Oak and Corn Stover. *ACS Sustain Chem Eng.*, 2015, 3, p. 892–902
- [73] Stiegel G. J. et al., Hydrogen from coal gasification: An economical pathway to a sustainable energy future. *Int J Coal Geol.*, 2006, 65, p. 173–190
- [74] Ursúa A. et al., Hydrogen production from water electrolysis: Current status and future trends. *Proc IEEE.*, 2012, 100, p. 410–426
- [75] Jin W. et al., Catalytic Upgrading of Biomass Model Compounds: Novel Approaches and Lessons Learnt from Traditional Hydrodeoxygenation – a

- Review. *ChemCatChem*, 2019, 11, p. 924–960
- [76] Nie R. et al., Transfer hydrogenation of bio-fuel with formic acid over biomass-derived N-doped carbon supported acid-resistant Pd catalyst. *Catal Sci Technol.*, 2017, 7, p. 627–634
- [77] Gilkey, M. J. et al., Heterogeneous Catalytic Transfer Hydrogenation as an Effective Pathway in Biomass Upgrading. *ACS Catal.*, 2016, 6, p. 1420–1436
- [78] Xiao Y. et al., Catalytic Deoxygenation of Guaiacol Using Methane. *ACS Sustain Chem Eng.*, 2015, 3, p. 2606–2610
- [79] Wang L. et al., Liquid phase in-situ hydrodeoxygenation of bio-derived phenol over Raney Ni and Nafion/SiO₂. *Int J Hydrogen Energy*, 2015, 40, p. 14790–14797
- [80] Lee J. H. et al., Catalytic upgrading of bio-tar over a MgNiMo/activated charcoal catalyst under supercritical ethanol conditions. *Catal Today*, 2018, 316, p. 237–243
- [81] Lee J. H. et al., Efficient upgrading of pyrolysis bio-oil over Ni-based catalysts in supercritical ethanol. *Fuel*, 2019, 241, p. 207–217
- [82] Jin W. et al., Investigating New Routes for Biomass Upgrading: “H₂-Free” Hydrodeoxygenation Using Ni-Based Catalysts. *ACS Sustain Chem Eng.*, 2019, 7, p. 16041–16049
- [83] Wang W. et al., Highly selective catalytic hydrodeoxygenation of Caromatic–OH in bio-oil to cycloalkanes on a Ce–Ni–W–B amorphous catalyst. *RSC Adv.*, 2014, 4, p. 37288–37295
- [84] Mukherjee D. et al., Ceria Promoted Cu-Ni/SiO₂ Catalyst for Selective Hydrodeoxygenation of Vanillin. *ACS Omega*, 2019, 4, p. 4770–4778
- [85] Wu X. et al., Vapor phase hydrodeoxygenation of phenolic compounds on group 10 metal-based catalysts: Reaction mechanism and product selectivity control. *Catal Today*, 2021, 365, p. 143–161
- [86] Zambrano D. et al., Kinetic Study of Dry Reforming of Methane Over Ni–Ce/Al₂O₃ Catalyst with Deactivation. *Top Catal.*, 2019, 625(62), p. 456–466.
- [87] González, J. J. et al., Biogas dry reforming over Ni–Ce catalyst supported on nanofibered alumina. *Int J Hydrogen Energy*, 2020, 45, p. 20568–20581



APPENDICES

APPENDIX A

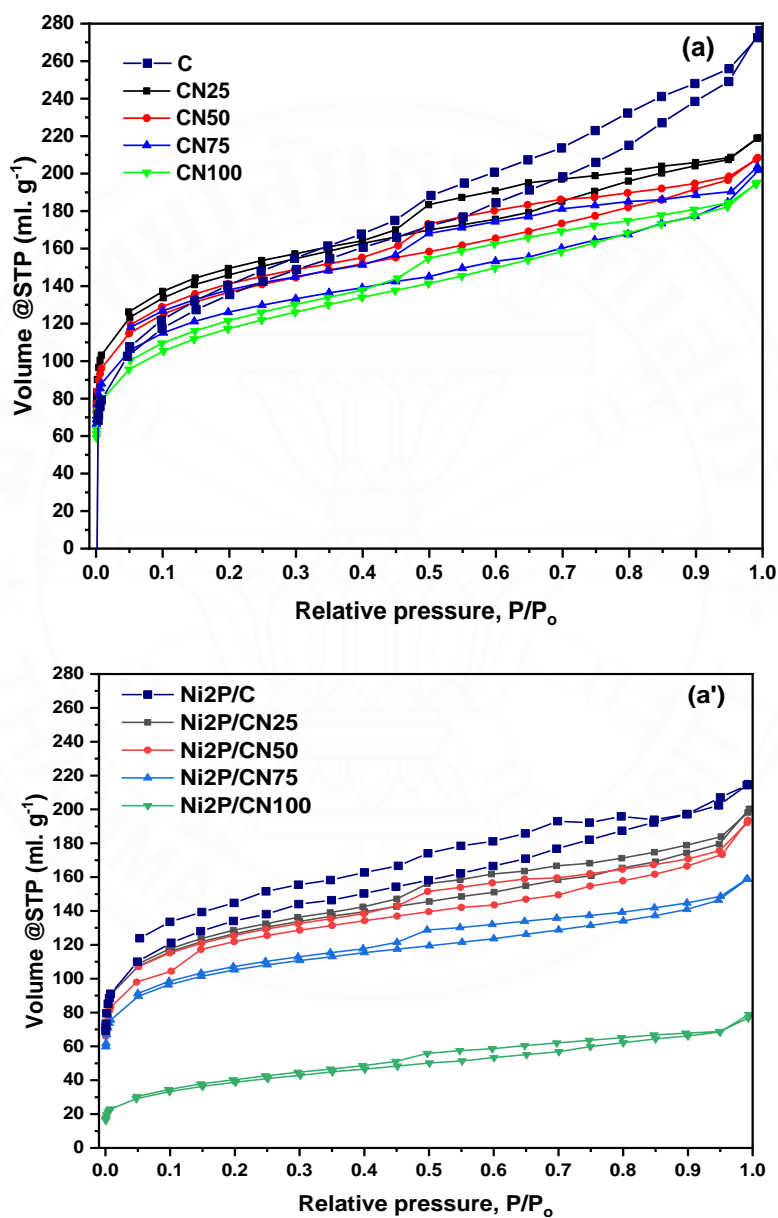
STUDY OF NICKEL PHOSPHIDE BASED-CARBONEOUS CATALYSTS ON
HYDRODEOXYGENATION OF PALM KERNEL SHELL PYROLYSIS VAPOR

Figure A.1 N_2 adsorption-desorption Isothermal samples of (a) activated carbon with and without N-doping support, and (a') Ni₂P doping on activated carbon with and without N-doping support

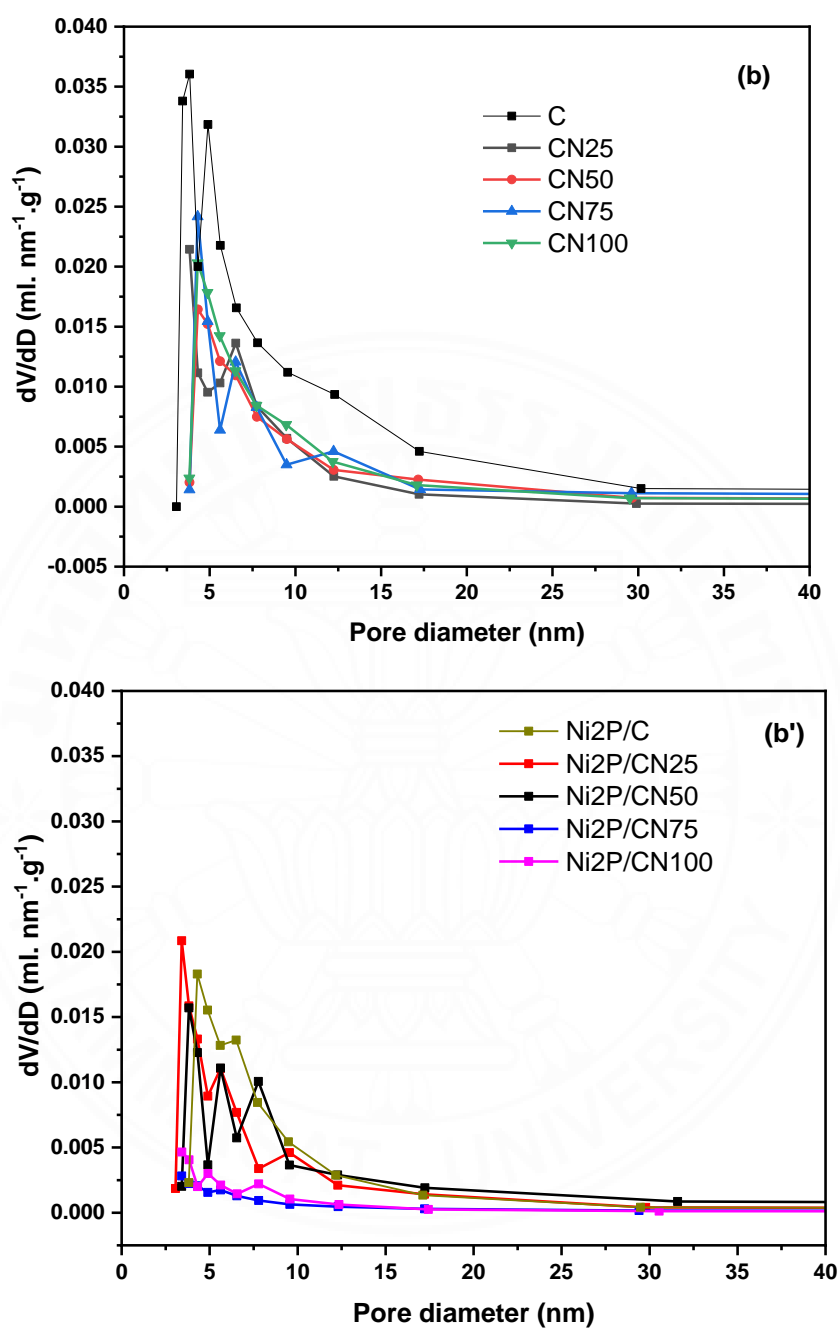


Figure A.2 Pore distribution of (b) activated carbon with and without N-doping support, and (b') Ni₂P doping on activated carbon with and without N-doping support

APPENDIX B

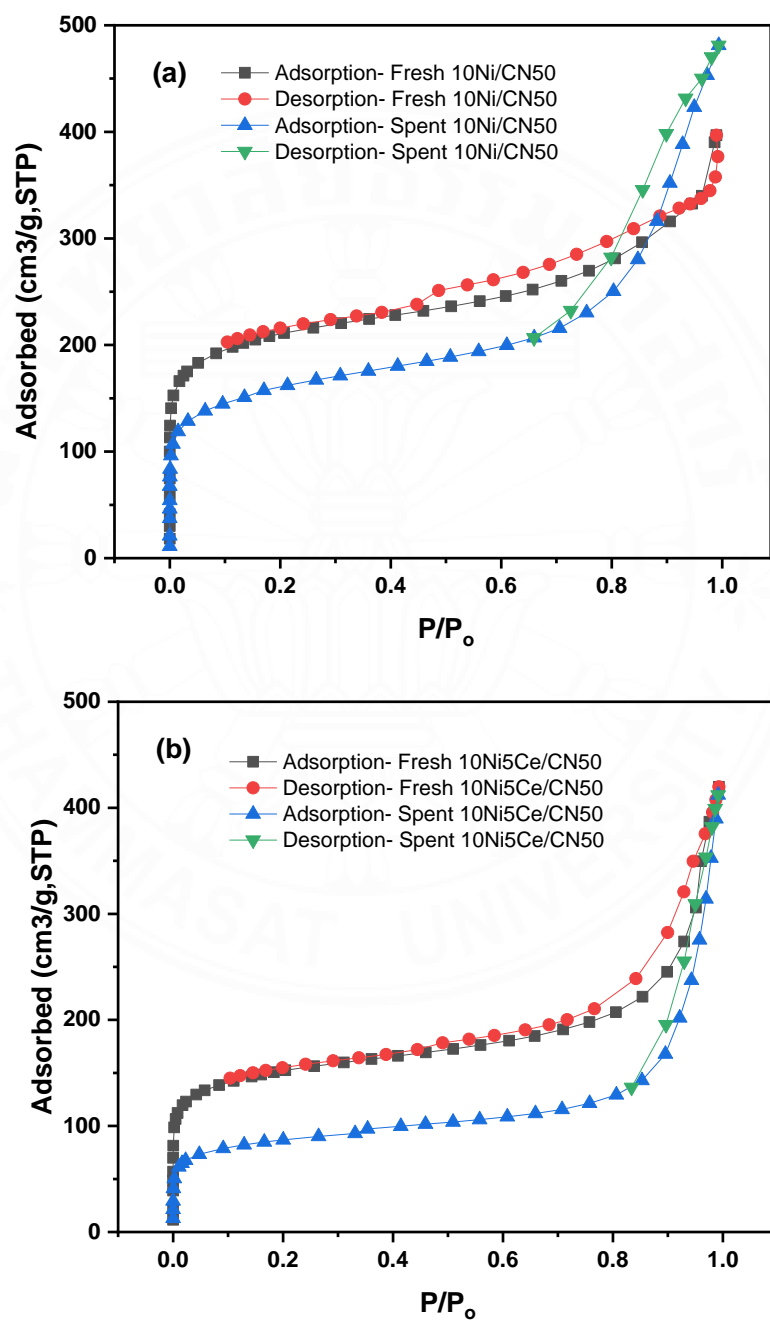
BIMETALIC Ni-Ce/CN50 CATALYST FOR IN-SITU HYDRODEOXYGENATION
OF PALM KERNEL SHELL PYROLYSIS VAPOR

Figure B.1 N_2 adsorption-desorption Isothermal fresh and spent catalysts of (a) 10Ni/CN50, and 10Ni5Ce/CN50

BIOGRAPHY

Name	Le Kim Hoang Pham
Educational Attainment	<p>2010 - 2014: Bachelor's degree (Petrochemical Engineering), Faculty of Chemistry Technology, Industrial University of HCM City</p> <p>2015 - 2017: Master of Science (Chemistry), Faculty of Science and Technology, Thammasat University</p> <p>2018 – 2022: Doctor of Philosophy (Chemistry), Faculty of Science and Technology, Thammasat University</p>
Scholarship	<p>2015: ASEAN scholarship of Thammasat University (Master study)</p> <p>2018: PRIDE Scholarship of Thammasat University (Doctoral study)</p>
Certification/Award	<ol style="list-style-type: none"> 1) Quality Assurance and Accreditation ISC/IEC 17025 and ISO/IEC 17020 2) Best oral presentation in International Symposium of Young Scholars on Carbon Recourses Conversion (YSCRC-2021), Oct. 14th – 16th 2021, Thailand
Conferences	<ol style="list-style-type: none"> 1) Oral presentation at the 29th International Symposium on Chemical Engineering (ISChE2016), December 2nd - 4th, 2016, Miyazaki, Japan 2) Oral presentation at the 4th Asian Conference on Biomass Science (ACBS2016b), Dec. 13th -14th, 2016, Penang, Malaysia 3) Oral presentation at the 5th Biotechnology International Congress

- (BIC2017), 6th - 8th September 2017, Bangkok, Thailand
- 4) Poster presentation at the 2nd TU-NSYSU bilateral workshop on chemistry, 3rd - 6th July 2018, Thammasat University, Thailand
 - 5) Oral presentation at the 31st International Symposium on Chemical Engineering (ISChE2018), December 2nd - 4th, 2018, Chiang Mai, Thailand
 - 6) Oral presentation at the 1st Thailand Biorefinery Conference, July 25th – 26th, 2019, Nakhon Ratchasima, Thailand
 - 7) Oral presentation in the International Symposium of Young Scholars on Carbon Recourses Conversion (YSCRC-2021), October 14th – 16th 2021, Pathum Thani, Thailand
 - 8) Oral presentation in the Vietnam-Taiwan Joint Symposium Applied Science and Emergent Two-Dimensional Materials 2022 (ASEM 2022), April 27th – 28th 2022, HCM city, Vietnam

Publications

Book Chapter

Pham, L. K. H. et al., Biofuel production with integrated pyrolysis and catalytic upgrading system. Innovations in Thermochemical Technologies for Biofuel Processing, 2022 Elsevier, p. 147–177

Articles

- 1) Pham, L. K. H. et al., Formation and activity of activated carbon supported Ni₂P catalysts for atmospheric deoxygenation of waste cooking oil. Fuel Processing Technology, 2019, 185, p. 117–125.
- 2) Pham, L. K. H. et al., Integrated catalytic hydrodeoxygenation of Napier grass pyrolysis vapor using a Ni₂P/C catalyst. Journal of Analytical and Applied Pyrolysis, 2019, 140, p. 170–178.
- 3) Pham, L. K. H. et al., Data-driven prediction of biomass pyrolysis pathways toward phenolic and aromatic products. Journal of Environmental Chemical Engineering, 2021, 9(2): 104836

- 4) Panpian P. et al., One-pot upgrading of coconut coir lignin over high-efficiency Ni_2P catalysts. *Journal of Environmental Chemical Engineering*, 2021, 9(6): 106702
- 5) Cao, A. N. T. et al., Boosted methane dry reforming for hydrogen generation on cobalt catalyst with small cerium dosage. *International Journal of Hydrogen Energy*, 2021, In press.
- 6) Pham, L. K. H. et al., High Catalytic Activity of a Nickel Phosphide Nanocatalyst Supported on Melamine-Doped Activated Carbon for Deoxygenation. *Topics in Catalysis*, 2022, 1–12

